8.
Wave modelling

CHAPTER COORDINATORS

Lotfi Aouf and Gabriel Diaz-Hernandez

CHAPTER AUTHORS *(in alphabetical order)*

Alexander Babanin, Jean Bidlot, Joanna Staneva, and Andy Saulter

8. Wave modelling

8.1. General introduction to wave characterization

8.1.1. Objective, applications, and beneficiaries

8.1.2. General characteristic of waves

8.1.2.1. General concepts

8.1.2.2. Definitions

8.1.3. Deep water wind-generated wave theory

8.1.4. Nearshore transformation of waves

8.1.4.1. Shoaling

8.1.4.2. Refraction

8.1.4.3. Diffraction

8.1.4.4. Wave current interaction

8.1.4.5. Dissipation (breaking and bottom friction)

8.1.4.6. Wave-structure interaction

8.2. Wave forecast and multi-year systems

8.2.1. Architecture singularities

8.2.1.1. Levels of complexity from deep to shallow water

8.2.1.2. Hybrid and clustering technique

8.3. Input data, available sources, data handling, and model pre-processing

8.3.1. Bathymetry and geometry

8.3.2. Forcing fields

8.3.3. Observations

8.3.4. Pre-processing and definition of the numerical problem

8.3.5. Boundary and initial conditions

8.4. Modelling component: general wave generation and propagation models

8.4.1. Types of models

8.4.1.1. Deep water

8.4.1.2. Shallow water

8.4.2. Discretization methods

Figure 8.1.   Waves panorama (credits: Gabriel Barajas Ojeda, IHCantabria).

8.1.
General introduction to wave characterization

Waves are extremely important in OOFS. This section gives an overview of the main challenges foreseen by OOFS for predictions to be able to numerically represent some relevant processes like that in Figure 8.1.

8.1.1. Objective, applications, and beneficiaries

Why is a comprehensive and reliable wave forecast so important?

In the last decade, the worldwide seas were hit by severe storms (see ECMWF, 2020), which caused serious damages in offshore and coastal zones, and attracted public attention on the importance of having reliable and comprehensive wave forecasts, especially when extreme events occur (Figure 8.2). Additionally, human activities, such as offshore wind power industry, oil industry, and coastal recreation also necessitate regular operational sea state information with high resolution in space and time.

Furthermore, extreme waves can cause serious impacts over coastal environments and infrastructures. The design of coastal and offshore structures requires a reliable estimation of maximum wave height. Efforts of sea state information are directed towards the improvement of environmental loads definition for lifetime of a ship or structure (e.g. wind energy turbines or oil and gas platforms). For example, long-term statistical and high-resolution predictions of significant wave height are necessary for planning the maintenance operations of offshore wind farms. Subject to wave forecasts, in the days and hours preceding a mission, "go/no go" decisions are made on operations and maintenance activities in offshore wind farms. Indeed, a reduction of uncertainties on metocean conditions will have a direct impact on structure and mooring loads, both for ultimate limit state and fatigue design, as well as for warning criteria for ships. These results can be obtained through hindcast and forecast studies including maximum wave parameters, which also aim at expanding the wave Copernicus Marine Service products catalogue[1] by providing novel wave diagnostics.

1. https://myocean.marine.copernicus.eu/ data?view=catalogue&initial=1
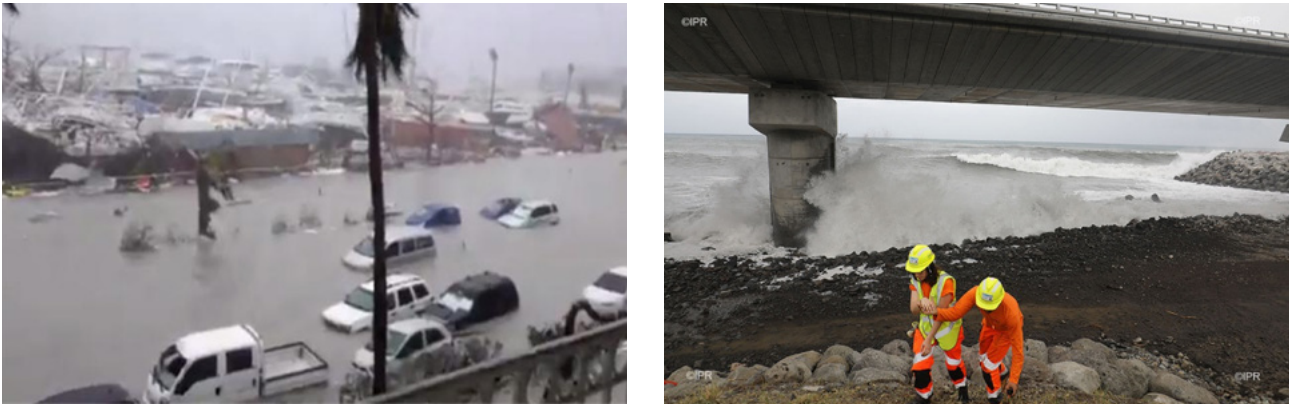
Figure 8.2. Left: high waves flooding after passage of Hurricane Irma in Saint Martin (Atlantic Ocean) in September 2017 (source: RCI-Guadeloupe). Right: high waves warning after passage of tropical cyclone Eliakim in La Réunion (Indian Ocean) on 15 March 2018 (copyright IPR Imaz Press Réunion).
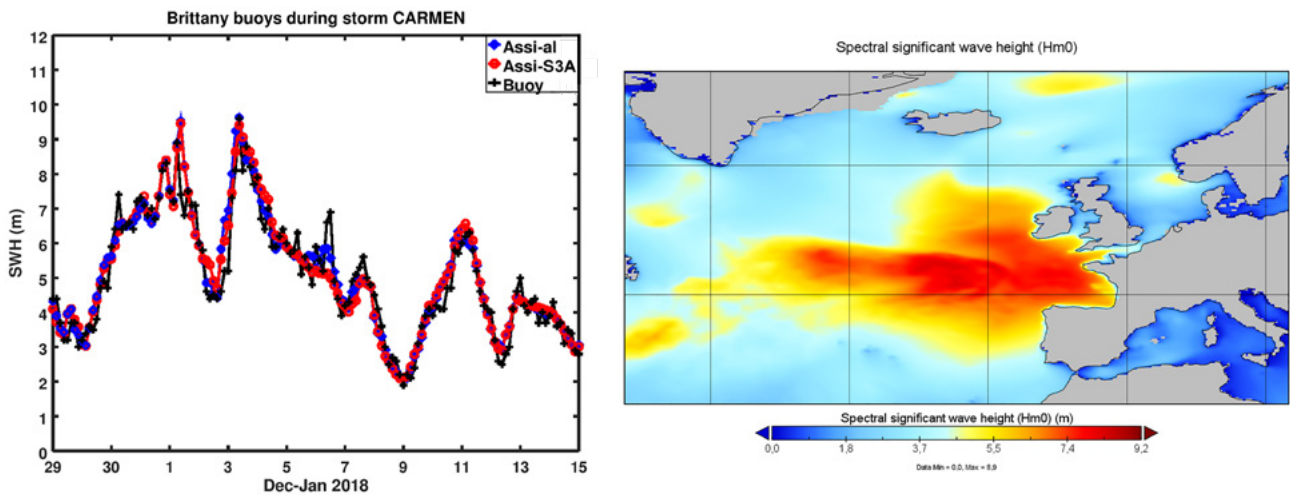
Figure 8.3. Left: time series of significant wave height at Brittany (France) buoy location during storm Carmen on 1 January 2018. Blue, red and black colours stand for hindcast from wave model MFWAM, analysis from model with assimilation of Sentinel-3 SWH and buoy SWH, respectively. Right: SWH map (in metres) from Copernicus Marine Service global wave reanalysis at peak of 1 January 2018 event, 09 UTC (source: Copernicus Marine Service).

The level of performance of wave forecasting products is of crucial importance. The assimilation of novel satellite data in global Monitoring and Forecasting Centres has pointed out the skill of the systems during storms generating high waves (Aouf, 2018). The joined satellite and model analyses also demonstrate the capability of the wave forecasting products to cover from global to regional scales (Copernicus Marine Service, OSR[2]), as well as the potential benefits of merging observational and modelled products (such as those shown in Figure 8.3) provided by the Copernicus Marine Service.

2. https://marine.copernicus.eu/access-data/ocean-state-report

Monitoring and forecasting

Monitoring and forecasting of wind waves are, in most cases, closely linked with ocean and atmospheric observations and modelling. The availability of systematic near-real time ocean observations is a prerequisite for the quality of weather and ocean state forecasts. Novel satellite wave observations are crucial for reducing the uncertainties in prediction skills for the wave simulations. Given that most of the buoy observations are coastal, remote sensing data are needed for tuning and validating the models offshore. On the other hand, ocean waves have a clear signature in most ocean remote sensing
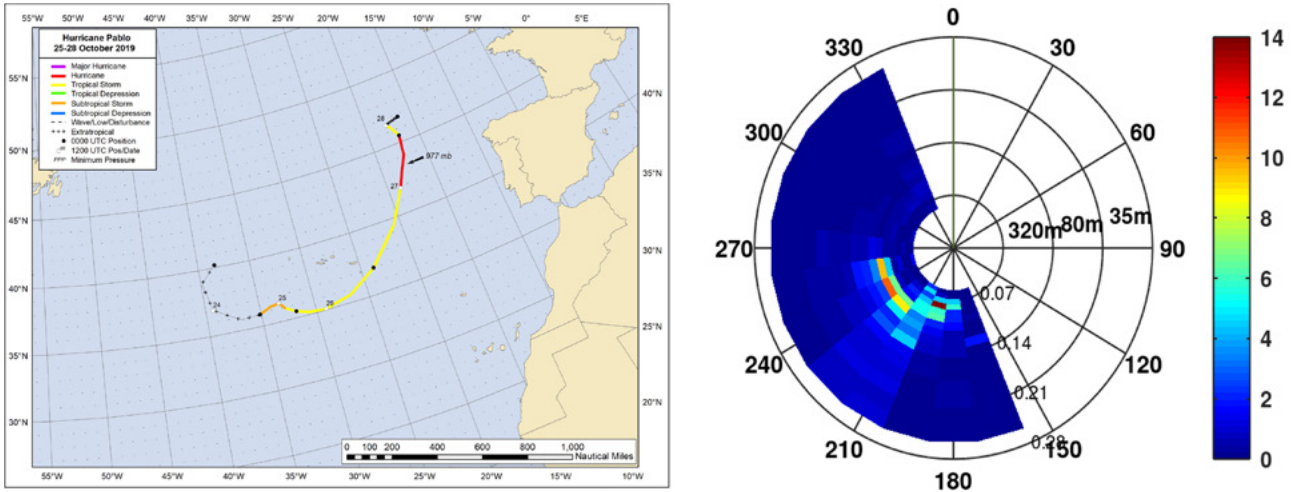
Figure 8.4. Left: trajectory of hurricane Pablo from 25 to 28 October 2019, NHC-NOAA tropical cyclone report. Right: wave spectrum observed by CFOSAT near the trajectory of hurricane Pablo (17°W-45°N) on 27 October 2019 at 18 UTC (source: Beven, 2019).

techniques, either adding noise or biases, and stable corrections and detection are very important for sea level and velocity estimates from altimetry (Climate Change Initiative Coastal Sea Level Team, 2020; Marti et al., 2021). It is important to underline that future regular monitoring of maximum wave heights is expected to improve understanding of the conditions that favour the generation of very large waves in the global ocean.

Sea state information for applications

There is a steady growth of the already intense interest in the wave conditions in coastal areas at different time scales. Increasing maritime traffic, recreational activities, urban development, ecosystem restoration, renewable energy industry, offshore management, all push in this direction (Cavaleri et al., 2018). Indeed, sea state affects most of the activities at sea (shipping, oil and gas industry, fisheries, offshore aquaculture, etc.), on the coast (marine protected areas, harbours, marine renewable energy, tourism, etc.). These activities require precise information on the sea state (hindcast, nowcast and forecast) and, in particular, on wave extremes. In addition to activities directly linked to the ocean, wind waves are of general interest to the Earth system.

Extreme events

Wind waves constitute the most relevant ocean process affecting the human activities and nearshore environment. The sea state and its related spatio-temporal variability dramatically affect maritime activities and the physical connectivity between offshore waters and coast-

al ecosystems, impacting also on the biodiversity of marine protected areas (Hewitt, 2003; González-Marco et al., 2008). Given their destructive effects in both the shoreline environment and human infrastructures, significant efforts have been devoted to predict extreme wave height events, prompting a wide range of adaptation strategies to deal with natural hazards in coastal areas (Hansom et al., 2015). In addition, there is also the emerging question about the effects of anthropogenic global climate change on present and future sea state conditions.

Tropical cyclones are commonly linked to devastation by hurricane force winds, storm surges and strong rainfall. They are also responsible for large exchanges of heat in the upper ocean and the atmosphere, and the transport of water from ocean to land. However, the dynamics inside these extremes are poorly sampled and understood. SAR overcomes these situations, but it is only able to recover one-dimensional information, which limits the ac<Zcuracy of estimated quantities like wind speed, total surface current, and wave spectra. In tropical cyclones, wave spectra (e.g. from Sentinel or by the CFOSAT) can only partly be recovered, as the quickly changing sea surface limits the resolution of SAR in the azimuth direction (Ardhuin et al., 2020) and from SWIM instrument of CFOSAT mission (Figure 8.4).

Coupling with circulation

The combined effect of high waves and sea level surge aggravate the storm risk potential. Integration of local wave and sea level forecasting systems (Álvarez-Fanjul et al., 2018; Staneva et al., 2020) and their associated alerts demonstrated

SSH (cfosat - Reference) for JFM2020
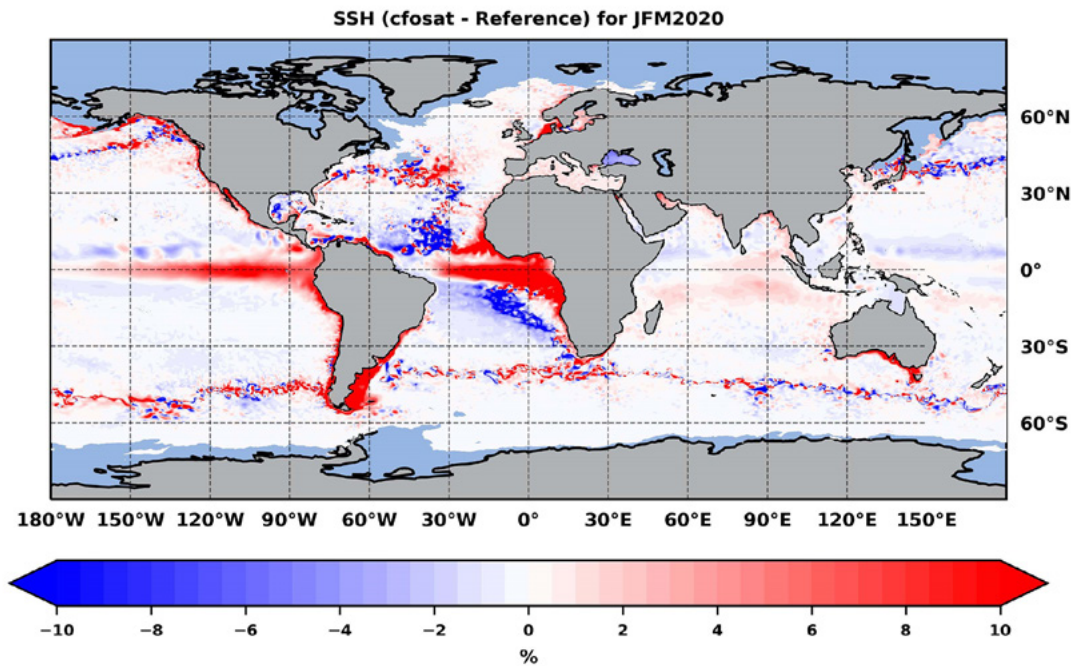
Figure 8.5. Mean difference (in percentage) of sea surface temperature induced by wave forcing in comparison with reference NEMO without waves (surface stress, Stokes drift and wave breaking inducing turbulence in the ocean mixed layer) for austral summer (January to March 2020) (source: Aouf et al., 2021).

the urgent need for such services. In respect to deep open waters, the relevance of currents is a difference emerging often. In the past, especially in the deep ocean, surface currents did not reach velocities to substantially affect wave conditions, which led to ignoring the wave induced currents in the ocean forecasts. However, close to the coast, the currents (barotropic and baroclinic) are geographically enhanced reaching values that, if not considered, can lead to substantial errors in wave model results (Cavaleri et al., 2018). Coupling between wind waves and circulation model waves can also affect the predictions of water levels, and thus of storm surges through changes in the stress of the upper-ocean mixing and circulation (Thomas et al., 2008; Staneva et al., 2021), providing more accurate offshore wave spectra (Cavaleri et al., 2018). Besides, forecasting the Lagrangian behaviour of surface currents is a key to identify high-risk scenarios for pollution of coastal areas, search and rescue, marine plastic, or quantify transport and retention of larvae or other planktonic organisms, with impact for fishery and Marine Protected Areas management.

Mixing

Human activities that take place at the atmospheric and ocean mixed layer (e.g. offshore wind energy sector) are largely driven by the air-sea exchanges of momentum, heat, and gas transfer. The fluxes between atmosphere and ocean are usually parameterized using bulk formulations, in which coefficients are often a function of wind speed alone. For example,

ocean waves largely define air-sea fluxes and upper ocean mixing (Babanin et al., 2012; Veron, 2015). A considerably enhanced momentum transfer from the atmosphere to the wave field is found during growing sea state (young sea) (Janssen, 1989). A wind stress formulation depending on wind stress and the wind–wave momentum released to the ocean was proposed by Janssen (1991). When running stand-alone ocean or atmosphere models, the surface waves that represent the air-sea interface are not taken into account. This can cause biases about the upper ocean, due to insufficient or, in some cases, too strong mixing (Breivik et al., 2015), or even because the momentum transfer is shifted in time and space compared to how the fluxes would behave in the presence of waves. Recent analyses show a moderate impact for intermediate wind speeds (Edson et al., 2013), even though it is expected that the surface roughness caused by waves should play a role (Donelan, 2004), although it is often correlated with the wind speed. The impact of waves on upper ocean mixing and sea surface temperature, in particular in cases of shallow mixed layers, is clearer at global and regional scales (Janssen, 2012; Staneva et al., 2017; Law Chune et al., 2018); see an example in Figure 8.5.

Engineering and near coastal applications

In order to design and operate ocean and coastal infrastructures (e.g. dikes, harbours, etc.) wave climate data and wave statistics are crucial. High-resolution, high-skill wave forecasts are important for coastal and marine engineering, given that waves can damage marine infrastructures and affect the safety
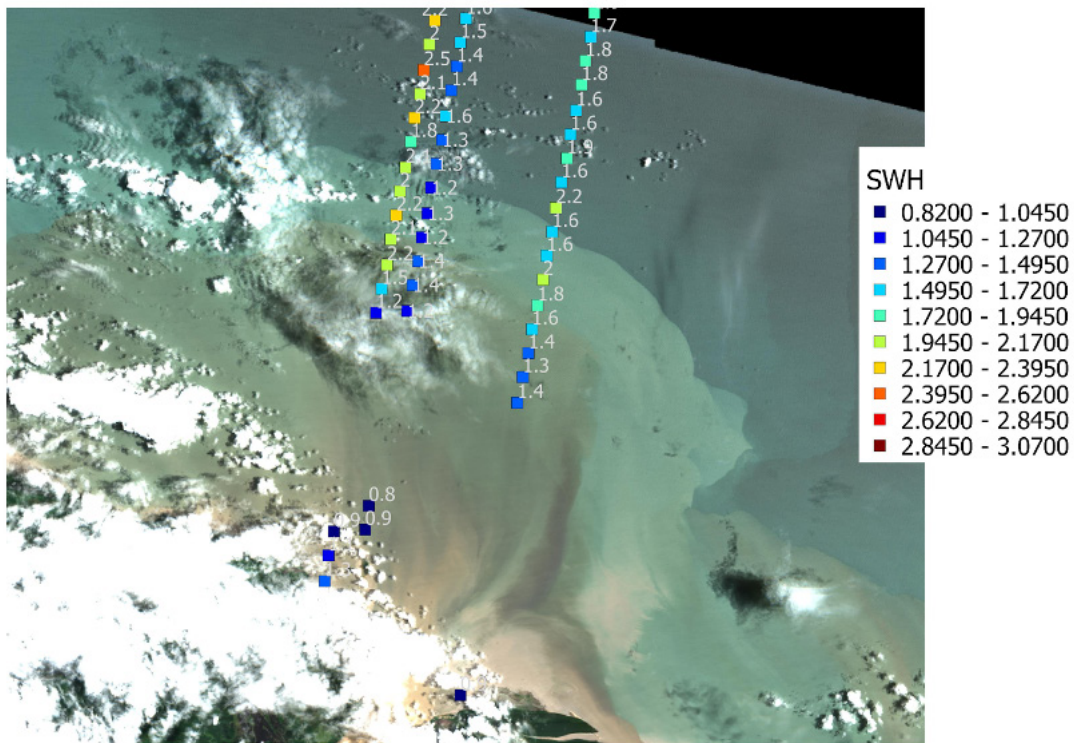
Figure 8.6. Sentinel-2 image observing coastal changes at Maroni estuary (French Guyana) overlapped by high resolution (1 km) significant wave heights on CFOSAT nadir tracks in March 2021. CFOSAT captures the decrease of SWH induced by very shallow water depth processes (courtesy of A. Dalphinet, MeteoFrance).

of shipping, ports, and offshore operations. Waves contribute to a large extent to shoreline erosion and flooding, which can influence coastal ecosystems and affect coastal communities. Realistic assessment and good understanding of historical wave climate is important to successfully address challenges and opportunities caused by present and future climate change, such as reduction of sediment supply by rivers to sand mining, blocking of longshore sediment transport by ports and other structures, sea level rise, particularly near tidal inlets, and land subsidence. Wind waves force coastal bathymetry changes and in coastline evolution, especially during extreme events or large swell events, waves can damage beaches, dunes, and/or dikes.

Early warning systems and risks

Warnings from integrated high-resolution wind waves surge forecasting systems can be sent in advance to the users. Several actions can be carried out to mitigate the impact of extreme hydrometeorological events. For example, harbours would stop operations to prevent accidents and assure safety. In some events material damages can be considerable but, as a result of preventive actions, personal injury can be avoided. Thanks to freely available satellite imagery (e.g.

Sentinel), it is now possible to observe from nadir altimeters, with good accuracy and increased sampling, the coastline changes by significant wave height, as shown in Figure 8.6.

The assimilation of newly available satellite-based wave data in wind wave models allows to more accurately hindcast and forecast coastal evolution in remote and ungauged areas, and to assess the effectiveness of coastal management strategies. Wind wave forecasts directly may improve the safety of people working offshore, such as those on oil platforms, fishers, etc. Professional sailors are constantly looking for wave forecast products that improve their knowledge and forecasts of sea state to be able to make the best decisions about routes and actions they will take during month-long competitions.

Sea state and coastal ecosystems

Some coastal ecosystems, such as salt marshes, coral reefs, mangroves, and seagrass meadows, play a fundamental role in shaping nearshore processes in a large portion of the world's coastline. Due to their capacity to naturally mitigate coastal flooding and erosion, the management and protection of these ecosystems is increasingly advocated within nature-based

coastal protection initiatives. Awareness that Nature-based solutions (NBS) can tackle societal challenges by utilising environmentally safe operations for vulnerability and risk assessment processes is growing. For example, marine seagrass is highly considered as a useful NBS, as it is capable of attenuating the impact of storm surges and coastal erosion. Ecosystem models usually have significant uncertainty in predictions. Understanding and better predicting wave-driven nearshore processes would help to improve our knowledge of hydrodynamic interactions with ecosystems across different time and space. Furthermore, wave forecast data are needed for activities involving protection, development, and enhancement of coastal and marine environments. Besides, sea state information can provide technical and scientific support to policy makers and stakeholders for environmental governance.

Wave data and the industry (e.g. marine energy sector, shipping operations, emergency response, etc.)

Wave data are critical for safe and efficient design, installation and operation of assets of the marine energy sector. High-resolution regional and coastal wave models can help to improve downscaling of general sea state forecasts, identify hotspots of different wave height properties, and prioritisation of maintenance jobs in offshore wind turbines, reducing their maintenance cost. Applications can further include initial resource assessment (wave power), environmental assessment, and planning (e.g. for installation and execution, operation and maintenance).

Sea state conditions have a significant impact on the design and structure of how vessels are built. The changes of the sea state impact on vessels operations and have always been a challenge for seafarers to which they have had to continually adapt. Besides, shipping/cargo operations are highly impacted by sea state and weather conditions. In addition, wave forecasts are needed for oil spill and emergency responses. The industry has developed various ways to adapt to the strength of the ocean. As evolving design and commercial needs push the boundaries of vessels' size and capacity, the demand for accurate sea state information increases.

Climate and waves as a part of the Earth system models

In our "blue" planet, interactions between the atmosphere and the ocean are crucial for the climate, and sea-related research plays a key role for a sustainable future (Visbeck, 2018), as advocated by international initiatives like the United Nations Decade of Ocean Science for Sustainable Development (2021-2030). Recent studies (e.g., Hewitt et al., 2017) have shown the relevance of air-sea interaction for a wide variety of phenomena (e.g. tropical/extratropical cyclogenesis, storm tracks, and global energy/radiation balances). Moreover, the IPCC has recognized the relevance of ocean waves for natural hazards in coastal areas, pointing out the

need for more mature regional (coupled) downscaling. Furthermore, air-sea transfers will become even more critical in the future, due to enhanced interface transients, temperature gradients, and possible other factors. To address the uncertainty and sensitivity of future projections due to global warming, it is necessary to fill the knowledge gaps related to air-sea feedbacks, which also limit present weather modelling, advancing from semi-empirical (bulk) formulations to sea-state dependent equations with an enhanced process basis. There is also an urgent need to advance the understanding and improve the modelling capabilities of the air-sea boundary, in which wind-waves play a key role.

The atmosphere-ocean feedback has now become state-of-the-art in weather prediction, but their bearing in climate simulations is somewhat limited and warrants a more detailed assessment (Breivik et al., 2015). The modulation of the active air-sea interface alters atmospheric and oceanic dynamics, as well as the associated bio-geo-chemical fluxes (e.g. CO_2 fluxes and storage at sea). Sea-state coupling should be accounted for in predictions/projections, so that the wave modulating effect on weather and climate evolution can be properly reproduced (Parkinson and Cavalieri 2012). Within an appropriate coupling and downscaling/nesting strategy, gaining understanding of air-sea interactions would reduce uncertainty in forecasting and be a critical advance for climate projections. Air-sea interface may have a role well beyond that conventionally accepted, and non-linear feedback should become more crucial under changing climate.

It is then essential to introduce the role of sea-state in both global and regional models for climate projection, addressing the resulting implications for bio geochemical and boundary (sea-ice and land) processes. Enhanced ESMs can be supported by new satellites (e.g. CFOSAT, Sentinel data, etc.) to achieve improved predictions for energetic conditions (e.g. tropical cyclones or Mediterranean tropical-like cyclones, often referred to as medicanes) and projections. In an ESM, the sea state needs to be considered at both global and regional scales, ensuring consistency and contributing to overcome uncertainties of projections at both short-term and long-term time scales. The advances on air-sea-wave-ice interactions in coupled models (including the land boundary) will contribute to bridge the gap between predictions/projections.

8.1.2. General characteristic of waves

8.1.2.1. General concepts

Within the catalogue of physical meteo-oceanographic variables and processes offered by any OOFS, waves can be considered one of the most relevant elements. Waves have high interaction with human activities located on the coast (coasts, ports, river mouths, etc.) given their energetic importance, and their cyclical and continuous presence in nature. Figure 8.7 dis-
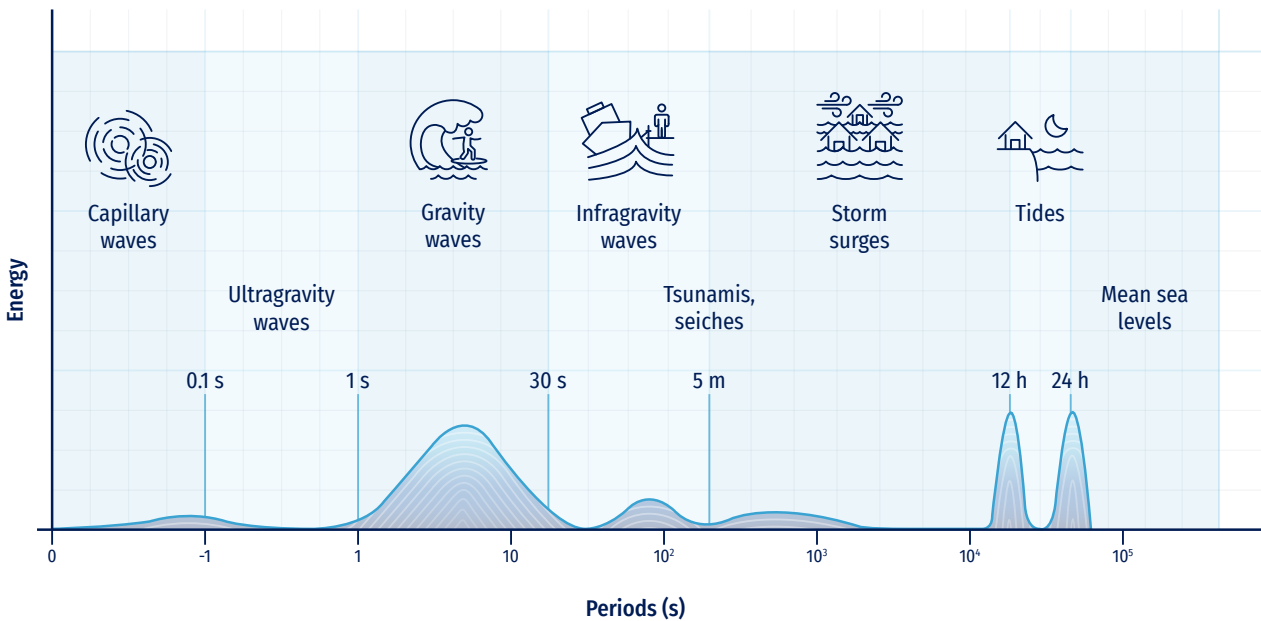
Figure 8.7. Frequencies and periods of the vertical notions of the ocean surface (adapted from Pérez et al. 2013, Holthuijsen (2007), after Munk (1950)).

plays the energetic relevance of wind-generated waves (with typical periods between 1 and 30s), in comparison with other oscillatory variables in the marine physical environment.

Traditionally, observations of ocean waves were obtained through visual databases (Gulev et al., 2003) limited in space and time, and with a high uncertainty about their qualitative genesis. Likewise, instrumental wave databases (Chelton and McCabe, 1985), obtained at discrete points in ocean and coastal areas, have been relevant in the understanding, quantification, and exploitation of this variable. However, only records of no more than two decades duration, generally non-continuous and acquired by equipment with non-homogeneous hardware characteristics, were available.

More recently, thanks to satellite technology it is possible to rely on a more extensive, continuous, accurate and homogeneous wave database (Barstow et al., 2004; Ribal and Young, 2019), with approximately two decades of development in the state of the art. The major disadvantage of this type of data consists in the spatial discontinuity conditioned by the satellite's own translation, which only manages to cover narrow trajectories (see Chapter 4, Section 4.2.3).

In the same way, thanks to technological advances in computers, in recent years it has been possible to obtain continuous, homogeneous, and realistic wave databases with global coverage (Saha et al., 2010; Reguero et al., 2012; Perez et al., 2017), in line with directional calibration techniques for post-processing this type of series. These new databases are in turn fed by global climate models of wind, pressure, ice cover, and other variables (Tolman, 2010). See in Figure 8.8 a general scheme of variables and processes for wind-generated waves.

The wave variable represents one of the fundamental bases of meteo-oceanographic knowledge, due to its energy and interactions with natural and human activities in open and coastal areas. Therefore, it is important to have a good quantification of wave characteristics, either from a statistical (long-term or multi-year / hindcast databases) or predictive (short- to medium-term / forecast strategies) approach. This information is needed to design, construct, and operate maritime activities from coastal areas to offshore locations exposed to extreme events, as well as for environmental management, climate analysis, and all situations in which the complex processes of wave transformation occur.
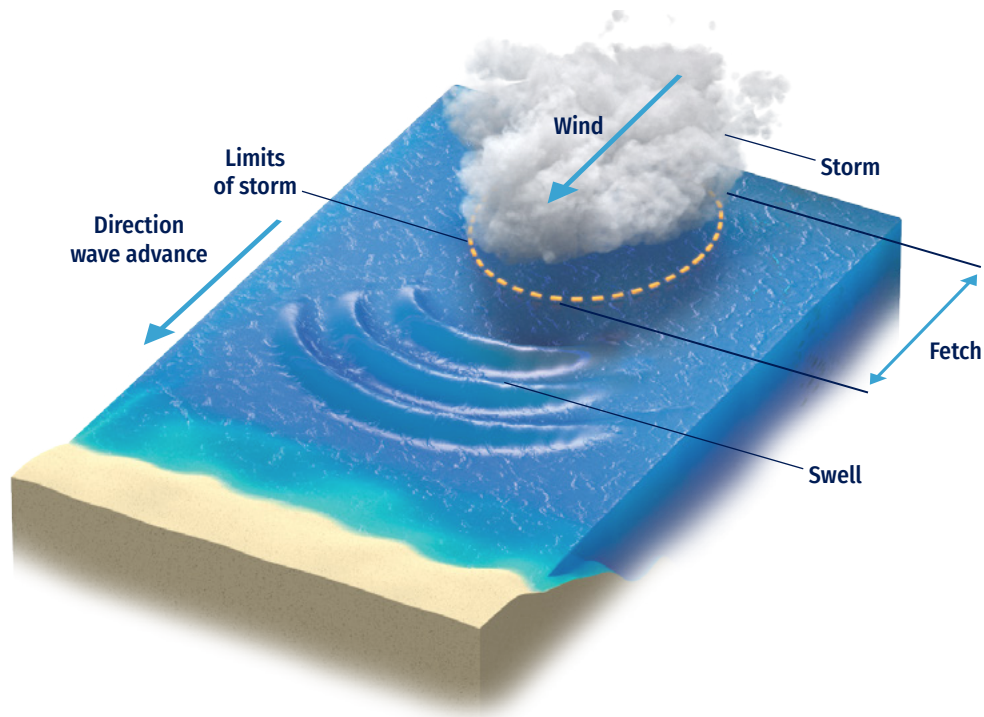
Figure 8.8. General scheme of variables and processes for wind-generated waves' characterization from offshore to coastal zones.

The current techniques require long-time (historical) series on the most relevant wave variables, associated to sea states (generally hourly) with a global coverage. These databases are already available, often free of charge, thanks to important technological efforts of different institutions worldwide (Rascle et al., 2008; National Centers for Environmental Prediction, 2012; Le Traon et al., 2019). This reliable information is subjected to validation, assimilation, and calibration protocols with instrumental data (Thomas, et al., 2008; Stopa, 2018) but, as it is only limited to open water areas, does not usually include the transformation processes that waves undergo in intermediate to reduced waters. Then, to include these relevant processes, it is necessary to address the concept of wave downscaling, and additional physics is needed to characterise in detail and with high resolution the waves in coastal areas, harbours, beaches, etc.

Modern downscaling relies almost entirely on the support of numerical models that, over the last decade, have evolved enormously in terms of resolution, including physical processes, spatial extensions; also the variables to be obtained go beyond the basic wave variables. However, the new processes/variables to be obtained, along with the new numerical tools, tend to increase the complexity of the solutions, since they call upon for increasingly sophisticated mathematical formulations, rise the dimensions of the computational scheme (from two-dimensional to three-dimensional scopes) and, consequently, boost the computational time for their solution.

This trend represents an important technical constraint in the assembly of numerical solutions for obtaining the wave variables, from hourly to multi-annual statistical analysis, as well as for any analytical project in the predictive or forecast environment, in which the results are expected to be available on a daily basis and within a calculation window of a few minutes/hours.
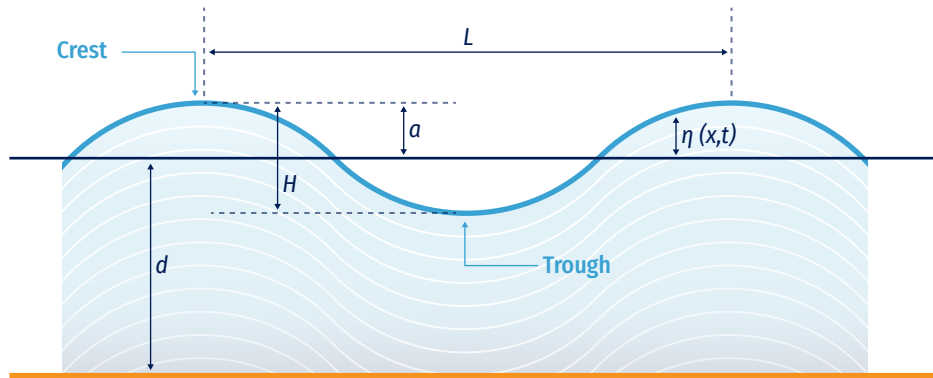
Figure 8.9. Characteristics of a 2D linear water wave.

Different methods have been proposed in the literature (Gaslikova and Weisse, 2005; Camus, et al. 2011 and Camus, et al. 2013) to overcome this problem, with the purpose of a better understanding of the complexity of the physical processes associated with the generation / propagation of waves, without paying a computational cost that moves the climate solution away from its practical and efficient objective.

In this chapter are discussed the most relevant concepts on the quantification of the wave variable in the meteo-oceanographic field, focusing on how to obtain time series (hourly) of this variable in the multi-annual field (hindcast) and the predictive field that are part of an OOFS. Basic concepts are:

- Theoretical definition of waves;

- Techniques, tools, and numerical models that are currently commonly used worldwide;

- Architecture and singularities in the solution schemes, assembly, and general approximation methods for the adequate exploitation of the tools;

- Basic and advanced variables associated with waves that can be obtained in different geographical areas;

- Some examples of multi-annual and forecast systems currently operating at the global level.

In line with the ten challenges of the UN Decade of Ocean Science for Sustainable Development, this chapter aims at making the readers able to obtain general and basic knowledge of wave climate, enabling them to establish their own multi-annual statistical prediction and interpretation systems for studies and projects in coastal engineering, offshore maritime works, beach design, integrated coastal management, harbour agitation, forensic analysis of extreme events, design formulations for coastal engineering, marine construction aid systems, etc.

8.1.2.2. Definitions

This section describes the general terminology for the physical features of the ocean waves. Theoretical water waves are described by their length (L), height (H), amplitude (a) or height (H), and water propagation depth (d). Other variables, such as velocities, pressures and accelerations can be explicitly mathematically calculated from the three basic quantities: amplitude (a), wavelength (L) and period (T). Two-dimensional wave schematic is traditionally visualised (Dean and Dalrymple, 1991) to better understand the wave main characteristics (Figure 8.9).

This scheme exemplifies ocean waves a as simple sinusoidal wave, where a represents the oscillatory and cyclic vertical distance between the mean water level and the crest height, and η(x,t) represents the vertical position of the free surface at a specific location x and time. The coordinate axis used to describe wave motion is located on the still water line z=0 and bottom of the water z=-d. Wavelength (L) can be defined using the dispersion relation (as described in Eq. 8.1), defined as the horizontal distance between two successive wave crests or troughs (wave lowest point) and directly related with the wave period (T, as the required time for two successive crests to pass from a fixed point in space or time respectively), over a water depth.

As waves propagate, water mass moves in orbital trajectories. Also, wave phase velocity or celerity (C), is equivalent to $C=L/T$.

This idealisation rarely appears in nature, neither in frequency nor in direction. Thus, irregular waves or real field waves can be organised as a superposition of a large number of sinusoidal components (monochromatic waves) going in multiple directions, each of them with different frequencies or periods, amplitudes and random phases. This idea allows the use of a classical Fourier analysis, statistical techniques, and well-known energy-spectral techniques to adequately

assimilate and describe ocean waves that exist within any location and time window (generally within 1 hour as sea-state definition).

Random or irregular ocean waves, as a summation of independent harmonic waves, can be described in detail with linear theory for surface gravity waves, only valid for small amplitude waves. Linear theory (also called Airy theory, or Airy waves), after a clear definition of basic governing equations and contour conditions, gives the solution of a long-crested harmonic propagating wave in the x-direction, as follows:

$$\eta(x, t) = a \sin(\omega t - kx) \tag{8.1}$$

That yields the general dispersion equation that relates the angular frequency $\omega = 2\pi/T$ and wavenumber $\omega = 2\pi/L$:

$$\omega^2 = gk \tanh(kd) \tag{8.2}$$

So, dispersion conditions can be used to calculate the wave propagation velocity at any depth, based only on the wave period. As a result, long waves travel faster compared to short waves. These waves, whose propagation speed depends on the wavelength and frequency, are called dispersive waves.

When waves travel and propagate in the ocean, they form groups of different components. Since the difference between the spectral sea-state frequencies is infinitely small (difference between adjacent wave numbers is also infinitely small), the velocity of the group (C_g) can be calculated from the phase velocity (C) as shown below:

$$C_g = \frac{1}{2} \left(1 + \frac{2kd}{\sinh(2kd)} \right) \tag{8.3}$$

It indicates that the phase velocity (speed of an individual wave) is always equal or greater than the speed of the group. The dependence of the group velocity on frequency results in the disintegration of the wave groups: this is physically visible as longer waves travel faster ahead of the shorter waves and wave energy disperses across the ocean. A consequence of this is the transformation of an irregular sea (called SEA-type) created by a storm into a more regular and phase-ordered sea (or SWELL-type).

In the basic linear theory, these variables can define three zones that clearly differentiate the overall behaviour of waves as they are generated and propagated towards the coast, as follows:

- **Deep water**: limited by *d>0.5 L* where wave-induced velocities decrease exponentially with increasing distance from the surface. Water particles move in circles of decreasing radius towards the sea bottom. Eventually, the amplitude of the wave is equal to the radius of the biggest circle on the free surface. Individual waves of the group travel faster than the group.

- **Shallow water**: limited between *d<0.05 L*, for shallow waters, particle kinematics shows that the amplitude of the horizontal velocity is constant over the vertical axis and it does not depend on the depth; also the amplitude of the vertical velocity increases linearly from the seabed to the surface. The orbits of the particles in shallow waters are elliptic. The celerity (*C*) is calculated only by the depth (*d*) and the wavelength (*L*) is proportional to the wave period (*T*). Individual components travel at the same speed of the group, maintaining their position in the group.

- **Intermediate depth**: all other cases in which both water depth and period (or wavelength) have a significant influence on the solution of linear wave theory. In addition, individual waves of the group travel faster than the group (as in deep waters).

This definition of waves into different theoretical zones allows to classify the physical behaviour of the oscillatory flow in three categories:

a. Wave generation in deep water by wind action;
b. Wave propagation and dispersion from deep to intermediate waters;
c. Wave transformation and dissipation towards the coastal zone, and its interaction with bathymetry, natural and artificial structures.

The general knowledge of these processes allows understanding their degree of complexity, importance, and application in statistical or predictive climate systems. It is imperative to properly identify the experimental, mathematical or numerical tools to be selected to solve processes (based on the most relevant wave transformation characteristics), to generate a hierarchy of the variables and processes to be considered and to establish the hypotheses in assembling climate systems.

The following sections discuss these topics, with the purpose of enabling the setup of a climatic (multi-year) or predictive system for ocean waves from deep water to the coast, tailored to the processes that the user wants to include, considering pros and cons of each numerical module, as well as the inherent and concatenated uncertainties of the integrated system.

8.1.3. Deep water wind-generated wave theory

Ocean wind-generated waves are one of the most challenging research objects in meteo-oceanographic physics. They are generated and forced by the wind fields acting at global

scale (Janssen, 2004, Chalikov, 2016) and are subject to important dissipation and strong nonlinear effects (Babanin, 2011), which drive the evolution of wave spectra at the scale of tens of thousands of wave periods (Hasselmann, 1962, Zakharov, 1968). Generation, dissipation, and interaction dynamics are the three main non-separable pillars for any wave model: once the waves are produced by the wind, no matter how small they are, the mechanisms of their attenuation and energy exchanges with other wave components within the wave spectrum are immediately activated. Moreover, each pillar is not a single physical process, but rather a plethora of various processes, often concurrent and with varying relative significance over the course of wave evolution.

The three main dynamics are always present but in particular circumstances, or from the point of view of a particular application, other processes can become relevant or even dominate. For example, various influences of surface currents (Babanin et al., 2017), sea ice (Thomson et al., 2018) or surface tension, as well as other forcings (Cavaleri et al., 2007).

In shallow-water environments and with extreme winds, waves become a different physical object and their respective wave models are notable for a lesser degree of physics and a larger degree of parametric and ad hoc tuning. For finite depths, dispersion is reduced or even ceases, nonlinearity grows but active nonlinear mechanisms change, balance between energy input and dissipation is no longer maintained, and a variety of new physical processes come into existence because of various wave-bottom interactions and sediment response (Young, 1999, Holthuijsen, 2007).

When winds exceed 30 m/s, a simultaneous change of physical regime takes place in all the three air-sea environments, i.e. atmospheric boundary layer, sea surface, and upper ocean (Babanin, 2018). For the waves on the ocean surface, this modifies wind input processes in which frequent flow separation and massive production of spray alters wind-wave exchanges and leads to the known effect of saturation of the sea drag. Wave breaking and dissipation are now driven by completely different dynamics, i.e. by direct wind forcing rather than nonlinear wave evolution.

8.1.4. Nearshore transformation of waves

Any ocean wave reanalysis (multi-year database) or prediction system, focusing on shallow waters of the coastal zone, will require detailed information on the most important processes involved in the transformation of ocean wave characteristics, which originated in deep water. This subsection presents a comprehensive description of these processes, their basic equations and the physics that need to be taken into account.

It is important to underline that the theories presented here treat each process as an isolated entity but, in reality, all these processes appear together and act concomitantly. Hence, it is necessary to create a hierarchy of the relevant processes for each sub-area of wave propagation towards the coast, so that developers of climate and forecasting systems can be aware and consider them appropriately.

8.1.4.1. Shoaling

Shoaling happens when waves start to interact with the ocean's bottom or bathymetry configuration. As the wave propagates over intermediate and shallow waters zones, it reduces its celerity and maintains its frequency (linear theory main hypothesis); both wavelength and phase speed decrease, and wave amplitude trends to grow (Figure 8.10). In other words, in shallow waters, ocean waves become less dispersive, meaning that the phase speed is less dependent on the wave frequency.

Waves interact with bottom

Deep water   **Shoaling zone**
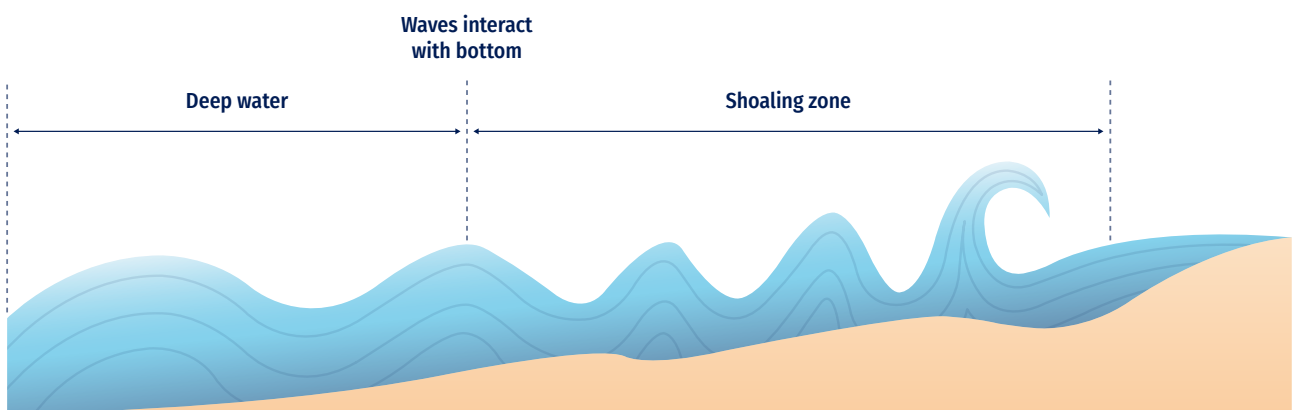
Figure 8.10.   Ocean wave shoaling main characteristics.
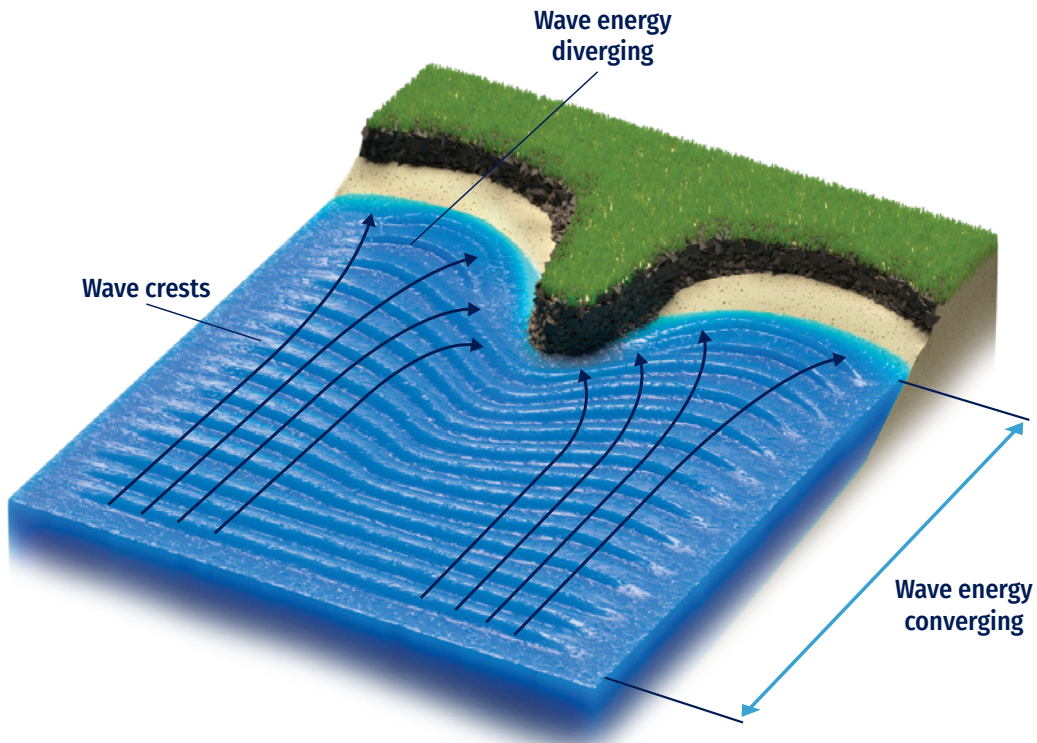
Figure 8.11.   Ocean wave refraction main characteristics.

The change in the wave height due to shoaling can be calculated from the following general relationship thorough a shoaling coefficient, K_s:

$$H_2 = H_1 \sqrt{\frac{C_{g1}}{C_{g2}}} = H_1 \cdot K_S \qquad (8.4)$$

In practice, wave shoaling phenomena can be observed as a local increase of wave heights due the reduction of the bathymetry profile or depths. Also can occur also in a reverse form, i.e. shoaled waves travelling into progressively deeper water. This results in a wavelength increase effect (wave speed also increases), while wave height decreases.

8.1.4.2. Refraction

When ocean waves change their direction of propagation from the bottom or for a bathymetry interaction, a refraction occurs, mainly due to the change of a same wave front travelling at different bathymetric depths, yielding partial reduction of its celerity. One section of a travelling wave moves faster than the other part, resulting in the wave fronts turning towards the coast (Figure 8.11). Ocean waves will al-

ways turn towards the region with lower propagation speed. Physically, wave refraction satisfies Snell's law:

$$\frac{\sin \theta}{C} = \frac{\sin \theta_0}{C_0} \qquad (8.5)$$

As waves propagate towards a coast, waves crests tend to become parallel to the coastline. Refraction can be visualised as the gradual change in waves' direction when they tend to approach a coastline at an angle 0°, known as oblique incidence.

Additionally, refraction can have an important effect (partial wave height reduction or increase) calculated with a refraction coefficient (K_R) as follows:

$$K_R = \sqrt{\frac{\cos \alpha_0}{\cos \alpha}} \qquad (8.6)$$

Finally, combined wave refraction and shoaling are always present simultaneously and affect wave height as follows:

$$H_2 = H_1 \sqrt{\frac{C_{g1}}{C_{g2}}} \sqrt{\frac{\cos \alpha_0}{\cos \alpha}} = H_1 \cdot K_S \cdot K_R \qquad (8.7)$$
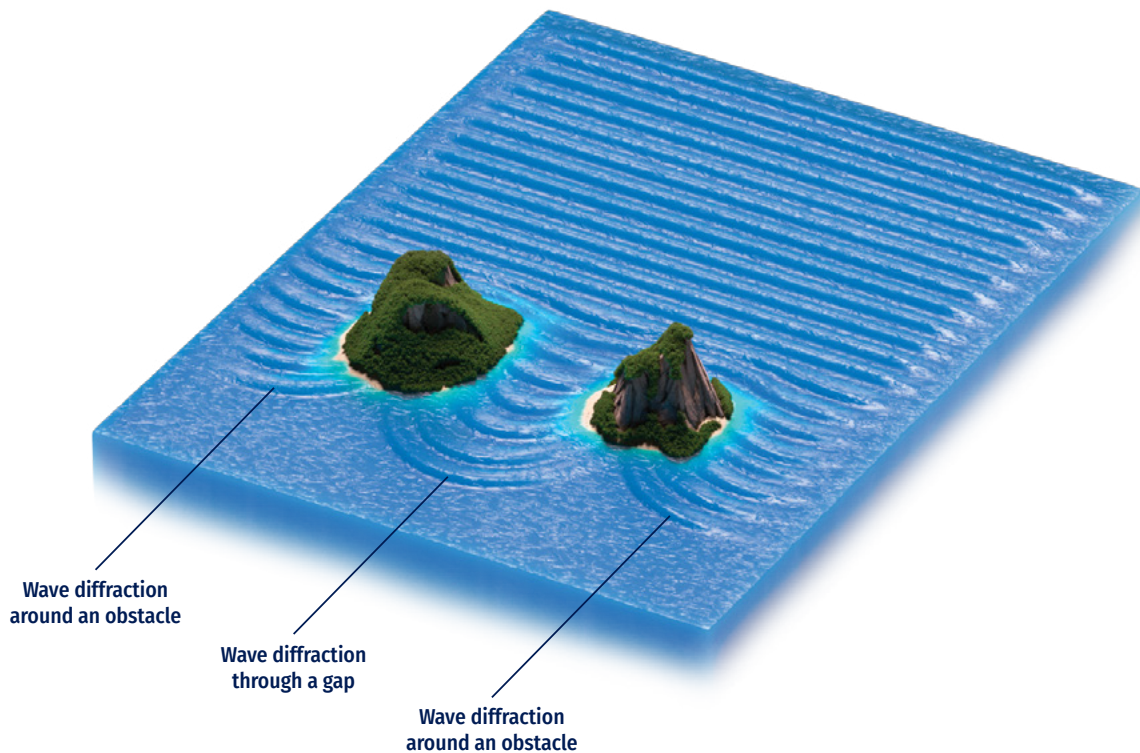
Figure 8.12. Ocean wave diffraction behind semi-infinite obstacles.

8.1.4.3. Diffraction

When ocean waves reach and interact with any structure (natural or artificial, totally or partially emerged), wave diffraction occurs, which is described as the blocking and spreading of energy laterally perpendicular to the dominant direction of wave propagation. The result is that wave fronts, angles, and energy spreads behind (so-called lee side) the obstacle and wave heights appear lower in sheltered areas (Figure 8.12). Also, wave fronts rearrange into more structured and radial/focused wave propagation patterns.

The circular pattern adopted by diffracted wave crests, as they penetrate in the lee side of obstacles, diminishes rapidly as waves are diffracted further behind the obstacles. This behaviour could be relevant for any OOFS near bays, harbours, islands, and peninsulas areas.

Diffracted waves are also still affected with both refraction and shoaling effects, especially for large sheltered zones with relevant bathymetric changes. Also, semi-diffraction effects can occur for those semi-submerged structures (break-

waters and/or steep bathymetric bodies) with a clear refraction-diffraction combined effect.

Analytical solution for diffracted waves can be handled through a diffraction coefficient for an idealised constant bathymetry and semi-infinite emerged bodies (CERC, 1984), ignoring wave reflection effects, and using instead graphical diagrams as a function of the wavelength, the angle of incidence between the emerged body and the distance between the head of the breakwater and the point of calculation (Koutitas, 1990). For more realistic configuration, numerical approaches (phase averaging or resolving strategies) should be invoked.

8.1.4.4. Wave current interaction

Ocean waves are also affected by currents (tides, storm surges, river discharges, ambient currents, etc.). Changes in the amplitude, frequency, and direction of the incident waves are expected (Dean and Dalrymple, 1991).

Current-derived local shoaling might occur if waves get blocked by a current. Also, current-induced refraction can induce chang-
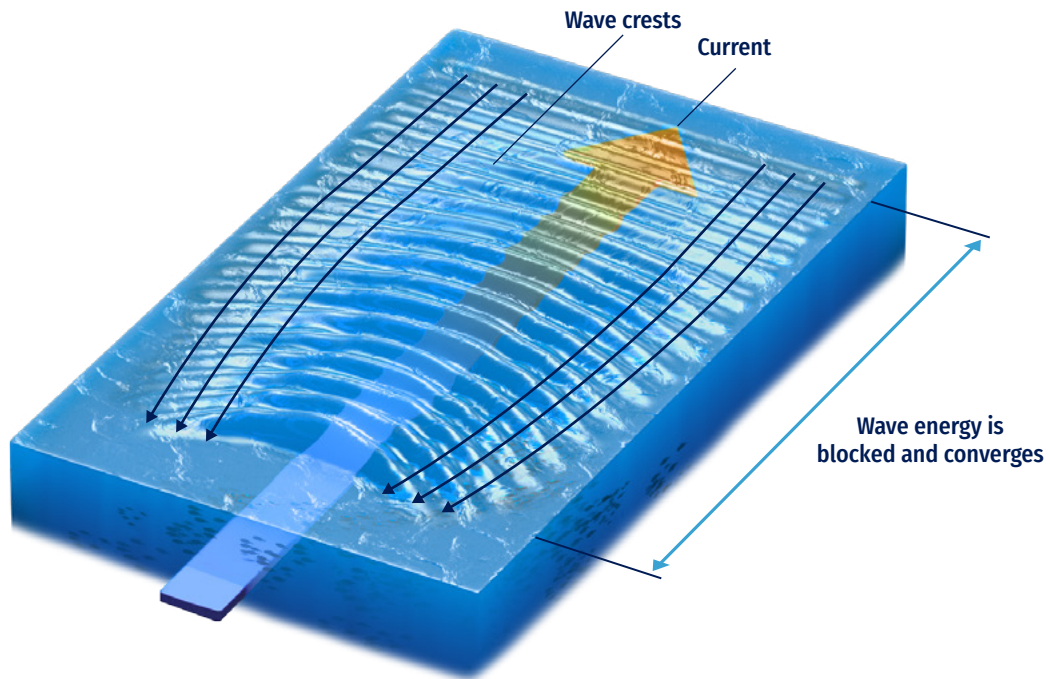
Figure 8.13.   Example of wave-current interaction.

es in the direction of speed/wave propagation, as well as energy exchange between the current and the wave can be present at coastal/mouth of the river zones and in some harbour entrances affected by littoral currents (Figure 8.13).

Linear theory is still valid and dispersion equation can be adapted to take into account currents (vertical integrated depth) as follows:

$$\omega = \sigma + kU_n \qquad (8.8)$$

where U_n is the component of the current in the wave direction.

8.1.4.5. Dissipation (breaking and bottom friction)

Wave breaking is maybe one of the most energy-dissipating phenomena that waves can experience. It occurs when a shoaling/growing wave propagates over a limited depth profile, reaching its own water volume stability. As waves propagate towards shallow water, they become steeper until a stability-limit when they break, generating a complex mechanism related to fluid turbulence and vorticity.

Depending on water wave incoming characteristics such as frequency, direction, and height, and the bathymetric char-

acteristics (slope), different types of wave breaking are expected to occur. A parameter called the Iribarren number (also known as surf similarity parameter) can be employed for these classifications (see Figure 8.14), defined as a function of the bottom gradient and wave steepness as:

$$\xi = \frac{\tan \alpha}{\sqrt{\frac{H}{L_0}}} \qquad (8.9)$$

where α is the bottom slope, H is the incident wave height and L_0 is the deep-water wavelength.

A simple way to estimate breaking limit depth is based on the breaking height equal to a fraction of the water depth, as established by McCowan (1984):

$$H_b = k \cdot h_b \qquad (8.10)$$

where $k=0.78$.

For coastal wave climate or forecast applications, realistic characterization of wave breaking could be one of the most challenging issues and should be handled numerically when dealing with prediction of structure damaged by waves inside the surf zone of the breaker line at beach profile.

Spilling

Spilling breaking which spans within the whole surf zone for mild-slope beaches.

Plunging

Plunging breaking what waves curls forward and impinges formatting a partial tube.

Collapsing

Collapsing breaking and it comprises of a combination of plunging and surging breaking (Dean & Dalrymple, 1991).

Surging

Surging breaking for very steep beaches forming a very narrow or even non-existing surf line or zone. Wave reflection in this case is relevant.

Figure 8.14.   Wave breaking type based on Iribarren number.

Additionally, wave dissipation due to bottom friction can be relevant when waves propagate into shallow water. Friction between the bottom and the orbital motion of water wave particles dissipates wave energy; it depends on both the orbital velocity and the roughness of the bottom.

8.1.4.6. Wave-structure interaction

As wave fronts reach any coastal obstacle, part of the to-tal-incident wave energy travels back into the open sea, basin, or sheltered area (Figure 8.15). Some of the original wave energy is reflected and some is dissipated. The amount of energy is reflected (stated as reflection coefficient or K_f) depending on both the vertical structure typology (natural cliffs, beaches, artificial breakwaters, quays, etc.) and the incident wave characteristics (mainly due to wave frequency).

An idealised vertical structure can reflect a 100% of the incoming wave energy ($K_R=1$) but in real imperfect coastal perimeters this value is commonly below ($K_f<1$), due to the combination of complex physical processes (e.g. wave break-

ing, friction, percolation, run-up, etc.) that occur in the structure-water interface.

For shallow water zones adjacent to coastal structures, it is important to include wave reflection in the list of relevant wave transformation processes, especially for those wave climate or forecast systems that needs a good characterization for both incident and reflected waves at the study zone (i.e. propagation of collateral reflection effects from far areas such harbours, cliffs, reefs, jetties, harbour agitation, etc.).

The mathematical description of wave reflection deals with the calculation of wave motion as a linear sum of the incident wave and the (partially) reflected wave, as a transient or standing wave effect (for a constant deep domain and 1D approach). This can be complex for real bathymetry and coastal perimeter configuration, when irregular wave trains interact with different structures and coastal typologies and, in this case, an ad-hoc numerical approach should be used.

Partial wave reflection can also be relevant for semi-submerged structures and/or steep bathymetric changes (e.g. dredged navigation channels), as it interacts with wave shoaling, diffraction, and refraction effects. For example, harbour agitation phenomena deal with a complex computation of diffracted and partially reflected wave patterns.

Along with wave reflection effect and wave breaking on coasts and rubble-mound structures, waves' energy and frequencies can overtop these elements, tide instants, and each particular structure's typologies and characteristics.

Within wave climate or forecast systems, for a detailed definition of wave effects interaction with coastal structures (natural or artificial) could be important: i) wave run-up height, defined as (Ru2%) the wave level, measured vertically from the still water line which is exceeded by 2% of the number of incident waves; and ii) wave overtopping discharge (Figure 8.16), defined as the average water discharge per linear metre of width of the structure.

In recent times, forecast systems dealing with wave overtopping along a pedestrian coastal zone are delivered worldwide. The precision of these early-alert systems depends on a good reproduction of both incoming water waves and the geometry of the structure (freeboard, crest width, roughness, slope, permeability, and porosity). In order to calculate these derived variables, EurOtop Manual (Van der Meer et al., 2016) gathered some empirical formulae
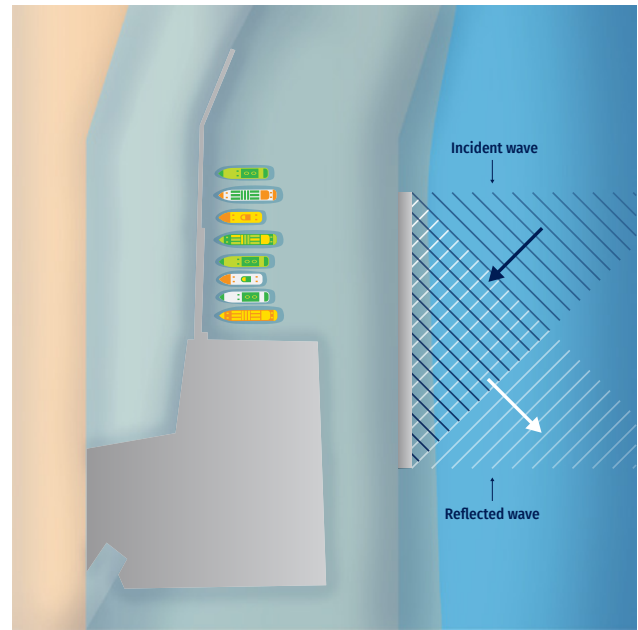
Figure 8.15. Ocean wave reflection.

to easily obtain them. Also, some advanced numerical models (based on Computational Fluid Dynamics) are available to obtain, with a very good approximation, overtopping values and discharge volumes (Losada et al., 2008).
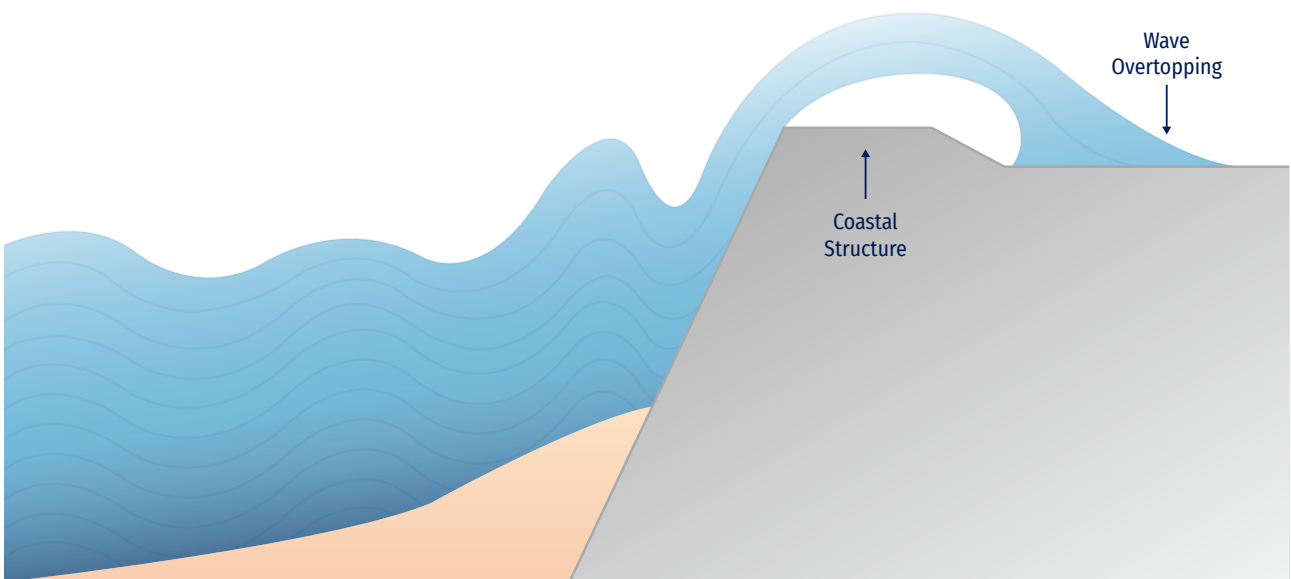
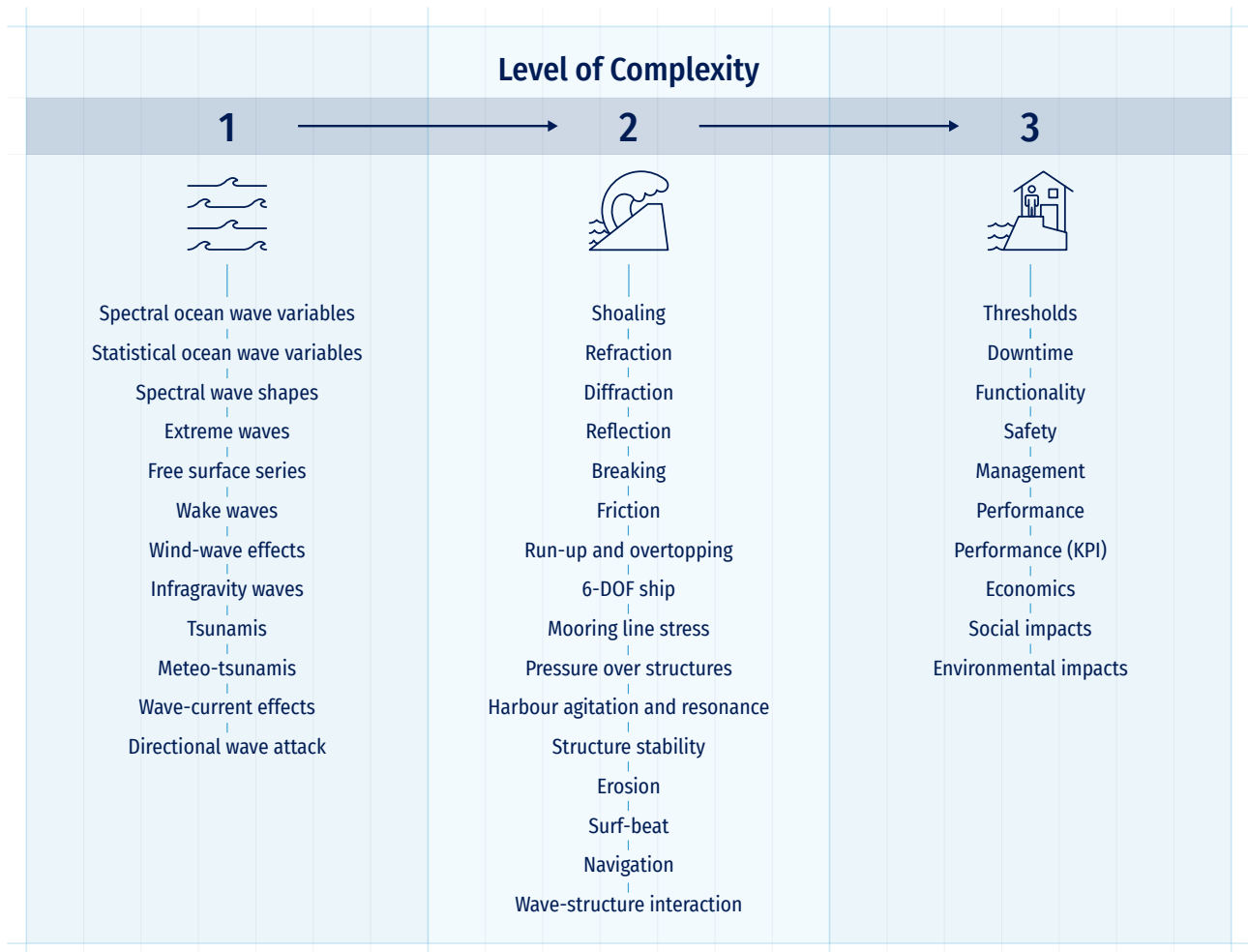**Figure 8.16.** Wave overtopping on a coastal perimeter example.

8.2.
Wave forecast and multi-year systems

Wave forecasting consists in describing the evolution of waves under the action of wind on the ocean surface and their propagation following interactions with currents, ice, and obstacles. Wave models numerically solve the variation of the wave spectrum from the energy balance equation taking into account the energy gain and loss terms. The evolution of wave models has followed improvements in the key processes of wind-wave growth, swell dissipation, and nonlinear wave interactions. Experimental works (Mitsuyasu, 1970; Hasselmann et al., 1973) have highlighted the importance of nonlinear wave interactions and wind-wave growth.

This has led to the improvement of wave models with, for example, a better simulation of the overshoot phenomenon which describes the transition of wave energy from high to low frequencies. Wave models must consider the computation time to ensure an operational forecast in near-real time conditions. So far, non-linear wave interactions have been simulated in the models in an approximate way, which sometimes generate errors.

Wave prediction is primarily a short-term process to ensure the safety of people, property, and maintenance of operation-

Level of Complexity

1	2	3
Spectral ocean wave variables	Shoaling	Thresholds
Statistical ocean wave variables	Refraction	Downtime
Spectral wave shapes	Diffraction	Functionality
Extreme waves	Reflection	Safety
Free surface series	Breaking	Management
Wake waves	Friction	Performance
Wind-wave effects	Run-up and overtopping	Performance (KPI)
Infragravity waves	6-DOF ship	Economics
Tsunamis	Mooring line stress	Social impacts
Meteo-tsunamis	Pressure over structures	Environmental impacts
Wave-current effects	Harbour agitation and resonance	
Directional wave attack	Structure stability	
	Erosion	
	Surf-beat	
	Navigation	
	Wave-structure interaction	

Figure 8.17.   Variables included in ocean wave OOFS grouped in levels from 1 to 3 depending on their complexity and codependency.

al activities that require an accurate description of the sea state. In addition, wave forecasting is necessary for long-term analysis of the wave climate, to learn lessons from extreme wave events, and to upgrade and improve operational wave forecasting systems. These last actions are part of wave reanalysis or so-called multi-year products, of which the most known by users are ERA5, WAVERYS - Global Ocean Waves Reanalysis - and CFSR.

8.2.1. Architecture singularities

8.2.1.1. Levels of complexity from deep to shallow water

Every OOFS, designed to provide ocean wave-related products for both historical (multi-year) and future predictions, would require a modular architecture and a common approach methodology (see Chapter 4).

The main components of a forecasting system and of its architecture (Figure 4.1) can be considered valid for almost any OOFS architecture as they are based on three general steps:

a. Forcing and observations for data assimilation;
b. Numerical model:
c. Post-processing tools and final product information (including validation, monitoring, and dissemination).

These steps should be followed when wave OOFS is used for deep water. However, when the main process to be assessed within the OOFS are ocean waves in the coastal zone, the second step could be a major problem if not well conceptualised. The reason is that the type of numerical models to be used would not be able to obtain the results efficiently or fast enough, especially for those forecast systems that need a robust and recurrent architecture for a 24/7 output. In addition, numerical wave propagation in the coastal zone could turn rapidly into a high-CPU requirement problem, especially when singular wave physics should be solved, such as wave reflection, wave current interaction, wave overtopping over structures, etc.

Usually, wave OOFS at deep water only provides simple prediction of basic variables (called here level 1). In coastal zones, downscaling approaches were not able to obtain more complex solutions involving derived variables (called level 2 and 3), because they could not be based on direct/trivial solutions but needed complex numerical calculations, and the use of advanced tools with high requirement of CPU time. A general list of the variables to be considered for each level (from 1 to 3) of sophistication and complexity within a wave OOFS, is shown in Figure 8.17.

The variables included will define the main architecture of the OOFS in which, through a method, effects, physical behaviour, and final prediction are linked, but allowing the pos-

sible future exchange/substitution of variables and methods in a simple and direct way.

The general architecture of modern ocean wave OOFS needs to meet certain characteristics of quality, interoperability, operation, and reliability. These characteristics should prevent anomalies that can lead to serious operational drawback such as:

- Unrealistic results without any protocol of quality control, with solutions only found with a dynamic approach (real-time sea-state by sea-state numerical runs, as explained by Rusu et al., 2008);
- Limited tools due to daily availability of CPU time;
- No learning/(feedback);
- Limited in space, geometrically inert (non-evolutionary);
- Unknown uncertainties (no error control/ measure);
- No communication between modules, only based on a deterministic nature.

To overcome these possible shortcomings, it is then necessary to identify some architectural specificities, which are described below.

a. Efficiency and speed of predictions. The need of creating a sufficiently agile and efficient system that can provide results within the time window pre-established by the future use. Generally, this window is reduced to the very competitive time of around 1 hour, necessary to trigger all processes, obtain results, and publish them. Therefore, the general assembly method, based on a hybrid architecture combining clustering methods, should be invoked, especially for the high-CPU modelling for shallow waters.

b. Robustness (24/7). The workflow must be light and computationally ordered, to guarantee an adequate triggering of the processes and obtaining of results.

c. Modular design. This refers to the ability of the system to interchange methods and tools directly, without major modifications to the backbone architecture of the system (plug & play). This way of working requires an adequate standardisation of the intercommunication formats between modules (input and output, I/O), so that the connection of each part is compatible with the coding of the general system.

d. Reliable and realistic results. This is one of the most important characteristics for a wave OOFS as it refers to the reliability of the tool, the credibility of the general method adopted, and the satisfaction of the end user. For this purpose, there should be proposed methods for validating the tool and its results with information measured in-situ. A common practice in the development

of this method is to prepare a document with instructions on how to carry out field campaigns, indicating locations, variables to be measured and type of equipment to be used, recommended schedules, suggested post-processing algorithms, and final validation products. It is important to note that the measurements will reflect the logical evolution/growth of the study area in the operational system (modification of bathymetries, evolutionary shelter elements, etc.).

e. Ad-hoc mathematical and numerical tools. This is closely related to the idea of a modular system mentioned above, and it is based on the precise integration of those tools aiming at the solution of physical processes of special interest. It is achieved through the appropriate use and adaptation of wave propagation tools (e.g. CFD models, Non-Linear Shallow Water Equations, Boussinesq-type equations, Mild Slope equations, third-generation wave generation and propagation models, etc.).

f. Self-diagnosis of results. This feature is based on the use of statistical methods that allow a detailed diag-

nosis of the results provided by the system on a daily basis, to identify and quantify the errors and uncertainties that are triggered throughout the execution of the system. This concept, closely linked to the "cascade of uncertainty" theory (Wilby and Dessai, 2010), makes it possible to optimise each method and reduce errors and uncertainties.

g. Nowcast integration. This refers to the capacity of the wave OOFS to take advantage of in-situ measurements provided continuously and in parallel with the use of the system during its operational phase. Algorithms should be developed for accessing, reading, post-processing, and assimilating the information measured to compare it with the predictions provided by the system, with the final capacity to generate readjustments of certain control parameters and, thus, of the predictions. This self-learning capacity of the system guarantees that, in a few months, the system will reach a mature operational level.

h. Tailor-made results. This is the OOFS's capacity to correctly prepare the formats in which the results are pre-
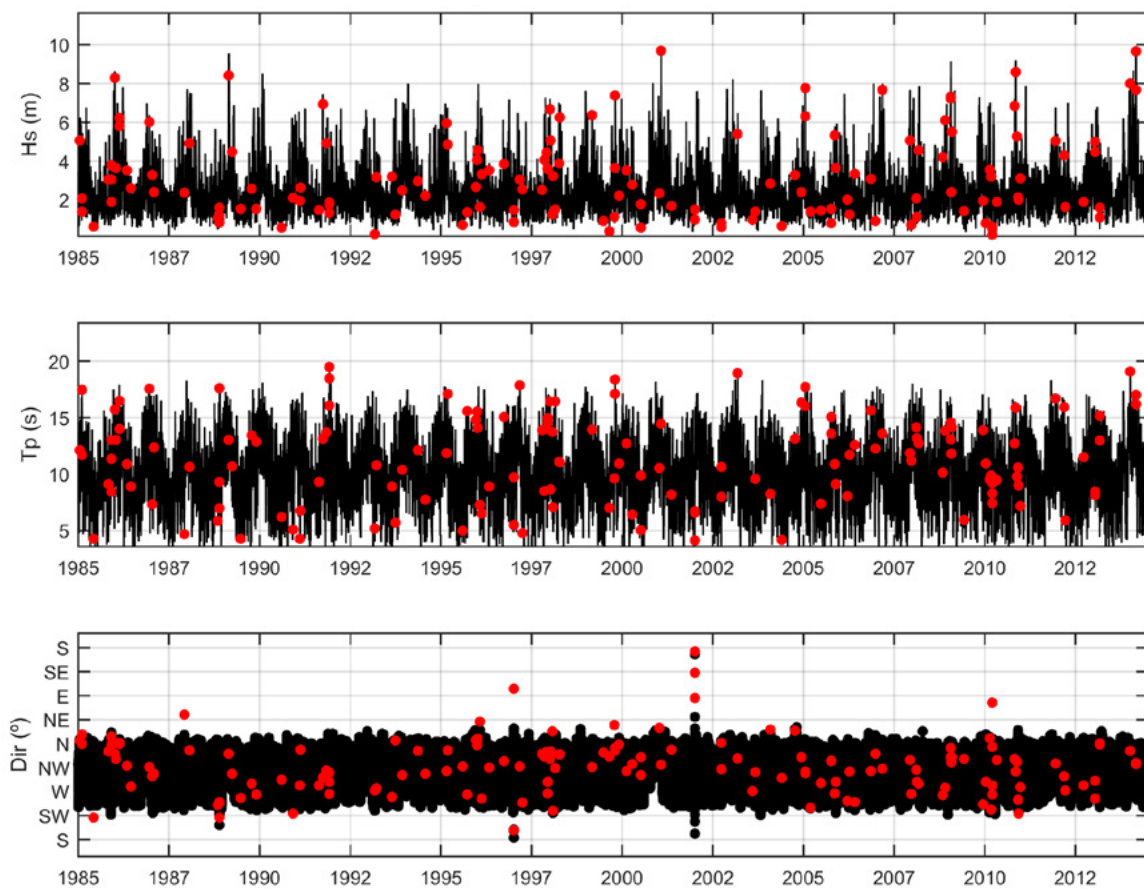
Figure 8.18.   Wave climate clustering using Max-Diss algorithm (source: University of Cantabria).

sented (summary tables, email bulletins, and web pages) for the appropriate decision-making process, adapting the formats to the user needs and showing the general uncertainties in the predictions.

The architecture specificities proposed here are able to provide: i) a multi-year wave (hindcast) and b) an operational/predictive product.

8.2.1.2. Hybrid and clustering technique

A hybrid approach has been recommended (Groeneweg et al., 2006, Stansby et al., 2006) when the complexity of the physics involved in the wave propagation assessment arises conditioning: i) the numerical model (CPU time) to be used; ii) the spatial resolution of the domains to be taken into account; and iii) the temporal relevance of new variables (such as variables above level 1) to be included in the final system/solution.

This approach allows a fast assessment of variables from level 2 to 3, regardless of the sophistication of the tool that performs it. This happens thanks to the concept of "pre-executed catalogue of cases" or clustering technique (also known as pre-cooked catalogue), which is responsible for assimilating the statistics of all the casuistry of processes involved, from the forcing involved to the final response.

The hybrid method, as described in various articles (Gaslikova and Weisse, 2006; Breivik et al., 2009, Herman et al. 2009), always follows the same steps:

- Access to the original forcing database (generally at deep water, sea-states, wind, and sea level series);

- Apply a self-selection algorithm of N pre-selected families of cases to be run, which will cover all the physics of the climate at the outer point (Figure 8.18);

- Transform level 1 variables to levels 2 and 3 through the execution of the N cases with the use of mainly mathematical/numerical tools;

- Statistically reconstruct the original database (Kalra et al., 2005; Browne et al., 2007) at the transfer point after having gone through the transformation processes, e.g. from the outer harbour zone to the quay area, making use of an algorithm that statistically interrelates the pre-run catalogue of N cases with the complete statistics of the forcing in the outer zone;

- Diagnose the data for historical diagnostic use.

8.3.
Input data, available sources, data handling, and model pre-processing

8.3.1. Bathymetry and geometry

Any global ocean wave OOFS needs accurate bathymetry data (see Section 4.2.4 for information about sources of bathymetric data). For systems downscaled towards the coastal/harbour zone, it is recommended a detailed bathymetry with resolution grid between 5 and 20 m.

Some solutions and models developed along the ocean wave OOFS strategy also need a topography (DEM). Main beach topographies, artificial structure sections, and elevations are recommended, with resolution grid below 5 m. In addition, vertical datumreference should be known and used to integrate all the different bathymetric, sections, topography references, along with sea level time series.

8.3.2. Forcing fields

Deep-water wave OOFS commonly need the following forcing met-ocean variables:

- Wind maps;
- Pressure maps;
- Ice coverage maps.

Shallow water / coastal / downscaled wave OOFS commonly need the following forcing met-ocean variables (generally obtained from the previous deep-water module or other hindcast/forecast global providers):

- Wave spectra in the form of:

    - Integrated variables (Hm0, Tp, Dir);
    - N-modal integrated variables (i.e. 2 SWELL and 1 SEA);
    - Wave spectral real forms if available;

- Sea level time series (both meteorological and astronomical tides);
- Mid to high-resolution wind maps;
- Free-surface elevation time series.

8.3.3. Observations

Observations are used as the main source for validation and calibration. The following observations are required.

For deep-water approach:

- Satellite observations of Hm0, Tp and Dir;
- Directional wave spectra definition (buoy).

For shallow-water approach:

- Directional wave spectra definition (buoy);
- Pressure gauge time series (burst with more than 20 minute length);
- Non-directional wave buoy;
- Wave overtopping measurements if available (non-intrusive camera deployment).

8.3.4. Pre-processing and definition of the numerical problem

Modern ocean wave OOFS uses a numerical model strategy to simulate the generation and propagation of the main phenomena in ocean (deep water) and coastal regions (shallow water). These numerical codes commonly contain three main elements: i) pre-process; ii) mathematical solver; and iii) post-process.

The first step takes place before the model execution and it is included in the pre-processing stage. Within this stage, the following sub-parts should be accomplished:

- Definition of the computational domain geometry where the equations will be applied and solved. This area is commonly discretized as cells, control volumes, or elements (depending on the solver-type), and all of them conform to a grid domain.

- Integration and adaptation of bathymetry data with the generated mesh (this is relevant for an adequate physical representation of the variables and for the stability of the model).

In general, accuracy increases with a greater number of cells but a longer computational time will be required. The choice will depend on the computer power available, on the type of architectural scope, and on the method to be used (for example, a hybrid approach could help to minimise the CPU time required). In general, the balance CPU-cost / physical definition can be tackled with the use of non-uniform meshes that have their nodes in the regions of special interest or where high variations of the physics properties take place.

Recently developed numerical wave models have incorporated self-adaptive meshes. That means that the mesh automatically adjusts its resolution (according to some tolerance criteria / physical mesh design defined by the user).

8.3.5. Boundary and initial conditions

Boundary conditions are the forcing values on the perimeters of the computational domain needed by any wave numerical model. In some cases, in the vicinity of any other body or another model incorporated in the domain.

Initial conditions are commonly the values of water waves that define a sea-state simulation (commonly with 1-hour frequency rate data for regional OOFS).

The following recommendations should be considered:

- Select an input forcing of the model (boundary conditions), adapt the formats, and assimilate the input data to a form that can be used later by the solver equations (data normalisation stage). Note to establish correct sea levels and DATUM elevations.

- Define any symmetry and cyclic boundary conditions at the perimeter boundaries.

- Define any open boundary conditions that are used to freely radiate water waves through infinite.

- For wave reflection models, define each individual reflection coefficient to be taken into account.

8.4.

Modelling component: general wave generation and propagation models

8.4.1. Types of models

Ocean wave modelling efforts and applications can be broadly classified into two large groups: i) phase resolving (or direct) models; and ii) phase average (usually spectral) models. Direct models can explicitly simulate basic equations of fluid mechanics for the water, air, or even two-phase media, and therefore extend the analytical research beyond its traditional range of approximate and asymptotic solutions of such equations. At oceanic scales, however, such models are not practical and not feasible, and therefore spectral models are employed for wind-wave forecasts.

In the next subsections, for both deep and shallow water analysis is given a general description, mathematical model, limitations, and main applications for each type of model.

8.4.1.1. Deep water

Spectral models

Evolution of wind-generated waves in water of finite depth d can be described by the wave action $N{=}F/\omega$ balance equation:

$$\frac{\partial N}{\partial t} + \cdot[(\mathbf{c}_g + \mathbf{U})N] + \nabla_{\mathbf{k}} \cdot [\mathbf{c_k}N] = \frac{I + L + D + B}{\omega} \quad (8.11)$$

where $F(\omega,\mathbf{k})$ is the wave energy density spectrum, ω is intrinsic (from the frame of reference relative to any local current) radian frequency, $\mathbf{k}$ is wavenumber (bold symbols signify vector properties). In the linear case, temporal and spatial scales of the waves are linked through the dispersion relationship (see Eq. 8.2).

The left-hand side of Eq. 8.11 represents time/space evolution of the wave action density because of the energy source terms on the right. On the left, $\mathbf{c}_g$ is group velocity, $\mathbf{c}_k$ means the spectral advection velocity, $\mathbf{U}$ is the current speed, and we note that $c{=}\omega/_k$ is phase speed of the waves. ∇ here is the horizontal divergence operator, and ∇_k is such an operator in spectral space.

On the right, source terms are physically represented by wind energy input from the wind, I; nonlinear interactions of various orders within the wave spectrum, L, whose role is to redistribute the energy within the spectrum; dissipation energy sinks, D; wave-bottom interaction processes, B; and more sources are possible in specific circumstances. Note that all the source terms, as well as the group and advection velocities, and the advection current are spectra themselves. Please refer to Cavaleri et al. (2007) for further details.

Among the source functions, L is a conservative term, i.e. its integral is zero, but the other integrals define energy fluxes in and out the wave system:

$$E_I = \int I(\omega, \mathbf{k})d\omega d\mathbf{k} \quad (8.12)$$

is the total flux of energy from the wind to the waves. Note that, depending on the relative speed of wind $\mathbf{U}_{10}$ and wave speeds $\mathbf{c}(\omega,\mathbf{k}){=}\omega/\mathbf{k}$, contributions to the total flux can be both positive (from the wind to the waves if $U_{10}{>}c$) and negative (from the waves to the wind if $U_{10}{<}c$). In the tropics, for example, where the wave climate is dominated by swells produced at high latitudes, the local winds are typically light and therefore the wind climate can be actually dominated by wave-induced winds (Hanley et al., 2010).

It should be noted that the energy input to the waves is generally accepted as a purely atmospheric exchange. In principle, however, energy input from the ocean side to the surface waves of scales accommodated in Eq. 8.11 is perceivable. For example, upper-ocean currents, tides, or internal waves can provide such dynamics. Given the amount of energy stored in the ocean movements, this could have large impacts on surface wave fields, even if localised, but it is fair to say that it has not been considered by the wave-ocean modelling community in practical terms.

Integrating the momentum-input spectrum gives the total momentum flux:

$$\tau_w = \int \frac{I(\omega, \mathbf{k})}{c(\omega, \mathbf{k})}d\omega d\mathbf{k} = \int I(\omega, \mathbf{k})\frac{\mathbf{k}}{\omega}d\omega d\mathbf{k} \quad (8.13)$$

which is an important measure of wind-wave interactions (Tsagareli et al., 2010). Together with the tangential viscous stress τ_v it forms the total wind stress at the ocean surface

$$\tau = \tau_w + \tau_v \quad (8.14)$$

and this stress is known independently (usually through empirical parameterisations of the so-called drag coefficient) and thus can be used as a constraint or for validation of the wind input term I. On the other hand, the total stress is often the main, if not the only property which expresses dynamic exchanges in large-scale air-sea models. Apart from situations of light winds, the wave-induced form drag (Eq. 8.12) provides a dominant contribution to this total stress (Kudryavtsev et al., 2001) and thus, if the wave-model physics is well defined and validated, such models can provide explicit rather than empirical estimates of fluxes for general circulation models if those are appropriately coupled with wave models.

The dissipation function D has a similar meaning in the context of wave-ocean dynamic exchanges, but with some essential distinctions. First, the integral

$$E_D = \int D(\omega, \mathbf{k}) d\omega d\mathbf{k} \qquad (8.15)$$

is the total flux of energy out of the wave field. The energy passed to the ocean is largely spent on generating turbulence near the surface and on work against buoyancy forces acting on bubbles injected during the wave breaking.

Unlike the input, however, which only occurs on the air side of the interface, the loss (8.15) can go both to the ocean below and to the atmosphere above the ocean surface. Numerical simulations of Iafrati et al. (2013) showed that up to 80% of wave energy due to breaking can be actually dissipated through the atmospheric turbulence.

The momentum-loss integral of dissipation function gives the so-called radiation stress:

$$\tau_r = \int D(\omega, \mathbf{k}) \frac{\mathbf{k}}{\omega} d\omega d\mathbf{k} \qquad (8.16)$$

which is presumed to be going to the currents (although some of it may in fact be going back to the wind, or to the bottom in shallow areas). In the present wave models, radiation stress is parameterized in terms of wave-height difference along the propagation direction. Obviously, such parameterization does describe the energy dissipation, and can then be used to estimate the momentum loss, but only in the areas where dissipation (Eq. 8.14) is much larger than the energy input (Eq. 8.14), i.e. usually in shallow waters. In deep water, the mean wave height is not a proxy for the energy loss. In fact, it may grow under wind action or not change if this action is balanced by the whitecapping dissipation, but the integral (Eq. 8.16) and hence the radiation stress is not zero.

Wave-ocean-bottom interactions in infinite depths, depicted by term B in Eq. 8.11, are very rich. Finite depths are characterised by the condition of $\mathbf{k}d\sim1$ (wavelength is comparable with the water depth d), and shallow non-dispersive environments by $\mathbf{k}d<<1$. Dispersive-wave nonlinear dynamics slowdown in finite and shallow depths, weaken or cease, but other nonlinear behaviours come into existence.

Wave exchanges with the bottom include bottom friction, formation of ripples, sediment suspension and transport if the sea bed is sandy, generation of bottom waves if the bottom is muddy, and percolation. Long-shore, cross-shore, and rip currents result from radiation stresses (Eq. 8.15), infragravity waves are produced by combined action of wave breaking and nonlinear wave groups, which can be subsequently reflected back to the deep ocean or trapped by coastal bays.

An example of this deep-water approach is the WAM (Hasselmann et al., 1988), perhaps the first one proposed as third-generation model, able to explicitly represent all the physics relevant for the development of the sea state in two dimensions, such as wind generation, whitecapping, quadruplet wave-wave interactions, and bottom dissipation. This modes is mainly forced by a two-dimensional ocean wave spectrum that develops freely with no constraints on the spectral shape, so that: a) a transfer source function of the same degree of freedom as the spectrum itself need to be developed; and b) the energy balance had to be closed by defining the dissipation source function. Hasselmann et al., (1985) and Komen et al., (1984) were employed to deal with these aspects, respectively. The dissipation was selected in order to replicate the observed fetch-limited wave growth and the fully developed Pierson-Moskowitz spectrum (WAMDI group, 1988).

Constant improvements and updates have led to a third-generation WAM model. A third-generation wave model explicitly represents all the physics relevant to the development of the sea state in two dimensions. Numerical solutions of the momentum balance of air flow over growing surface gravity waves have been presented in a series of studies by Janssen et al. (1989), and Janssen (1991). The main conclusion was that the growth rate of the waves generated by wind depends on the ratio of friction velocity and phase speed and on several additional factors, such as the atmospheric density stratification, wind gustiness, and wave age. This work has also introduced the surface stress dependency with the sea state, and the feedback of wave-induced stress on the wind profile in the atmospheric boundary layer.

WAM is an Eulerian phase-averaged model. Designed as a deep-water model, it can be used to predict directional spectra and wave properties (significant wave height, mean wave direction and frequency, swell wave height). The model can be used in finite depth as well by introducing bottom dissipation source function and refraction. The model runs on a spherical latitude-longitude grid.

The first WAVEWATCH model was developed at TU Delft (Tolman, 1989; Tolman 2014), followed by the NASA Goddard

Space Flight Centre in 1992. Recently, WAVEWATCH III was presented as a worldwide used and full-spectral third-generation wind-wave model. It was developed at NOAA/NCEP and it is based on the first WAM model's principles. This latest version includes many improvements in the governing equations, model structure, numerical schemes, and physical parameterizations. The model solves the random phase spectral action density balance equation for wavenumber-direction spectra. The medium properties, namely the water depth and current properties, as well as the wave field, vary in time and space in scales much larger than a single wave. WAVEWATCH is an open-source model that is freely available[3], including the whole source code and all documentation.

The discretization of the wave energy spectra in all directions is achieved by using a constant directional increment and a spatially varying wavenumber grid, which corresponds to an invariant logarithmic intrinsic frequency. In order to achieve high accuracy, both first order and third order schemes are available for wave propagation. For the integration of source terms in time, a semi-implicit scheme is used similar to that used in WAM, which includes a dynamically adjusted time stepping algorithm.

Following the work of Battjes and Janssen (1978), WAM and WAVEWATCH III models have been upgraded to account for the dissipation by wave breaking induced by depth in the surf zone. However, wave models still have difficulties with strong three-wave interactions that occur in finite-depth and shallow waters. That has led to simplified empirical calculations with large errors, especially for complex wave trains with multi-model spectra. In addition, both models lack of diffraction processes, which implies that only open coastal zones could be solved accurately, plus only linear behaviour of wave propagation could be assessed and non-linear corrections to linear wave should be imposed, by triad and quadruplet wave-wave interactions in shallow waters, where the waves break (Booij et al., 1999).

8.4.1.2. Shallow water

Spectral models

For shallow water domains and wave propagation (Eckart, 1952), the SWAN model could be a good choice. This also is a third-generation wave model developed at the Delft University of Technology, with the purpose of obtaining realistic estimates of wave parameters in coastal areas, lakes, and estuaries from given wind, bottom, and current conditions. The SWAN model can be also used on any scale relevant for wind-generated surface gravity waves. The model equations are based on the wave action balance equation with sources and sinks.

3. https://polar.ncep.noaa.gov/waves/wavewatch/wave-watch.shtml

SWAN has been developed to simulate coastal wave conditions (with friction, breaking, whitecapping, triad, and quadruplet wave-wave interaction). SWAN can be also coupled with previous models such as WAM or WAVEWATCH III, and inherit the boundary conditions. SWAN can provide a computational representation of directional and no directional spectrum at one point, and several spectral and time-dependent parameters of waves, such as significant wave height, peak or mean period, direction, and direction of energy transport. SWAN is a freely available[4] open-source software.

SWAN model is based on the spectral action balance equation, which describes the evolution of the wave spectrum (Booij et al., 1999).

In Cartesian coordinates the evolution of the action density is governed by the following balance equation:

$$
\frac{\partial N}{\partial t} + \frac{\partial (C_x N)}{\partial x} + \frac{\partial (C_y N)}{\partial y}
$$
$$
+ \frac{\partial (C_\theta N)}{\partial \theta} + \frac{\partial (C_\sigma N)}{\partial \sigma} = \frac{S_{total}(x, y, t, \theta, \sigma)}{\sigma} \tag{8.17}
$$

where σ is the wave frequency, θ is the wave direction component, t is the time, x and y the 2D coordinates in space, N the wave action density spectrum defined as:

$$
N(x, y, t, \theta, \sigma) = \frac{E(x, y, t, \theta, \sigma)}{\sigma} \tag{8.18}
$$

where E is the wave energy density spectrum; S_{total} is the source term and C,S are the wave propagation velocities in space and wavenumber, given by:

$$
C_x = C_g \cos \theta + U_x \tag{8.19}
$$

$$
C_y = C_g \sin \theta + U_y \tag{8.20}
$$

$$
C_\sigma = -\frac{\partial \sigma}{\partial h} \frac{\partial h}{\partial s} - K \frac{\partial U}{\partial s} \tag{8.21}
$$

$$
C_\theta = -\frac{\partial \sigma}{\partial h} \frac{\partial h}{\partial m} - K \frac{\partial U}{\partial m} \tag{8.22}
$$

where k is the wavenumber, C_g is the group velocity; s is a coordinate in θ direction and m is a coordinate perpendicular to s; h is the mean water depth and K the wavenumber vector.

The left hand side of Eq. 8.16 corresponds to the kinematic terms, as derivatives for the propagation in space; and are the propagation velocities. The term with the derivative with respect to θ is the refraction term. The term with respect to σ causes a change of frequency. The right hand side is the

4. https://swanmodel.sourceforge.io/
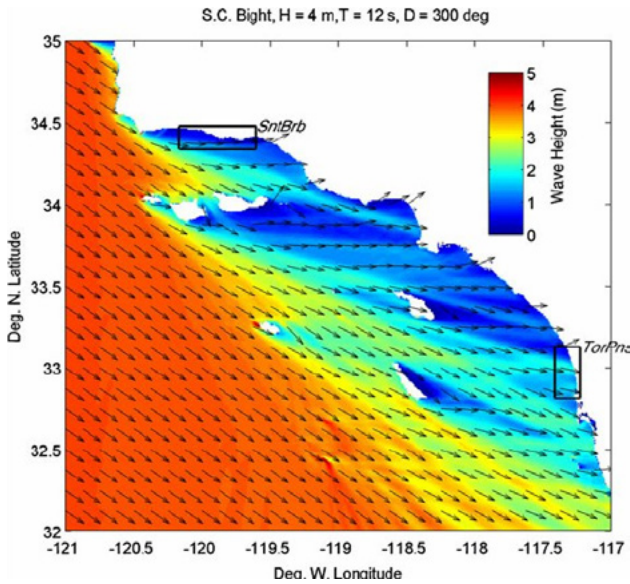
Figure 8.19. Example wave height and direction output from SWAN wave transformation model over the Southern California Bight (source: University of Florida).

source term and contains the effects of wind generation, whitecapping, dissipation, bottom friction, surf breaking, and nonlinear wave-wave interaction. This equation is implemented with finite difference schemes in all directions: time, geographic space, and spectral space.

The essential input data to run the model is the bathymetry for a sufficiently large area, the incident wave field, and the wind field. Various general and nested grids can be selected, depending on the availability of high-resolution data and the computational efficiency. Nesting is a very important implementation that can save computational time and increase accuracy. The model is validated with analytical solutions, field observations and experimental measurements, and has shown good agreement (Booij et al., 1999). Moreover, SWAN can operate with unstructured grids as well. Zijlema (2009) presented a method of vertex-based, fully implicit, and finite differences that is designed for unstructured meshes with high variability in geographic resolution. It is useful for complex bottom topographies in shallow areas and irregular shorelines.

SWAN is basically designed for applications in open coastal scale, with no-diffraction effects. That means that the model should be used in areas where variations in wave height are large within a horizontal scale of a few wavelengths.

SWAN organises its output in tables, maps (Figures 8.19 and 8.20) and time series, as well as 1D and 2D spectra, significant wave height and periods, average wave direction and directional spreading, one- and two-dimensional spectral

source terms, root-mean-square of the orbital near-bottom motion, dissipation, wave induced force (based on the radiation-stress gradients), set-up, diffraction parameter, etc.

Mild slope equations models

MSE originally developed to describe the propagation of the waves over low gradient seabeds. MSE is commonly used in coastal engineering, since it can account well the effects of simultaneous diffraction and refraction of the waves due to coastlines or structures (Berkhoff, 1972). Mild-slope equations are a type of depth-averaged equation, within a x-y domain (2DH), applied in both deep and shallow waters for monochromatic waves (Lin, 2008).

The equations can be found in various forms, including the effects of wave breaking, nonlinearity of waves, wave-current interactions, and seabed friction. They calculate the wave amplitude or wave height but, if there is a constant water depth, the mild-slope equation reduces to the Helmholtz equation for wave diffraction. First introduced by Berkhoff (1972), the MSE assumed that the wave is linear and the slope is mild, obtaining the following main equation, improved by including the effects of friction dissipation and wave breaking:

$$\nabla(CC_g\nabla\widehat{\eta}) + \left(\frac{C_g}{C}\sigma^2 + i\sigma w + iC_g\sigma\gamma\right)\widehat{\eta} = 0 \qquad (8.23)$$

where C is the wave celerity and C_g the group velocity; $\hat{\eta}$ is the complex wave surface function; k is the wavenumber; σ is the wave frequency; w is a friction factor and γ is a wave breaking parameter. Friction is then obtained with:

$$w = \left(\frac{2n\sigma}{k}\right)\left[\frac{2f_r}{3\pi}\frac{ak^2}{2kh + \sinh(2kh)\sinh(kh)}\right] \qquad (8.24)$$

where a is the wave amplitude, and f_r is a Reynolds dependent friction coefficient related to the bottom roughness; n is the Manning dissipation coefficient.

For weave breaking parameter, the following formulation is commonly used:

$$\gamma = \frac{0.15}{h}\left(1 - \frac{0.4^2 h^2}{4\sigma^2}\right) \qquad (8.25)$$

The original MSE has limitations because it is only applicable to linear waves and on mild bottom geometry. In addition, the equation does not contain energy dissipation, but in recent years there have been numerical advances to include energy dissipation and weakly non-linear waves with steeper bottom slopes. Mild-slope equation has been developed with different formulations that can be described by hyperbolic (Dingemans, 1997), elliptic (Berkhoff, 1972), and parabolic (Lin, 2008) formulation of the mild-slope equation respectively.

The practical application of wave transformation usually requires the simulation of directional random waves; thus, the

principle of superposition of different wave frequency components can be applied. In general, MSE models for spectral wave conditions require inputs of the incoming directional random sea at the offshore boundary. The two-dimensional input spectra are discretized into a finite number of frequency and direction wave components.

For the parabolic approach, the evolution of the amplitudes of all the wave components is computed simultaneously. Based on the calculations for all components and assuming a Rayleigh distribution, statistical quantities such as the significant wave height Hs can be calculated at every grid point. Figure 8.20 shows an example for a near-coast wave propagation obtained with a parabolic approximation of the mild slope equation for spectral wave conditions.
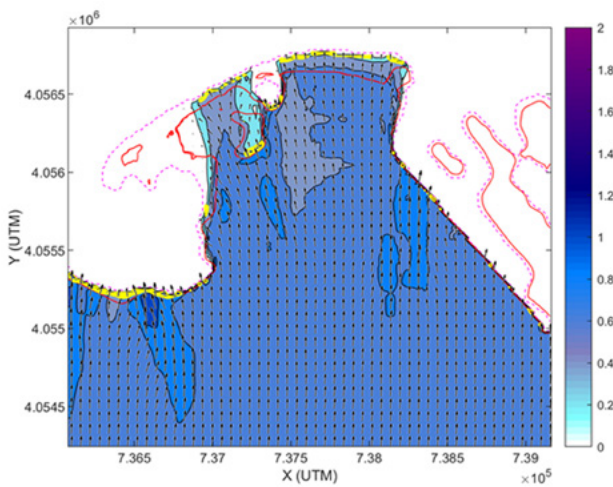
Figure 8.20. Significant wave height propagation map for Los Galeones Beach (Cadiz, Spain) computed with a parabolic Mild-Slope based model (REF-DIFF, OLUCA model) (source: University of Cantabria).

When wave reflection becomes relevant for wave propagation and transformation (i.e. within bays, harbours, sheltered areas, etc.), models should be based on the elliptical approximation of the mild-slope equation (Berkhoff, 1972; Madsen and Larsen, 1987; Tsay et al., 1989). This approach allows engineers to obtain the energetic response of reflected (totally or partially) waves, under the penetrating wave action.

Elliptic mild slope models solve the extended mild-slope equation to reproduce the main processes that control dynamics of waves when approaching coastal areas and entering into harbours (Figure 8.21): geometric refraction, shoaling, diffraction by obstacles, and full or partial reflection. Radiation conditions and free infinite outflow conditions are also available in the model. It also considers the complete

spectral frequency distribution and the directional spreading of the wave energy spectrum.

In addition to the above mechanisms, nonlinear waves may be simulated by incorporating amplitude-dependent wave dispersion, which has been demonstrated to be important in certain situations (Kirby and Dalrymple, 1983).

This practical approach for harbour agitation and wave propagation can be assessed with the following, among others, commercial and non-commercial models: CGWAVE; ARTEMIS MIKE21; PHAROS, and MSP.
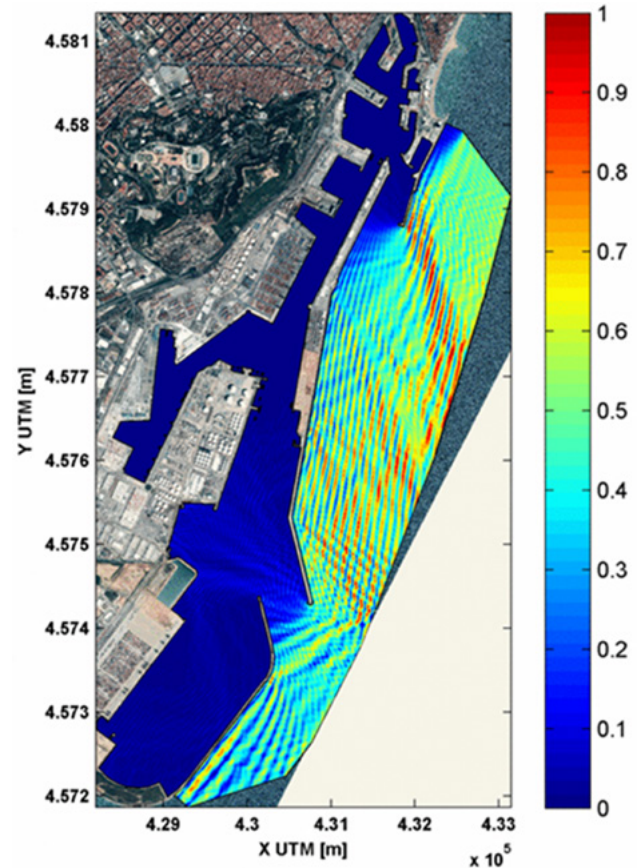
Figure 8.21. Significant wave height map within Barcelona Port computed with an elliptic Mild-Slope based model (MSP model) (source: University of Cantabria and Puertos del Estado).

Phase resolving models (SWE, NSWE, and Boussinesq)

The Shallow Water Equations (SWE) are applied when water waves enter very shallow domains. Particles move basically horizontally and the vertical accelerations are negligible.

In this case, the propagation of the wave can be described by the SWE (Holthuijsen, 2007). These equations are derived from averaging the depth of the Navier-Stokes equations (NSE) assuming that the horizontal length scale is much greater than the vertical. The profile is uniform in depth and the vertical components very small. Using the conservation of mass, it can be shown that the vertical velocity is small, while using the momentum equation the vertical pressure gradients are hydrostatic. Therefore, the velocity profile is uniform in depth and the vertical components very small, and this is the reason for which SWE are also known as "long-wave equations", given that they can be applied only to waves which are much larger to the bottom depth.

In the case of ignoring the Coriolis force, the frictional and viscous forces, the formulas of SWE are:

$$\frac{\partial \eta}{\partial t} + \frac{\partial(\eta u)}{\partial x} + \frac{\partial(\eta v)}{\partial y} = 0 \qquad (8.26)$$

$$\frac{\partial(\eta u)}{\partial t} + \frac{\partial}{\partial x}\left(\eta u^2 + \frac{1}{2}g\eta^2\right) + \frac{\partial(\eta uv)}{\partial y} = 0 \qquad (8.27)$$

$$\frac{\partial(\eta v)}{\partial t} + \frac{\partial}{\partial y}\left(\eta v^2 + \frac{1}{2}g\eta^2\right) + \frac{\partial(\eta uv)}{\partial x} = 0 \qquad (8.28)$$

Equation 8.26 is derived from mass conservation and Eqq. 8.27 and 8.28 from momentum conservation, where η is the total fluid column height, (u,v) - a 2D vector - is the fluid's horizontal velocity in the xy 2D domain.

To represent the ocean waves frequencies and physical behaviour, an improvement within the original SWE is needed, including the non-linearity terms and dispersive functions. The solution for this is the NSWE, as a non-hydrostatic wave-flow solution model. It can be used for predicting transformation of dispersive surface waves from offshore to the beach, solving the surf zone and swash zone dynamics, wave propagation and agitation in bays and harbours, and rapidly varied shallow water flows typically found in coastal flooding (e.g. dike breaks, tsunamis and flood waves, density driven flows in coastal waters), as well as large-scale ocean circulation, tides and storm surges (typically solved by the original SWE models).

Main governing equation considers a 2DH wave motion over a domain represented in a Cartesian coordinate system (x,y). The depth-averaged, non-hydrostatic, free-surface flow can be described by the NSWE and comprise the conservation of mass and momentum. These equations are given by:

$$\frac{\partial \zeta}{\partial t} + \frac{\partial(hu)}{\partial x} + \frac{\partial(hv)}{\partial y} = 0 \qquad (8.29)$$

$$\frac{\partial u}{\partial t} + u\frac{\partial u}{\partial x} + v\frac{\partial u}{\partial y} + g\frac{\partial \zeta}{\partial x}$$
$$+ \frac{1}{h}\int_{-d}^{\zeta}\frac{\partial q}{\partial x}dz + C_f\frac{u\sqrt{u^2+v^2}}{h} \qquad (8.30)$$
$$= \frac{1}{h}\left(\frac{\partial h\tau_{xx}}{\partial x} + \frac{\partial h\tau_{xy}}{\partial v}\right)$$

$$\frac{\partial v}{\partial t} + u\frac{\partial v}{\partial x} + v\frac{\partial v}{\partial y} + g\frac{\partial \zeta}{\partial y}$$
$$+ \frac{1}{h}\int_{-d}^{\zeta}\frac{\partial q}{\partial y}dz + C_f\frac{u\sqrt{u^2+v^2}}{h} \qquad (8.31)$$
$$= \frac{1}{h}\left(\frac{\partial h\tau_{yx}}{\partial x} + \frac{\partial h\tau_{yy}}{\partial v}\right)$$

where t is the time; ζ is the free surface elevation, d is the water depth and $h=d+\zeta$, u and v are depth-averaged flow velocities, q is the non-hydrostatic pressure, g the gravitational acceleration, C_f the bottom friction coefficient, and the group of τ are the horizontal turbulent stress terms.

The SWASH (Zijlema et al., 2011) is one of the latest worldwide available 🔗[5] NSWE models. It is a numerical tool for simulating unsteady, non-hydrostatic, free-surface, rotational flow, and transport phenomena in coastal waters as driven by waves, tides, buoyancy, and wind forces. It provides a general basis for describing wave transformations from deep water to the beach, port or harbour, as well as complex changes to
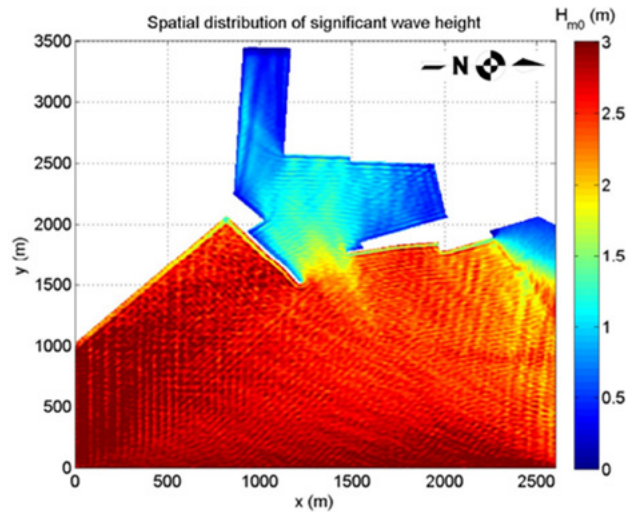
Figure 8.22. Results from the SWASH model for the wave condition at Limassol Port (Cyprus) (from Van der Ven et al., 2018).

rapidly varied flows, and density driven flows in coastal seas, estuaries, lakes, and rivers. SWASH is an efficient and robust model that allows the application of a wide range of time and space scales of surface waves and shallow water flows in complex environments (Figure 8.22). The model can be also

5. https://swash.sourceforge.io/

employed to resolve the dynamics of wave transformation, buoyancy flow, and turbulent exchange of momentum, salinity, heat, and suspended sediment in shallow seas, coastal waters, estuaries, reefs, rivers, and lakes.

SWASH may be run in depth-averaged mode or multi-layered mode in which the computational domain is divided into a fixed number of vertical terrain-following layers. SWASH improves its frequency dispersion by increasing the number of layers rather than increasing the order of derivatives of the dependent variables like Boussinesq-type wave models do.

BE can be applied as an alternative to NSWEs as the region between deep and shallow waters can be also well described by the Boussinesq model. In BE models, the horizontal component of the velocity is assumed to be constant in the water column and the vertical component of the velocity varies almost linearly over depth (2DH hypothesis). Essentially, these equations are the shallow-water equations with corrections for the vertical acceleration, and third order derivatives are the result of the Laplace equation forcing the vertical velocity of the velocity potential function to be expressed in terms of the horizontal velocity distribution. These equations can be readily expanded into two horizontal dimensions.

Researchers have introduced many different implementations of the Boussinesq equations, creating Boussinesq-type models to be applied for propagation in deep water and the process of wave-breaking (Brocchini, 2013). A vast majority of Boussinesq equations models (for fully non-linear approach) can be presented as follows:

$$\eta_t = -\nabla \cdot [(h + \epsilon\eta)(V + \mu^2 M] + O(\mu^4) \tag{8.32}$$

$$V_t + \frac{\epsilon}{2}\nabla(V^2) = -\nabla\eta - \mu^2 \left[\frac{1}{2}z_\alpha^2\nabla\nabla \cdot V_t + z_\alpha\nabla\nabla \cdot (hV_t)\right]$$
$$+ \epsilon\mu^2\nabla(D_1 + \epsilon D_2 + \epsilon^2 D_3) + O(\mu^4) + N + E \tag{8.33}$$

with

$$M = \left[\frac{1}{2}z_\alpha^2 - \frac{1}{6}(h^2 - \epsilon h\eta + \epsilon^2\eta^2)\right]\nabla\nabla \cdot V$$
$$+ \left[z_\alpha + \frac{1}{2}(h - \epsilon\eta)\right]\nabla\nabla \cdot (hV) \tag{8.34}$$

$$D_1 = \eta\nabla \cdot (hV_t) - \frac{1}{2}z_\alpha^2 V \cdot \nabla\nabla V$$
$$- z_\alpha V \cdot \nabla\nabla \cdot (hV) - \frac{1}{2}(\nabla \cdot (hV))^2 \tag{8.35}$$

$$D_2 = \frac{1}{2}\eta^2\nabla \cdot V_t + \eta V \cdot \nabla\nabla \cdot (hV)$$
$$- \eta\nabla \cdot (hV)\nabla \cdot V \tag{8.36}$$

$$D_3 = \frac{1}{2}\eta^2[V \cdot \nabla\nabla \cdot V - (\nabla \cdot V)^2] \tag{8.37}$$

where index of *t* denotes time; *h* is the equilibrium depth; η is the free-surface elevation, *V* is the horizontal velocity, and ∇ is the 2DH gradient operator. *N* and *E* respectively represent bottom drag and diffusion (artificial).

On the other hand, a similar family of equations exist and are applied in the region between deep and shallow waters; the Boussinesq equation-based model. For this approach, the main hypothesis is that the horizontal component of the velocity is assumed to be constant in the water column, and the vertical component of the velocity varies almost linearly over depth.

One of the most complete Boussinesq models, the fully nonlinear Boussinesq wave model (FUNWAVE) in its TVD version known as FUNWAVE-TVD model (Fengyan, et al., 2012), was developed at the Centre for Applied Coastal Research at the University of Delaware (USA). It includes several enhancements: i) a more complete set of fully nonlinear Boussinesq equations; ii) a MUSCLE-TVD finite volume scheme together with adaptive Runge Kutta time stepping; iii) shock-capturing wave breaking scheme, iv) wetting-drying moving boundary condition with HLL construction method for the scheme; and v) code parallelization using MPI method. The development

Figure 8.23. Free surface snapshot from the FUNWAVE-TVD applied in Sardinero Beach and Santander Bay (Spain) outer and inner zone (source: University of Cantabria).

of the FUNWAVE-TVD was prompted by the need to model tsunami waves in regional and coastal scale, coastal inundation, and wave propagation at basin scale (Figure 8.23). FUNWAVE is an open-source model available to the public 🔗 [6].

6. https://fengyanshi.github.io/build/html/index.html

Numerical solutions of Boussinesq equations can be significantly corrupted if truncation errors, arising from the differencing of the leading order wave equation terms, are allowed to grow in size and become comparable to the terms describing the weak dispersion effects. All errors involved in solving the underlying nonlinear SWE are reduced to 4th order in grid spacing and time step size. Due to non-linear interaction in the model, higher harmonic waves will be generated as the program runs. These super harmonic waves could have very short wavelengths and the classic Boussinesq model is not valid. For this reason, a numerical filter suggested by Shapiro (1970) can be used.

In summary, both Boussinesq and NSWEs modelling approaches are the preferred solutions in their respective physical regions: Boussinesq where nonlinearity and dispersion are both significant, typically prior to breaking; and NSWE where nonlinearity predominates, from the mid-surf to inner surf zone shoreward, although it should be noted that there can be a significant overlap of these regions. Therefore, the NSWE models, which work well from the surf zone shoreward and naturally model wave breaking and the moving shoreline, find their main weakness in the absence of frequency dispersion, so that in deeper water waves will propagate incorrectly at the shallow water wave speed and, sooner or later, break again, which is not usual and correct in this region.

Two- and three-dimensions wave structure interaction model

CFD utilises numerical approaches to examine fluid flows, heat transfer and chemical reactions. Therefore, within wave propagation and structure interaction problems, the CFD term mainly refers to computer codes that solve the fully nonlinear Navier-Stokes equations in all three dimensions (3D).

CFD is then a state-of-the-art techniques for industrial and research applications, although its often high computation cost demands the use of high-performance computers. Within the wave propagation and wave structure interaction field, two of the most used CFD programs are: IH2VOF (two-dimension approach, derived from COBRAS original model) and OpenFOAM (three-dimension approach); these two codes are also well validated for many marine and ocean engineering applications.

As a classic Eulerian approach, both models are based on the RANS equations. These equations represent the continuum properties of the flow. By averaging the Navier-Stokes equations, more recent VARANS equations are obtained. The VARANS equations can have different terms, depending on the assumptions applied; for example, they include a k-ω turbulence model closure within the porous media, which make them the most suitable formulation for coastal engineering as the advantages of VARANS equations are numerous. The solving process yields very detailed solutions, both in time and space. Pressure and velocity fields are obtained

cell-wise, even inside the porous zones, so that the whole three-dimensional flow structure is solved. Furthermore, non-linearity is inherent to the equations, and therefore all the complex interactions among the different processes are also taken into consideration. Finally, the effects of turbulence within the porous zones can be also easily incorporated with closure models.

IH2VOF model (Lara et al., 2006) solves 2D RANS equations for the oscillatory fluid and VARANS equations for the porous media. This 2D model can simulate the most relevant hydrodynamic near-field processes that take place in the interaction between waves and low-crested breakwaters. It considers wave reflection, transmission, overtopping, and breaking due to transient nonlinear waves, including turbulence in the fluid domain and in the permeable regions for any kind of geometry and number of layers. This model is highly validated, with different wave conditions and breakwater configurations, achieving a high degree of agreement with all the studied magnitudes, free surface displacement, pressure inside the porous structure, and velocity field.

IH2VOF is based on the decomposition of the instantaneous velocity and pressure fields into mean and turbulent components, the κ-ε equations for the turbulent kinetic energy κ, and its dissipation rate ε. This permits the simulation of any kind of coastal structure (e.g. rubble mound, vertical or mixed breakwaters). The free surface movement is tracked by the volume of fluid (VOF) method for one phase only, water and void. In order to replicate solid bodies immersed in the mesh instead of treating them as sawtooth shape, the model uses a cutting cell method. The main purpose of this technique is to use an orthogonal structured mesh in the simulations to save computational cost.

IH2VOF includes a complete set of wave generation boundary conditions, which cover most water depth ranges. These include a Dirichlet boundary condition and a moving boundary method, which are linked with an active wave absorption system to avoid an increase of the mean water level and the agitation. An internal source function can be also used to generate waves, but it has to be linked with a dissipation zone.
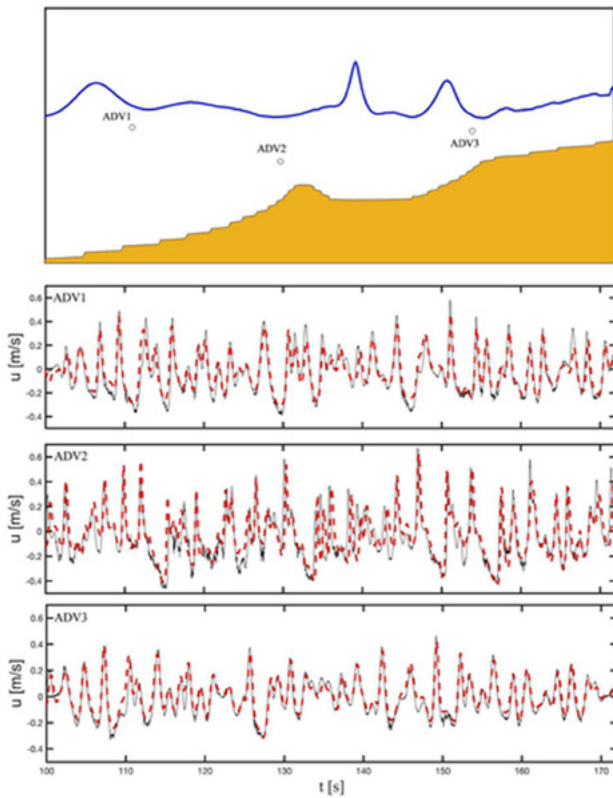
The RANS equations (clear fluid region) are redefined as follows:

$$\frac{\partial(\theta u_i)}{\partial x_i} = 0 \qquad (8.38)$$

$$\frac{\partial(\theta u_i)}{\partial t} + \theta u_j \frac{\partial(\theta u_i)}{\partial x_i} = -\frac{\theta}{\rho}\frac{\partial p}{\partial x_i} + \rho g_i + \frac{\theta}{\rho}\frac{\partial(\tau_{ij})}{\partial x_j} + f_b \quad (8.39)$$

Generally, IH2VOF application is within a detailed incident-wave and structure interaction (rubble-mound breakwaters, vertical structures and beaches), taking into account

Figure 8.24. Irregular wave propagation towards a real profile beach. Free surface snapshot and wave velocity validation against field measurements (source: National University of Mexico).

The OpenFOAM (Higuera et al., 2014a and 2014b) is an extensive software package that has been widely used in industrial and academic applications. It is freely distributed 🔗[7] as an open source CFD Toolbox, and it includes a broad range of features. IHFOAM 2.0 is an extension of the original software for coastal applications, newly developed with a three-dimensional numerical two-phase flow solver, specially designed to simulate coastal, offshore, and hydraulic engineering processes. It contains an advanced multiphysics model, widely used in the industry. A wide collection of boundary conditions, which handle wave generation and active absorption at the boundaries with a high practical application to coastal and harbour engineering (Figure 8.25), makes IHFOAM 2.0 different from the rest of solvers. Maza et
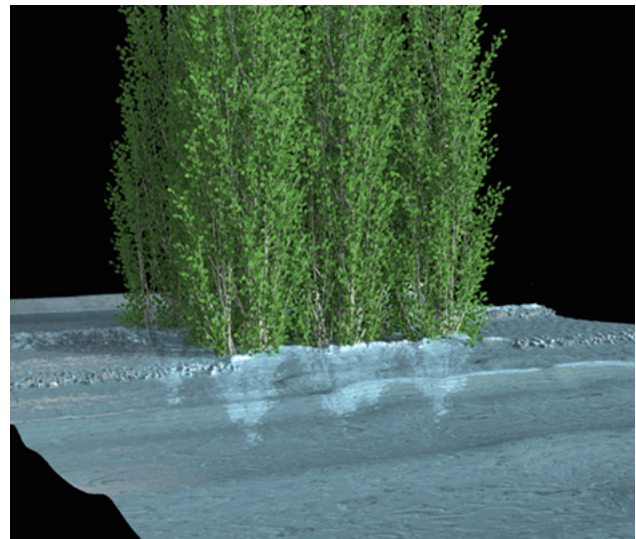
Figure 8.25. Free surface snapshot of irregular wave interacting with a natural-based protection (a tree patch) calculated with IHFOAM 2.0 (source: University of Cantabria).

a realistic wave breaking and porous media interaction (see Figure 8.24).

al. (2016) have studied and proposed natural-based solutions for coastal protections using IHFOAM.

The general VARANS equations include conservation of mass (8.39), conservation of momentum (8.40), and the VOF function advection equation (8.41) as follows:

8.4.2. Discretization methods

Various discretization methods are used in water wave solving problems, a brief description for each of them is presented below (for additional references see Sections 5.4.2.4 and 7.2.3.5):

$$\frac{\partial}{\partial x_i} \frac{u_i}{n} = 0 \tag{8.40}$$

$$\frac{\partial}{\partial t} u_i + u_j \frac{\partial}{\partial X_i} \frac{u_i}{n} = -\frac{n}{\rho} \frac{\partial}{\partial x_i} p$$
$$+ n g_i + n \frac{\partial}{\partial x_i} \left(\nu \frac{\partial}{\partial x_i} \frac{u_i}{n} \right) - a u_i - b u_i \mid u_i \mid -c \frac{\partial}{\partial t} u_i \tag{8.41}$$

$$\frac{\alpha_1}{\partial t} + \frac{\partial}{\partial x_i} \frac{u_i}{n} \alpha_1 = u_i \tag{8.42}$$

where u is the extended averaged Darcy velocity; n is the porosity (volume of voids over the total volume); ρ is the density; p is the pressure; g is the acceleration of gravity; ν is the kinematic viscosity, and α_1 is the VOF function indicator (quantity of water per unit of volume at each cell).

- • FDM. Maybe the most used and simplest ways to solve numerically partial differential equations (PDEs). The method establishes the value of the flow variable at a given point based on the number of neighbour

7. https://www.openfoam.com/

Figure 8.26.   Finite Element Metod (FEM) based on irregular sized triangles applied to Galicia (Spain) for SWAN model (source: University of Cantabria).

points. The numerical domain forms a grid. The governing equations of the fluid are considered in their differential form at each point in the domain, so that the solution is solved by replacing the partial derivatives with approximations by means of the nodal values of the functions. This method is recommended for structured grids and low-order equation schemes.

• FEM for the solution of PDEs employs variational methods to minimise the error of the approximated solution, similarly to the Galerkin method. FEM was used in structural mechanics but this technique developed for computational fluid dynamics applications being introduced to common wave propagation and agitations models. FEM technique, similarly to the FDM, is based on the concept of subdividing a continuum computational domain into elements, forming a grid of triangular or quadrilateral un-

structured elements or curved cells (Figure 8.26). Therefore, the method can handle problems with great geometric complexity, such as harbour perimeter definition, concentration of nodes at relevant parts of the domain, etc.

FEM used variational methods, which in practice means that the solution is assumed to have a prescribed form and to belong to a function space. The function space is built by varying functions, such as linear and quadratic. The varying functions connect the nodal points, which can be the vertices, mid-side points, mid-element points, etc., of the elements. As a result, the geometric representation of the domain plays a crucial role in the outcome of the numerical simulation. The original PDEs are not solved by the FEM. Instead, the solution is approximated locally by an integral form of the PDEs. The integral of the inner product of the residual and the weight functions are constructed. The integral is set to zero and trial functions are used to minimise the residual. The most general integral form is obtained from a weighted residual formulation. The process eliminates all the spatial derivatives from the PDEs and, therefore, differential type boundary conditions for transient problems and algebraic type boundary conditions for steady state problems can be considered, hence the differential equations become algebraic. Only one equation is solved per grid node, which has one variable as unknown. The same variable is also unknown at the neighbouring cells.

• FVM solves PDEs by transforming them to algebraic equations around a control volume (subdivisions of the computational domain). The variables are calculated at the centre of each control volume. General interpolation methods are used to derive the values of the variables at the surfaces of the control volume considering the neighbour control volumes as well. The FVM has two major advantages: i) it is able to accommodate any type of grid, making it applicable for domains of high complexity; and ii) it is conservative by definition, since the control volumes that share a boundary have the same surface integrals, describing the convective and diffusive fluxes. FVMs are very popular in the numerical wave propagation community, succeeding in free surface flow simulations, especially when highly nonlinear processes are involved, such as wave breaking.

8.5.
Data assimilation systems

In a wave forecasting system, data assimilation plays a key role in order to provide the best description of sea state, and also to correct uncertainties related to wind forcing from the atmospheric systems. Since the beginning of the 1990s, with the arrival of altimeter missions such the pioneer one Topex-Poseidon, the assimilation schemes have been implemented to use significant wave height in the WAM model (Janssen et al., 1989; Bauer et al., 1992; Lionello et al., 1992). Basically, the scheme uses an optimal interpolation through a weighted correction of the first SWH guess with that one from altimeters. The correlation model to spread the correction from altimeter SWH to other grid points is essentially a Gaussian function, depending on the distance between the observation and model locations, and a correlation length, which can vary with the wave regime (Greenslade and Young, 2004). The assimilation of SWH corrects the two-dimensional spectrum by introducing appropriate rescaling factors to the energy and frequen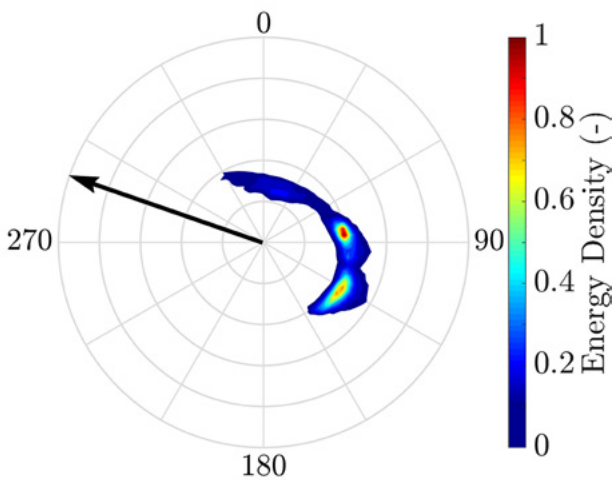cy scales of the wind sea and swell components of the spectrum, and also updates the local forcing wind speed. The rescaling factors are computed for two classes of spectra: i) wind sea spectra, for which the rescaling factors are derived from fetch and duration growth relations; and ii) swell spectra, for which it is assumed that the wave steepness is conserved. Currently, there is abundant information on SWH (see Figure 8.27), as it is provided by eight satellite missions (Jason-3, Saral/Altika, Cryosat-2, Sentinel-3A and 3B, CFOSAT, HY2B, Sentinel-6MF). This ensures an excellent coverage for open ocean and it is evolving to a good coverage for coastal areas.

A variational technique has been also used in regional wave forecasting (Saulter et al., 2020) to assimilate SWH from altimeters. This scheme is an adaptation of the assimilation code NEMOVAR to wave assimilation.
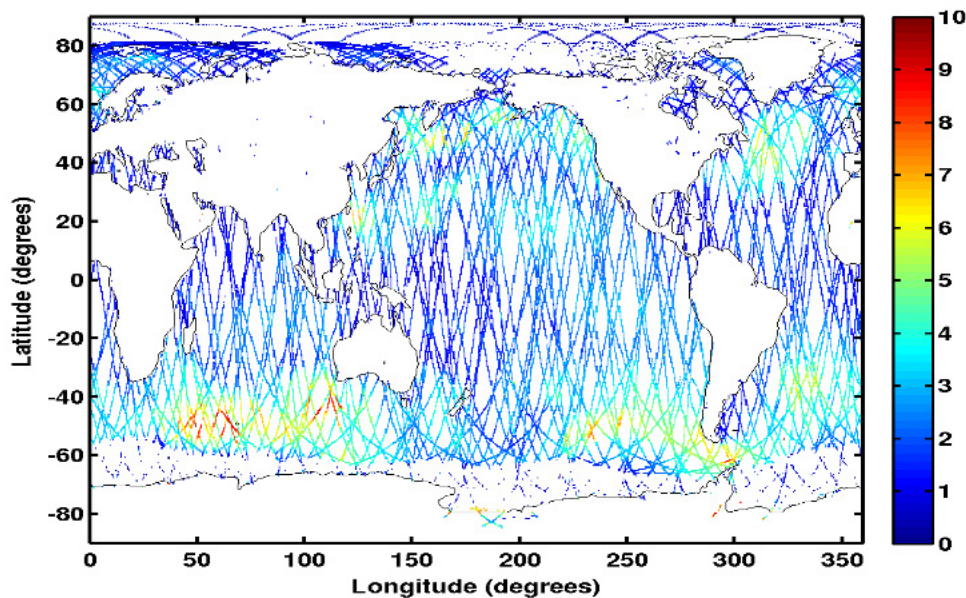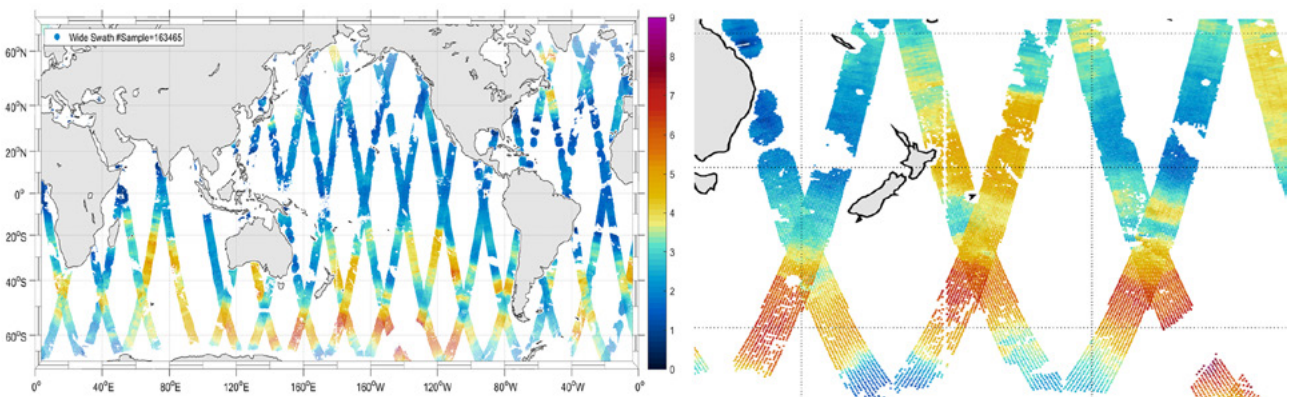

Figure 8.27.   Significant wave height (in meters) observed by altimeter radars of six satellite missions (Jason-3, Saral/Altika, Cryosat-2, Sentinel-3A and 3B, CFOSAT) during the whole day of 11 October 2021 (source: Aouf et al., 2021).
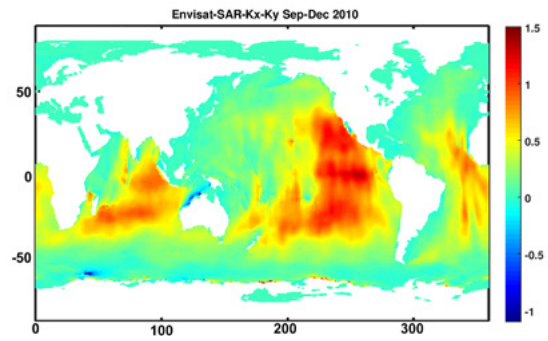
Since the launch of the ERS-1 and 2 and ENVISAT (2002) satellites, the waves are observed with more detailed information (Hasselmann et al., 2013), characterised by the directional wave spectrum that can describe the different dominant wave trains (see Figure 8.28). The assimilation of such observations needs several steps and has been initiated at the end of 1990's. The method is based on the assimilation of wave systems as derived from a spectral partitioning scheme, which works on the principle of the inverted catchment area (Hasselmann et al., 1997; Voorrips et al., 1997; Breivik et al., 1998; Aouf et al., 2006). The different wave systems are characterised by their mean energy, frequency, and direction. The mean parameters are assimilated using an optimal interpo-

Figure 8.29. Difference of mean wave period (in seconds) from the model MFWAM with and without assimilation of wavenumber components of SAR partitions from ENVISAT during the period from September to December 2010; positive and negative values stand, respectively, for overestimation and underestimation of the model, (source: Aouf et al., 2021).

lation (OI) scheme, following a cross-assignment procedure that correlates the observed and modelled wave systems. The analysed spectra are reconstructed by resizing and reshaping the model spectra based on the mean parameters obtained from the OI scheme.

The SAR, from the ERS, ENVISAT and Sentinel-1 satellites, provides directional wave spectra with a limitation in azimuth direction of detecting waves with wavelength greater than 150 m. Such wave spectra are very useful to describe several wave trains in energy and wave numbers components. MF-WAM started to assimilate wave partition parameters, such wavenumber components, by using optimal interpolation. This has provided a significant improvement of long swell propagation, and an assimilation impact which remains efficient at least 3 days in the period of forecast. Figure 8.29

Figure 8.28. Directional wave spectra observed by Synthetic Aperture Radar of Sentinel-1 (source: Derkani et al., 2021).

Figure 8.30. Wide swath significant wave height from the CFOSAT mission. Left: global view. Right: zoom focused on high SWH in Southwest Pacific Ocean (source: Wang et al., 2021).

shows the impact of the assimilation of wavenumber components of partitions from ENVISAT on the mean wave period. The different anomalies are strongly correlated with swell track propagation from the Southern Ocean.

Future wave forecasting systems will be able to assimilate both the wave heights and the directional components represented by the partitions. The impact of these assimilation systems ensures reliable integrated wave parameters in the 3-day forecast. The processing of satellite wave data is evolving rapidly; in a recent study by Wang et al. (2021), it is shown the retrieval of significant wave height on a scatterometer swath by using a deep learning technique. With this type of

wave data, the amount of data to be assimilated is significantly increased, which keeps consistent the correction of the model over a swath distance of 200 km. An example of a wide swath SWH obtained from the CFOSAT mission is shown in Figure 8.30. The assimilation of wide swaths of significant wave heights improves the initial conditions of the sea state generated by storms, for instance in the Southern Ocean, and also enhances the impact in coastal regions. Furthermore, with the trend of improved spatial resolution of the wave model, altimeters are providing better sampled wave heights, e.g. 5 hz (~1km), with the ability to correctly describe small scale variations such wave-current interactions.

8.6.
Ensemble modelling

Forecasts are subject to uncertainty by their nature. Some of the uncertainty is due to errors in model parameterizations of real-world processes, while some others can be attributed to observation errors. However, a significant amount of uncertainty is also introduced as a result of small differentials between the analysis and the state of environmental conditions at forecast initiation. These differences can lead to much wider discrepancies between the forecast and actual state at longer lead times, depending on the stability of the background meteorological conditions. One approach to forecasting is attempting to quantify the uncertainties, and view the forecast as sampling from a probability distribution of likely conditions rather than as a single "deterministic" outcome. Continuing increases in computing resources have enabled modelling centres to adopt a probabilistic forecasting approach based on running wave EPSs.

The aim of an EPS is to provide forecasters with a measure of model and climatic uncertainty associated with a given forecast. The ensemble will indicate lower forecast uncertainty in well- specified and stable weather conditions than in unstable conditions, where the present weather state might be poorly analysed and weather system development is more dynamic. As a forced-dissipative system, wave-forecast uncertainty is mostly determined by variations in the driving atmospheric data. Thus, the requirement for a complex EPS based on data assimilation, using perturbed initial conditions to generate starting conditions for ensemble members as in ensemble weather prediction, is limited. Pioneering applications have been developed for global medium-range

forecasts (1-4 weeks ahead) at centres such as the ECMWF (Molteni et al., 1996; Saetra and Bidlot, 2004), NCEP (Chen, 2006), and FNMOC (Alves et al., 2013). Research into short-range regional ensemble systems, which have a stronger requirement for uncertainty to be well specified at forecast initialization, is ongoing at the UKMO (Bunney and Saulter, 2015), the Italian Meteorological Service (Pezzutto et al., 2016), and the Australian Bureau of Meteorology (Zieger et al., 2018).

The data provided by an ensemble (see Figures 8.31 and 8.32) allow more than one approach to be adopted when interpreting and issuing a forecast. For example: i) individual members can be identified and used to describe alternative forecast scenarios deterministically; ii) dynamic changes in ensemble spread can be used to estimate the uncertainty associated with a deterministic product derived from the ensemble; or iii) probability information about a given outcome (for instance, the probability of wave height exceeding a certain operating threshold) can be used directly. The choice of approach requires an understanding of the end-user requirements and of the ensemble's performance.

However, a well-specified ensemble should show a good reliability relationship. Similarly, a good ensemble will show a strong correlation between spread in the EPS forecast and error in the ensemble control/mean forecast and observations. All these behaviours are fundamentally reliant on the quality of the underlying model. In the example in Figure 8.33, reliability is shown to be significantly affected for a short-range ensemble forecast when
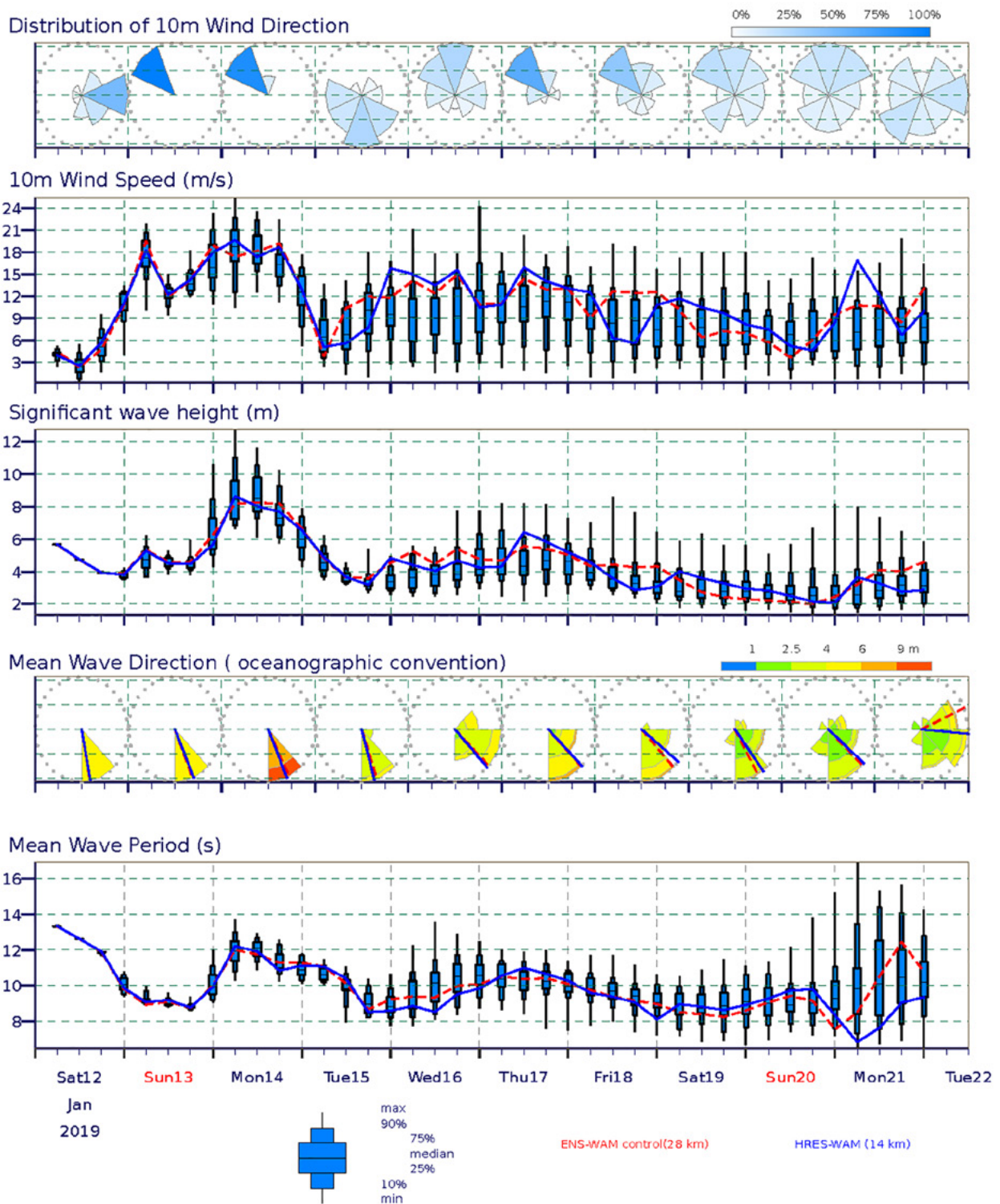
Figure 8.31. Point time-series ensemble wave forecast product by ECMWF. Top two panels: direction variability and wind speed. Lower three panels: forecast of total wave parameters. In this instance, a high-resolution deterministic model and the ensemble control are overlaid using the blue and red lines, respectively (source: WMO, 2020).
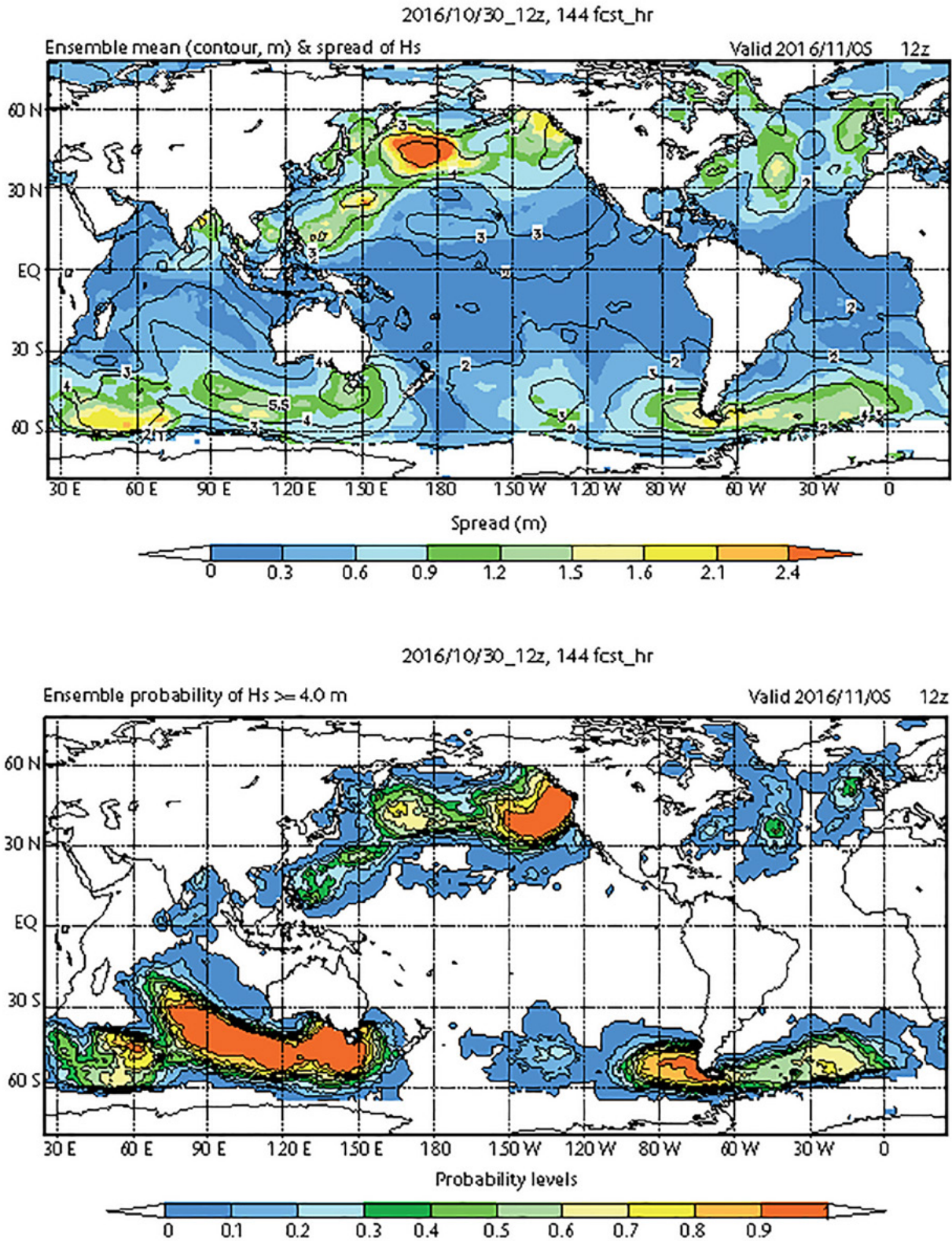
Figure 8.32. Ensemble forecast charts. Top: ensemble mean significant wave height (contours) and spread (shading). Bottom: probability of significant wave height exceeding 4 m (source: WMO, 2020).

6.0m Exceedance Reliability Diagram (North Sea)

Hs>6m reliability diagram (North Sea)
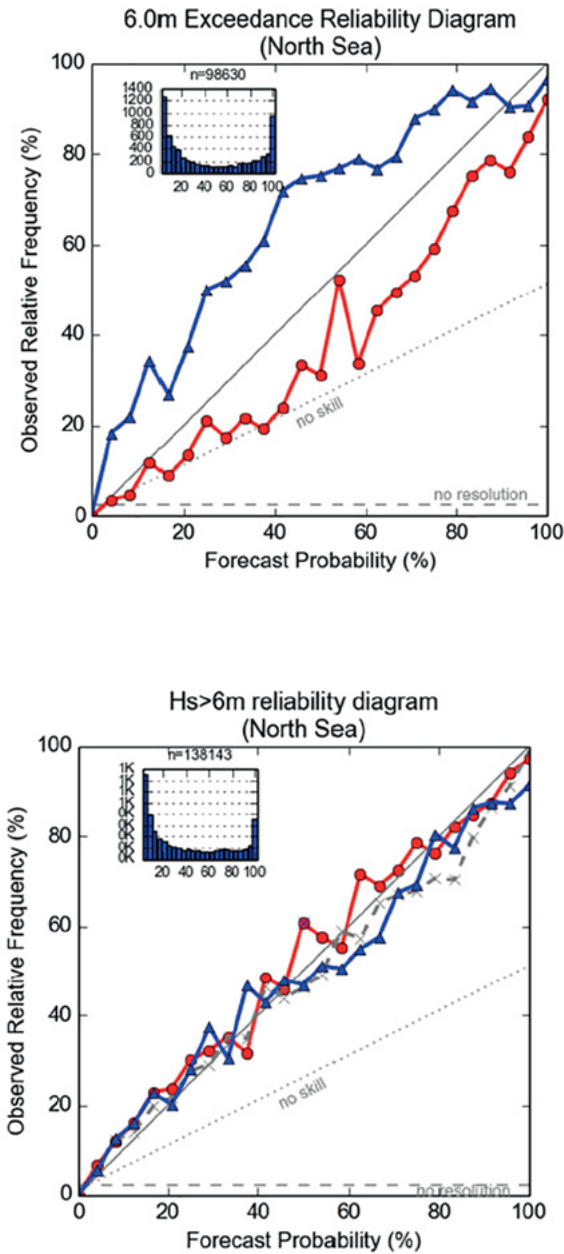
Figure 8.33. Reliability diagram for two wave EPS forecasts of significant wave height above 6 m at a forecast range of 2 d (blue: Atlantic regional model; red: regional model of the United Kingdom). The forecasts are considered reliable when the forecast probability and frequency of subsequent observations are similar (the data fall onto the 1:1 line). In this example, the effect of bias correcting the forecast is significant; in the bottom panel, the lines representing forecasts after bias correction are much closer to the 1:1 line than the raw forecasts in the top panel (source: WMO, 2020).
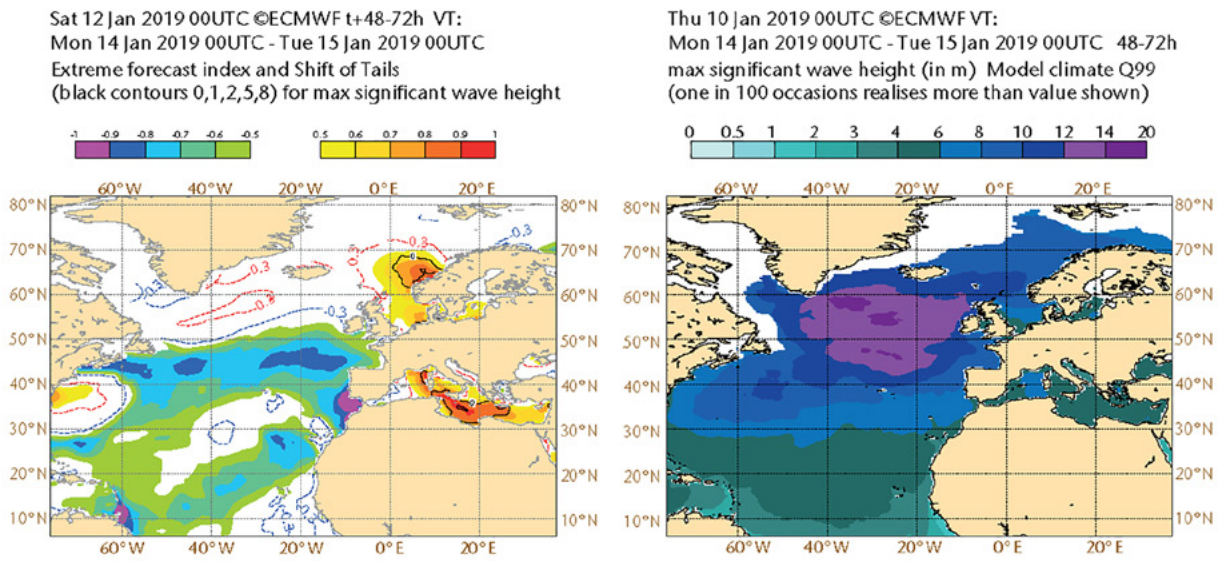
an underlying bias is corrected. A recommended practice when assessing probability of threshold exceedance is to evaluate the probability and also the quantity by which the threshold is exceeded. For example, a forecast where 90% of ensemble members exceeded a threshold by 1 m Hs should be given a stronger level of confidence than a forecast with a similar probability of 90%, but which threshold exceeds by only 10-20 cm.

One aspect of ensemble prediction that may have particular application is the identification of low-probability, high-impact occurrences of a "dangerous" sea state within the ensemble at long range (Petroliagis and Pinson, 2012). In extreme cases, the accuracy of the underlying model may be more questionable than everyday forecasting, but this can be mitigated using a background model climatology. Lalaurette (2003) described the ECMWF EFI methodology for wind, temperature, and precipitation parameters, in which forecast members were compared against a model climate. This EFI has also been extended to waves. Figure 8.34 shows an example in which the figure on the left is EFI (with range -1 to 1) for significant wave height, with values nearing 1 over the Norwegian Sea. The figure on the right is the corresponding 99th percentile of the wave-height distribution for that day. Therefore, EFI indicates that the model is predicting wave heights above 4 m and that this is not usual for that time of the year.

A computationally cheaper version of a full ensemble system is the so-called "poor man's ensemble" (Ebert, 2001), which combines some independent model forecasts from several operational centres. The availability of such a set of forecasts can also contribute to a "consensus forecast" in which the forecasts are weighted and bias corrected according to past performance to produce an "optimal consensus forecast", which typically outperforms any of the individual model forecasts (Durrant et al., 2009).

An example is given below for the interest of using a wave ensemble in the frame of emergency and wave submersion warning. Figure 8.34 right panel shows the high uncertainty between members on the location of the strong wave area generated by a storm event. The propagation of the storm is observed differently. Several members, including the deterministic forecast, estimate SWH of 10m on Brittany coasts at 102-hour forecast (06:00 UTC), as illustrated in Figure 8.35 left panel. In fact, the wave submersion warning in this case was triggered for the evening. It can be seen that about 20% of the members considered a probability of waves with SWH greater than 10m near the analysis. Uncertainty was also related to the location of the storm on the North-South axis.

Sat 12 Jan 2019 00UTC ©ECMWF t+48-72h VT:
Mon 14 Jan 2019 00UTC - Tue 15 Jan 2019 00UTC
Extreme forecast index and Shift of Tails
(black contours 0,1,2,5,8) for max significant wave height

Thu 10 Jan 2019 00UTC ©ECMWF VT:
Mon 14 Jan 2019 00UTC - Tue 15 Jan 2019 00UTC   48-72h
max significant wave height (in m) Model climate Q99
(one in 100 occasions realises more than value shown)

Figure 8.34.   Extreme Forecast Index (left) and associated 99th percentile of significant wave height derived from the model's long-term climate simulation (right panel) (source: WMO, 2020).
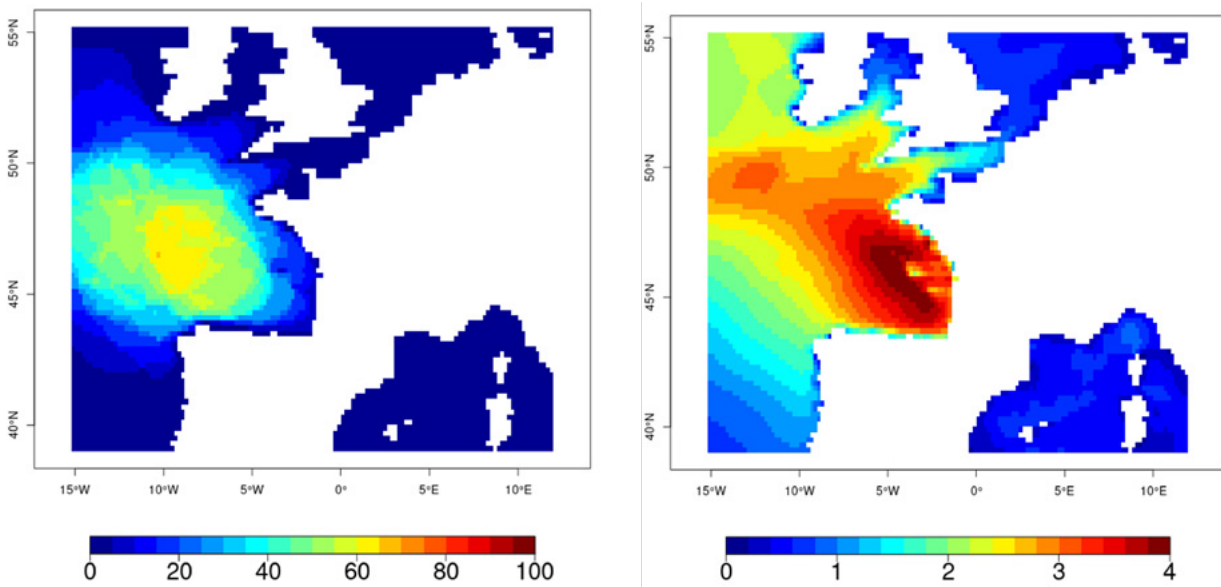
Figure 8.35.   Left: probability (in %) of SWH exceeding 10m at 102-hour forecast from the wave ensemble system. Right: standard deviation of SWH (in metre) between ensemble members, 30 January 2021 at 06:00 UTC (courtesy: A. Dalphinet, MeteoFrance).

8.7.
Validation and calibration strategies

For all operational ocean forecast systems, verification of wave models is dependent on the choice of metric, sampling strategy, and parameter(s) to be verified. Verification and measurement of model uncertainty include describing the difference between the model and observed conditions and their statistical properties; assessing the value of the model in accurately predicting specific ocean conditions for user decision making; providing a long term view of performance and measuring the impact of model changes; and/or investigating the model's ability to represent particular ocean processes or conditions. As with any statistical analysis, it is useful to frame the question or hypothesis that the verification should answer and ensure that the metrics provided are appropriate to the expertise of the audience.

For the verification, it is fundamental the sampling strategy applied to both model and observations. Sampling should consider spatial and temporal correlations with respect to data to be verified. These correlations will be dependent on the verification setting, for example in the open ocean wave fields may be well correlated over scales of hundreds of kilometres and several hours, whilst in coastal settings with a strong tidal component correlation in wave conditions, scales can diminish about tens of kilometres and periods of less than an hour (Saulter et al., 2020). The degree of correlation between data affects the sample size required to consider robust statistical verification. The verification can be affected if scales represented by models and observations are substantially different. In-situ observations tend to sample on scales equivalent to approximately 5-20 km depending on dominant wave periods, whilst a 1 Hz altimeter observation of significant wave height is derived over a spatial footprint that covers approximately 6-7 km in the along-track direction with a diameter 2-10 km increasing with the sea-state (since the backscatter increases as waves get bigger and wavelengths longer). Wave models can generally be considered to scale at a factor of 3-4 times of either the wave or forcing atmospheric model horizontal grid and integration time step (Janssen et al., 2007). It is recommended to define a benchmark representative scale for comparison with the data processed to that scale, as well as metadata describing this processing supplied alongside with metrics. It may also be important to communicate limitations in the data, for example in the case in which the available observations and processing methods cannot be extended to a full coverage of the model domain, such as coastal zones.

Existing standards for baseline performance metrics can be found via the WMO/LC-WFV established at ECMWF (Bidlot, 2016), and Product Quality Dashboard of the Copernicus Marine Service (🔗 8). Left panel in Figure 8.36 shows an example of scatter index of SWH monitoring provided by different operational
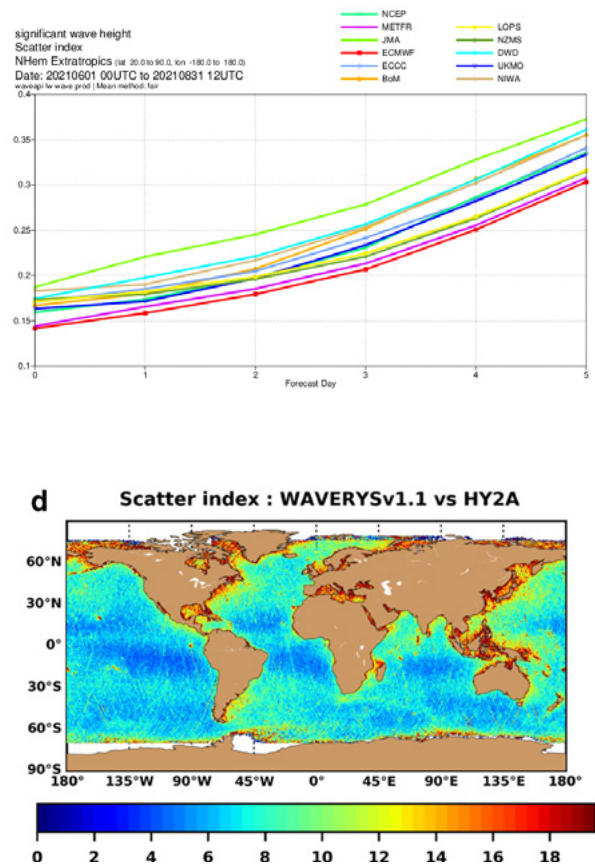
Figure 8.36. Top: variation of scatter index of SWH in a forecast compared to wave buoys from June to August 2021, colours stand for operational centres names (source: WMO/LC-WFV). Bottom: map of scatter index of SWH from Global Ocean Wave Reanalysis (WAVERYS) compared to altimeter HY2A during the 2013-2018 period (source: CMEMS-GLO-QUID-001-032 🔗 9).

8. https://pqd.mercator-ocean.fr
9. https://catalogue.marine.copernicus.eu/documents/QUID/CMEMS-GLO-QUID-001-028.pdf

centres in the framework of the WMO/LC-WFV. As illustrated by the Copernicus Marine Service global wave reanalysis (right panel in Figure 8.36), the altimeters have the advantage of covering all ocean basins, allowing the monitoring of the spatial variation of wave models errors.

Standards will continue to evolve with the increased use of ensemble forecast systems and reductions in horizontal scales of wave, atmosphere, and ocean models. However, model performance is better described by metrics that exploit the uncertainty in forecasts, either from the ensemble (Pezzutto et al., 2016) or using variability in spatial neighbourhoods surrounding an observation point (Ebert, 2008; Mittermaier and Csima, 2017). For long-term monitoring, an important ensemble prediction metric is the Cumulative Ranked Probability Score (Hersbach, 2000), which can be directly compared with Mean Absolute Error for deterministic predictions, therefore enabling the benefits of transition to high resolution or ensemble models from lower resolution or deterministic systems to be measured.

Wave observational data are dominated by SWH measurements available from in-situ sources and remote sensing via satellite missions and HF radar. SWH data are a primary health indicator for the wave model, describing the wave energy of the surface ocean as a response to momentum supplied by the atmosphere and redistributed through wave dispersion. SWH is often the main parameter of interest for users and decision makers about sea-state conditions (see also Chapter 4). However, to properly verify a wave model's performance at a process level, observations of further parameters describing the distribution of wave energy within the two-dimensional frequency-direction spectrum should be also used. Full spectral coverage in the frequency (period) domain of ocean surface waves is currently obtained only by in-situ measurements. Attention is needed to understand the limitations imposed by a given platform's response to wave action, which determines a high frequency cut-off, and the distinction between directional spectra derived from the 'first five' approach used by in-situ data (Swail et al., 2010) versus the full frequency-direction distributions generated from models and remote sensing. Remote sensed data are strongly affected by frequency (wavelength) cut-off constraints as , for example, SAR will capture long period swells but not short wind-waves. From a verification perspective, it can be difficult obtaining a sufficient sample of data across the full directional wave spectrum to enable a robust statistical analysis over multiple frequencies and directions, and hence it is often preferable to compare wave heights, periods, and directions integrated over a reduced number of partitioned regions of the wave spectrum (Ardhuin et al., 2010). Since wave models are strongly influenced by the uncertainty inherited from the forcing atmosphere (Cavaleri et al., 2018), when evaluating wave models at the process level, it is recommended to verify wave parameters alongside contemporary measures of wind speed or stress.

A useful tool in the verification process is the wave rose analysis. Figure 8.37 shows a comparison between the directional wave properties by the Copernicus Marine Service WAVERYS and the buoy 51202 deployed by the NOAA NDBC at Oahu (Hawaii, USA).
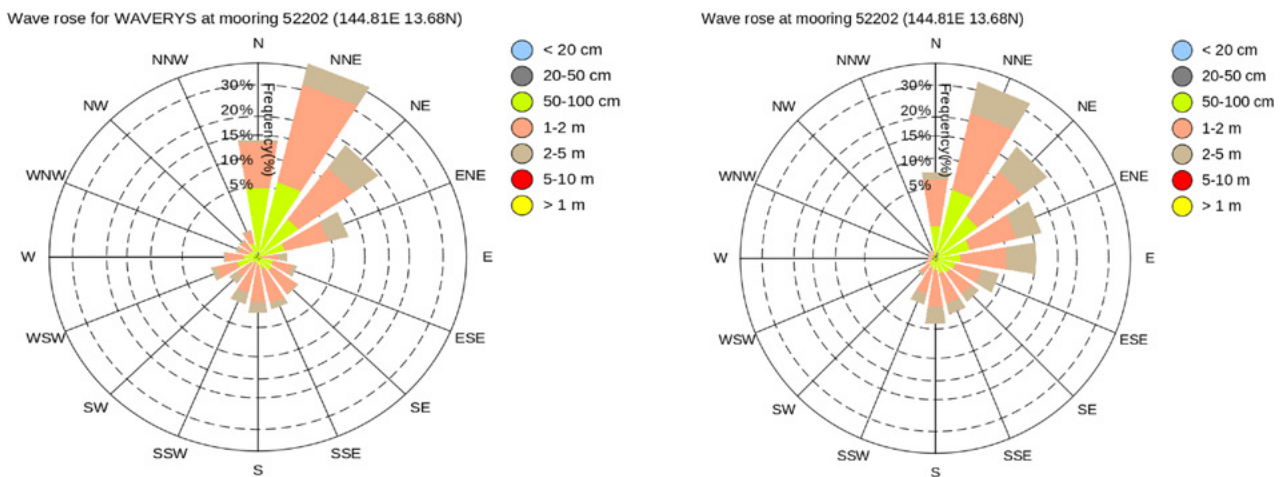
Figure 8.37.   Left: wave rose for Copernicus Marine Service WAVERYS. Right: wave rose at NDBC buoy 51202 (Hawaii, USA).

8.8.
Outputs and post processing

8.8.1. Post-processing of the wave model results for the final delivery

Wave models provide at each grid point two-dimensional wave spectrum $F(f, \theta)$, which describes how the wave energy is distributed as a function of frequency f and propagation direction θ. In general, the wave spectrum F is discretized in 30 frequencies and 24 directions. To simplify the study of wave conditions, integrated parameters are derived from weighted integrals of $F(f, \theta)$. The moment of order n, m_n is defined as the following integral:

$$m_n = \int \int f^n F(f, \theta) df f \theta \qquad (8.43)$$

The integrations are performed over all frequencies and directions or over a spectral subdomain when the spectrum is split between wind sea and swell or partitioned into main components. The wind sea wave component is subject to the wind forcing, and then wave phase speed is smaller than the wind speed at the ocean surface. The remaining part is considered swell. It is established in the WAM model for in-

stance, the spectral energy is subject to wind forcing when the following approximation is satisfied:

$$1.2 \times 28 \left(\frac{u^*}{c} \right) \cos(\theta - \varphi) > 1 \qquad (8.44)$$

where u^* is the friction velocity, c is the phase speed as derived from the linear theory of waves and φ is the wind direction. The integrated parameters are therefore also computed for wind waves and swell by only integrating over the respective components of $F(f, \theta)$ that satisfies 8.43 or not.

Significant wave height

The wave energy is the 0th order of the moment m_0 and significant wave height (Hs) is defined as follows (Hs snapshot shown in Figure 8.38):

$$Hs = 4\sqrt{m_0} \qquad (8.45)$$
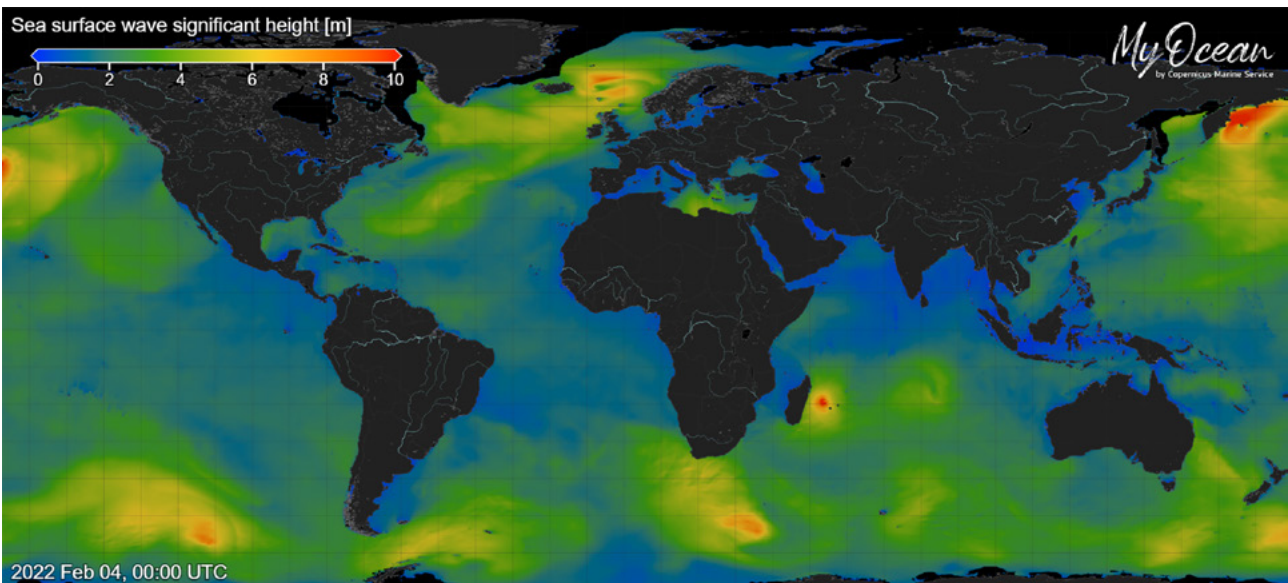
Figure 8.38. Snapshot of Hs (in meters) from Copernicus Marine Service global wave system (3 February 2022 at 21 UTC).

Mean period

The mean period (snapshot in Figure 8.39) is expressed in several ways. The most used is Tm_{-1} which is based on the moment of order $_{-1}$, that is

$$Tm_{-1} = \frac{m_{-1}}{m_0} \qquad (8.46)$$

Tm_{-1} is also commonly known as the energy mean wave period. By considering Hs, it can be used to determine the wave energy flux per unit of wave-crest length in deep water, also indicated as the wave power per unit of wave-crest length P.

To analyse different aspects of the wave field, other moments can be used to define a mean period. Periods can be based on the first moment Tm_1 given by:

$$Tm_1 = \frac{m_0}{m_1} \qquad (8.47)$$

Tm_1 is essentially the reciprocal of the mean frequency. It can be used to estimate the magnitude of Stokes drift transport in deep water and periods based on the second moment Tm_2 given by:

$$Tm_2 = \frac{m_0}{m_2} \qquad (8.48)$$

Tm_2 is also known as the zero-crossing mean wave period, as it corresponds to the mean period that is determined from observations of the sea surface elevation using the zero-crossing method.

Peak period

The peak period is defined for total sea and can be expressed as the reciprocal peak frequency of the 1D wave spectrum $F(f)$ integrated over directions. There is a second way to compute the peak frequency and it is obtained from a parabolic fit around the discretized maximum of the two-dimensional wave spectrum $F(f,\theta)$.

Mean wave direction

The mean wave direction is defined by weighting the wave spectrum $F(f,\theta)$. It is expressed as follows:

$$< \theta > = \arctan \frac{S_1}{C_1} \qquad (8.49)$$

where S_1 is the integral of $sin(\theta)*F(f,\theta)$ over frequencies and directions, while C_1 is the integral of $cos(\theta)*F(f,\theta)$ over f and θ.

Directional spread

The wave directional spread gives the information on the directional distribution of the total sea, or it can be applied for different wave components. It is expressed as follows:

$$s_\theta = \sqrt{2(1-M)} \qquad (8.50)$$

where M is I/m_0 and I is the integral of $cos(\theta-<\theta>)*F(f,\theta)$ over f and θ. $<\theta>$ is the mean direction. The directional spread can be computed for wind, sea, and swell components.
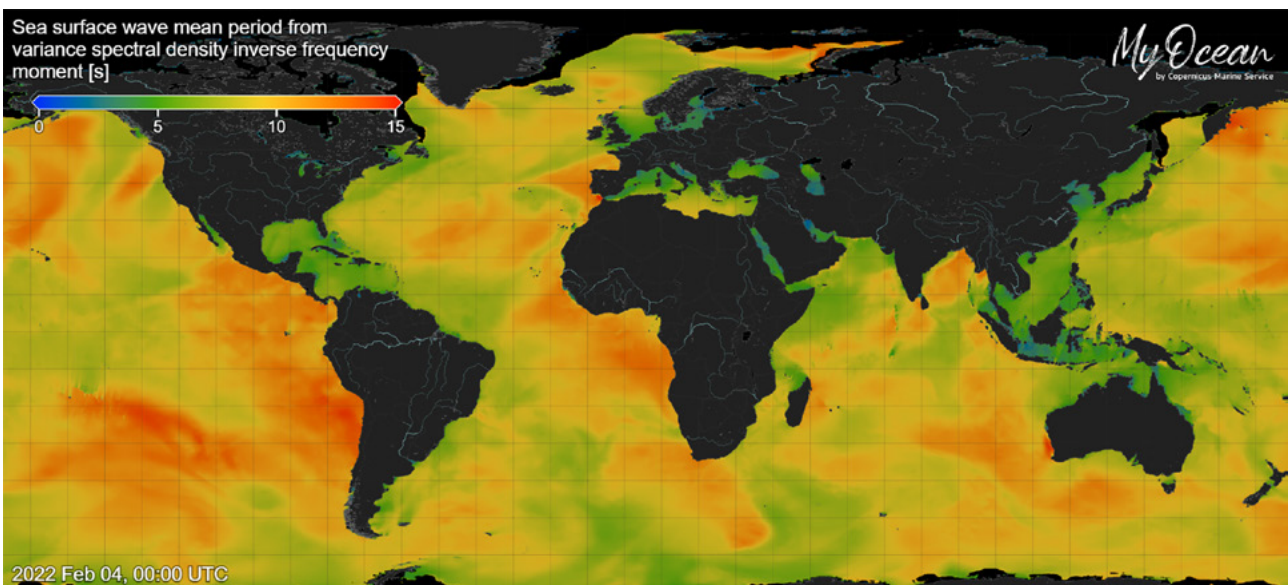
Figure 8.39. Snapshot of mean period Tm_{-1} (in seconds) from Copernicus Marine Service global wave system (3 February 2022 at 21 UTC).

Surface Stokes Drift

The Stokes drift impacts the turbulence in the upper ocean layers and contributes to the source of energy of the ocean circulation, particularly the Langmuir circulation. The surface Stokes drift Us is computed from the wave spectrum in deep water by the following relation:

$$U_s = \frac{16\pi^3}{g} \int \int f^3 \cdot k \cdot F(f,\theta)dfd\theta \qquad (8.51)$$

where the integration is over all frequencies and directions. k is the unit vector in the direction of the wave component. In the high frequency range, the Phillips spectral shape is used with accounting of spectral level of the last frequency bin. Figure 8.40 shows the ratio of Stokes drift magnitude to 10 m wind speed.

Partitioning wave spectrum

In general, wave forecasters firstly analyse the integrated parameters over the full wave spectrum describing the total sea. Then, they refine their analysis by examining the different dominant wave trains representing wind, sea, and swell. Most wave models include a partitioning procedure, which aims to separate the different wave systems represented by energy peaks in the wave spectrum. The most used partitioning procedure is adapted from Hanson and Phillips (2002) and is based on the watershed method inspired from image processing. After splitting the wind sea and swell wave spectrum, the method consists in identifying the energy peaks in

the wave spectrum and isolating a partition with decreasing energy from the peak to a limit corresponding to an increase in energy. Several partitions or wave systems can be detected in a wave spectrum, and they are classified by decreasing order of their wave height. An example of partitioning is shown in Figure 8.41, where three partitions are detected with two swells and one wind sea. The average height, period and direction can be calculated on each partition.

Wave energy flux

The wave energy flux per unit of wave-crest length in deep water can be computed by using the wave period Tm_{-1} and significant wave height H_s:
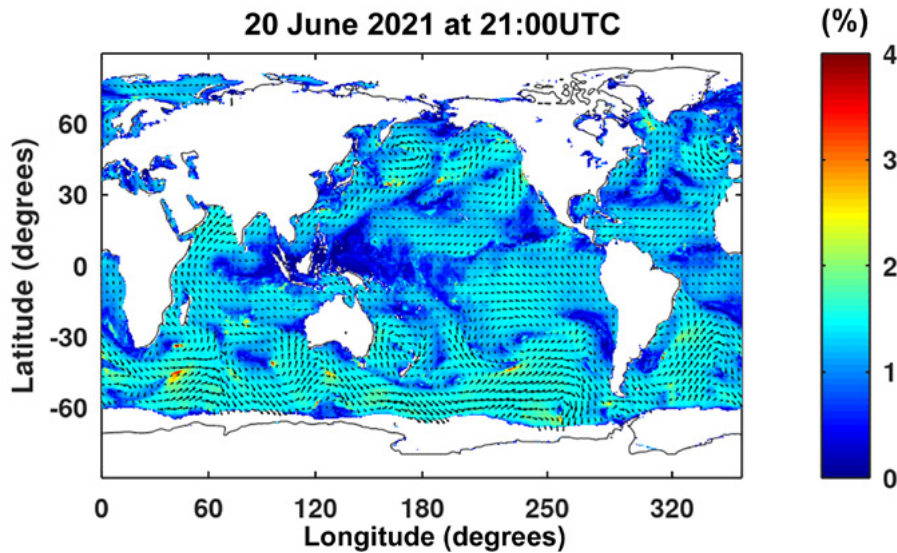
$$P = \frac{\rho_w \cdot g^2}{64\pi} Tm_{-1} H_s^2 \qquad (8.52)$$

where rw is the water density and g is the acceleration due to gravity.

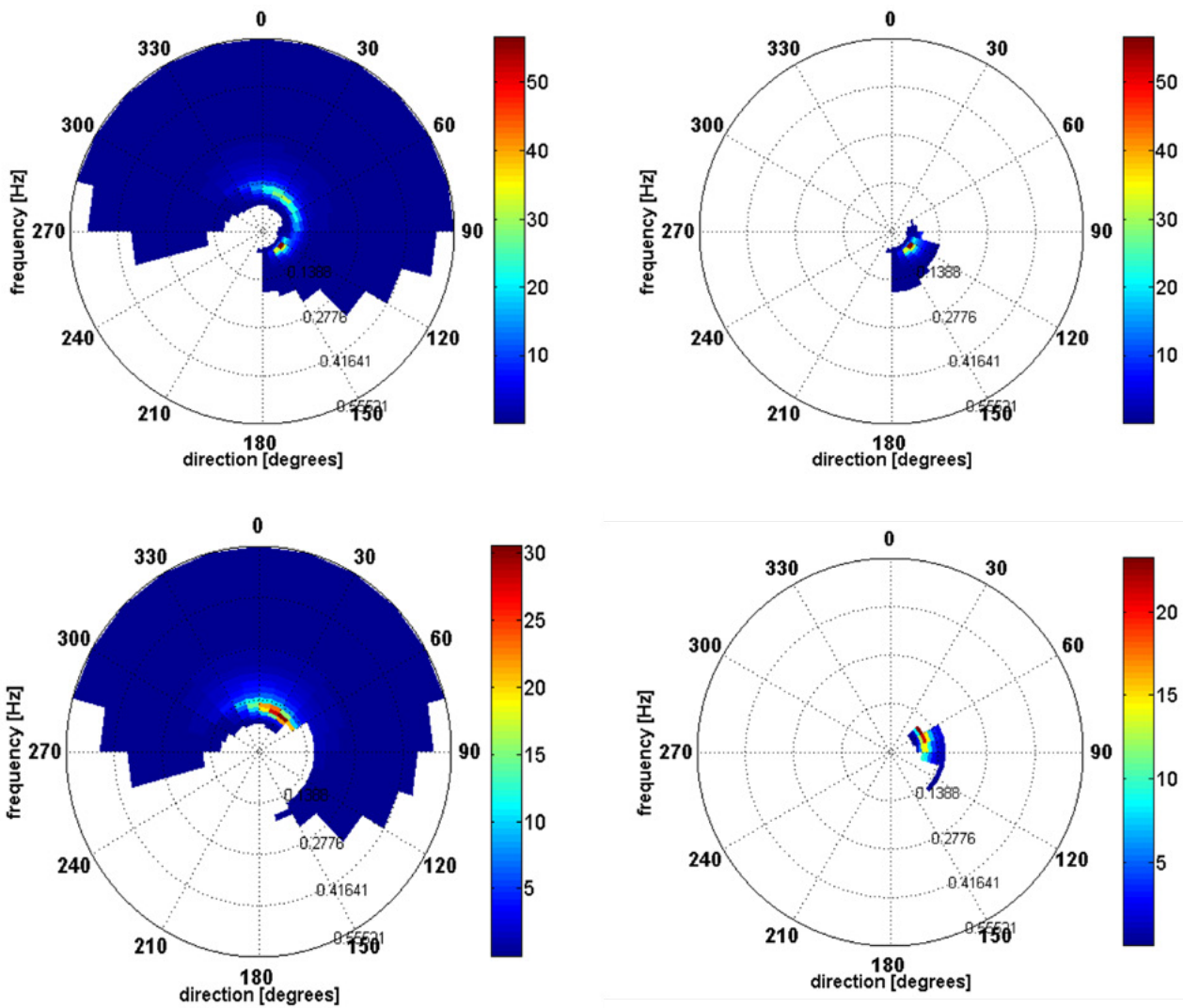The wave energy flux can be expressed by integrating the flux of each spectral component.

$$P = 2\pi g \int \int C_g \cdot F(f,\theta)dfd\theta \qquad (8.53)$$

where Cg is the group velocity in deep water.

Figure 8.40.   Ratio (in percentage) between surface Stokes drift and wind speed from Copernicus Marine Service global wave system on 20 June 2021 at 21 UTC. Arrows show the Stokes drift direction.

Figure 8.41. Top left: full wave spectrum for the location of the Prestige ship accident (Trulsen et al., 2015). Top right: swell partition-1, the most energetic propagating to the South-East direction. Bottom left: long wind sea partition-2 propagating to the North-East direction. Bottom right: swell partition-3 propagating to the East-North-East direction (source: Copernicus Marine Service).

8.8.2. Common output variables

Numerical models for wave generation and propagation can provide different variables to be used in multi-year and pre- dictive systems. Table 8.1 lists variables that are commonly provided by numerical and that may be of special relevance for users, as well as for developers who wish to set up future wave OOFS and multi-year systems.

Table 8.1.   Common names of wave variables.

Common variable names *(usually provided by third-generation spectral wave model and/or a mild slope approximations)*	Symbol	Units
Significant wave height	Hs	m
Peak period	Tp	s
Mean wave period	Tm	s
Mean and Peak wave direction	Θ	$°N$
Complete wave spectra matrix	S	$m^2/Hz/°N$
Mean parameters of wave partitions (Hs,Tm,Tp and Dir) for: 2 Swells and 1 wind sea	$Hsi, Tpi, Diri$	$m, s, °n$
Maximum wave height	$Hmax$	m
Maximum wave period	$Tmax$	m
Meridional component of Stokes drift	Us	m/s
Zonal component of Stokes drift	Vs	m/s
Drag coefficient with waves	Cd	
Normalised stress to ocean	$Tauoc$	
Mean square slope	mss	

Advanced variable names (usually provided by phase resolving models and CFD approaches)	Symbol	Units
Free-surface time series at points and maps	η	m
Wave breaking-induced currents	U-V	m/s
Instantaneous wave run-up	Ru	m
Instantaneous wave overtopping volume	q	m^3/s per m
Infragravity wave oscillations	ηIG	m
Multi-directional wave spectra matrix (agitation)	S	$m^2/Hz/^oN$
Instantaneous wave pressures over structures	P	N/m^2
Instantaneous forces over structures	F	N
Instantaneous wave currents	u-v	m/s

8.9.
Inventories

The purpose of this section is to provide an initial inventory of the operational ocean wave NearRealTime (NRT) and MultiYear (MY) operating at international level. Details about each specific system, resolution, implemented numerical tool, and data assimilation are provided in Tables 8.2 and 8.3 and, where existing, the website address to directly link to systems products and other relevant information.

8.9.1. Inventory of Near-real time wave forecasting systems

The present state-of-the-art operational ocean wave systems for NRT products from global to local scale is presented in Table 8.2.

Also, current contributors to the ocean wave forecast, either global or regional, are (among others): European Centre for Medium-Range Weather Forecasts, UK; Met Office, UK; Fleet Numerical Meteorology and Oceanography Centre, USA; Environment and Climate Change Canada, Canada; National Centres for Environmental Prediction, USA; Météo France, France; Deutscher Wetterdienst, Germany; Bureau of Meteorology, Australia; Service Hydrographique et Océanographique de la Marine, France; Japan Meteorological Agency, Japan; Korea Meteorological Administration, Republic of Korea; Puertos del Estado, Spain; Danmarks Meteorologiske Institut, Denmark; National Institute of Water and Atmospheric Research, New Zealand; Det Norske Meteorologiske Institutt, Norway; Servicio de Hidrografía Naval, Servicio Meteorológico, Argentina.

Table 8.2. Initial inventory of global (G) and regional (R) Near-real time wave forecasting systems.

Type	System (Producer)	Area	Grid type and resolution	Wave model core	Data used for assimilation	Products	Website
G	Global Wave Forecasting System (MeteoFrance, France)	Global ocean	Regular grid, 0.083° - 0.083° - 9km; 1 level (surface)	MFWAM	SWH from satellite	3-hourly instantaneous for SWH MWT VMDR VSDXY WW, SW1 SW2	https://marine.copernicus.eu
R	Arctic Wave Forecasting System (The Norwegian Meteorological Institute, Norway)	Arctic region	3km; 1 level (surface)	WAM	NA	Hourly instantaneous for SWH MWT VMDR VSDXY WW, SW1 SW2	https://marine.copernicus.eu
R	Baltic Wave Forecasting System (FMI, Finland)	Baltic region	2km; 1 level (surface)	WAM	NA	Hourly instantaneous for SWH MWT VMDR VSDXY WW SW1 SW2	https://marine.copernicus.eu
R	European North West Shelf Seas Wave Forecasting System (UK MetOffice, United Kingdom)	European North-West shelf Seas	0.014° - 0.03°; 1 level (surface)	WW3	NA	Hourly instantaneous for SWH MWT VMDR VSDXY WW SW1 SW2	https://marine.copernicus.eu
R	Iberia Biscay Ireland Regional Seas Wave Forecasting System (Puertos del Estado, Spain)	Irish-Biscay-Iberian shelves	0.05° × 0.05°; 1 level (surface)	MFWAM	SWH from satellite	Hourly instantaneous for SWH MWT VMDR VSDXY WW SW1 SW2	https://marine.copernicus.eu
R	Mediterranean Wave Forecasting System (HCMR, Greece)	Mediterranean Sea	0.042° - 0.042° - 5km; 1 level (surface)	WAM	SWH from satellite	Hourly instantaneous for SWH MWT VMDR VSDXY WW SW1 SW2	https://marine.copernicus.eu
R	Black Sea Wave Forecasting System (HEREON, Germany)	Black Sea	0.025° - 0.025° - 3km; N/A level (surface)	WAM	NA	Hourly instantaneous for SWH MWT VMDR VSDXY WW SW1 SW2	https://marine.copernicus.eu

Type	System (Producer)	Area	Grid type and resolution	Wave model core	Data used for assimilation	Products	Website
R	High resolution wave and current forecast within Santander Bay entrance (Spain)	Santander, Spain	10 x 10 km; 10 m level (surface)	SWAN - Elliptic mild slope and tidal currents model (ROMS)	In situ measurements, buoys and radar	instantaneous data for waves SWH MWT VMDR VSDXY WW SW1 SW2 and currents	https://nowcastsdr.ih-cantabria.com/
R	Local Wave Forecasting System at the Harbour Authorities (SAPO)	Spain	Regular grid, 0.1° - 0.1°; 1 level (surface)	SAPO	In situ measurements, Coastal buoys	Hourly instantaneous for SWH MWT VMDR VSDXY WW SW1 SW2	https://portus.puertos.es/index.html?locale=en#/
R	Foras Na Mara / Marine Institute Wave Forecasts	Ireland	Regular grid. 0.025 degrees (approximately 1.5km)	SWAN	NA	Hourly instantaneous for SWH TP VMDR SW2	http://www.marine.ie/Home/site-area/data-services/marine-forecasts/wave-forecasts
R	Foras Na Mara / Marine Institute Wave Forecasts	Ireland	Regular grid. 0.025 degrees (approximately 1.5km)	SWAN	NA	Hourly instantaneous for SWH TP VMDR SW2	http://www.marine.ie/Home/site-area/data-services/marine-forecasts/wave-forecasts
R	Foras Na Mara / Marine Institute Wave Forecasts	Ireland	Regular grid. 0.025 degrees (approximately 1.5km)	SWAN	NA	Hourly instantaneous for SWH TP VMDR SW2	http://www.marine.ie/Home/site-area/data-services/marine-forecasts/wave-forecasts
R	AUSWAVE	Australia	AUSWAVE-G Global (78°S-78°N, 0°E-359°E) AWAVE-R Regional (60°S-12°N, 69°E-180°E)	WW3	NA	Hourly instantaneous for sig_wav_ht pk_wav_per pk_wav_dir mn_dir_wnd_sea (for SW1, SW2, SW3, and WND)	http://www.bom.gov.au/nwp/doc/auswave/data.shtml

Type	System (Producer)	Area	Grid type and resolution	Wave model core	Data used for assimilation	Products	Website
R	NOAA/NWS Marine Weather Forecasts	USA	Regional 0.1º aprox.	WW3	Offshore buoys	Marine, Tropical and Tsunami Services Branch	https://www.weather.gov/marine/
G	NOMADS NOAA Operational Model Archive and Distribution System	Global	Regular grid (global 0.251 to 0.5º and regional 11 km aprox.)	WW3	Offshore buoys	Hourly instantaneous for SWH MWT VMDR VSDXY WW SW1 SW2	https://nomads.ncep.noaa.gov/
R	CARICOOS Nearshore Wave Model	Puerto Rico and Virgin Islands	1 km grid to 200 m and 10 m grid	SWAN	NA	Hourly instantaneous for SWH MWT VMDR VSDXY WW SW1 SW2	https://www.caricoos.org/waves/forecast/SWAN/PRVI/hsig

8.9.2. Inventory of Multi-year wave systems (reanalysis, hindcast)

Table 8.3. Initial inventory of global (G) and regional (R) Near-real time wave forecasting systems.

Type	System (Producer)	Area	Grid type and resolution	Wave model core	Data used for assimilation	Available timeseries	Products	Website
G	Global Ocean Waves Reanalysis (MOi, France)	Global Ocean	0.2° × 0.2°	MFWAM	Sea Wave Height (SWH)	1993-2021	3-hourly instantaneous for SWH MWT VMDR VSDXY WW, SW1 SW2	https://marine.copernicus.eu
R	Arctic Ocean Wave Hindcast (MetNo, Norway)	Arctic Sea	3km × 3km	WAM	NA		Hourly instantaneous for SWH MWT VMDR VSDXY WW SW1 SW2	https://marine.copernicus.eu
R	Baltic Sea Wave Hindcast (FMI, Finland)	Baltic Sea	2km × 2km	WAM	NA	1993/01/01 - 2020/12/31	Hourly instantaneous for SWH MWT VMDR VSDXY WW SW1 SW2	https://marine.copernicus.eu

Type	System (Producer)	Area	Grid type and resolution	Wave model core	Data used for assimilation	Available timeseries	Products	Website
R	Baltic Sea Wave Hindcast (FMI, Finland)	Baltic Sea	2km × 2km	WAM	NA	1993/01/01 - 2020/12/31	Hourly instantaneous for SWH MWT VMDR VSDXY WW SW1 SW2	https://marine.copernicus.eu
R	Mediterranean Sea Waves Reanalysis (HCMR, Greece)	Mediterranean Sea	0.042° × 0.042°	WAM	Sea Wave Height (SWH)	1993/01/01 - present	Hourly instantaneous for SWH MWT VMDR VSDXY WW SW1 SW2	https://marine.copernicus.eu
R	Atlantic -Iberian Biscay Irish-Ocean Wave Reanalysis (Puertos del Estado, Spain)	Irish-Biscay-Iberian shelves	0.05° × 0.05°	MFWAM	Sea Wave Height (SWH)	1993/01/01 - 2020/12/31	Hourly instantaneous for SWH MWT VMDR VSDXY WW SW1 SW2	https://marine.copernicus.eu
R	Atlantic- European North West Shelf-Wave Physics Reanalysis	European North-West shelf Seas	0.017° × 0.017°	WW3	NA	1980/01/01 - present	3-hourly instantaneous for SWH MWT VMDR VSDXY WW, SW1 SW2	https://marine.copernicus.eu
R	Black Sea Waves Reanalysis (HEREON, Germany)	Black Sea	0.037° × 0.028°	WAM	Sea Wave Height (SWH)	1979/01/01 - present	Hourly instantaneous for SWH MWT VMDR VSDXY WW SW1 SW2	https://marine.copernicus.eu
G	Global ocean wave reanalysis from Climate data service copernicus ERA5	Global	0.5°x0.5°	ECWAM	SWH	1980 - present	Hourly	https://climate.copernicus.eu/climate-reanalysis
G	Global wave reanalysis CFSR	Global	0.5°x0.5°	WW3	NA	1979 - 2017		https://polar.ncep.noaa.gov/waves/hindcasts/
G	Global wave reanalysis CAWCR (CSIRO)	Global	0.4°x0.4°	WW3	NA	1979 - 2010		https://data.csiro.au/collection/csiro:39819

8.10.
References

Álvarez-Fanjul, E., García-Sotillo, M., Pérez Gómez, B., García Valdecasas, J. M., Pérez Rubio, S., Rodríguez Dapena, A., et al. (2018). Operational oceanography at the service of the ports. In: "New Frontiers in Operational Oceanography", Editors: E. Chassignet, A. Pascual, J. Tintoré, and J. Verron (Cambridge: GODAE OceanView), 729-736, https://doi.org/10.17125/gov2018.ch27

Alves, J.-H.G.M., Wittmann, P., Sestak, M., Schauer, J., Stripling, S., Bernier, N.B., Mclean, J., Chao, Y., Chawla, A., Tolman, H., Nelson, G., and Klotz, S. (2013). The NCEP–FNMOC combined wave ensemble product: expanding benefits of inter-agency probabilistic forecasts to the oceanic environment. *Bulletin of the American Meteorological Society,* 94(12), 1893-1905, https://doi.org/10.1175/BAMS-D-12-00032.1

Aouf, L., Hauser, D., Law-Chune, S., Chapron, B., Dalphinet, A., and Tourain, C. (2021). New directional wave observations from CFOSAT: impact on ocean/wave coupling in the Southern Ocean. EGU General Assembly 2021, online, 19-30 Apr 2021, EGU21-7412, https://doi.org/10.5194/egusphere-egu21-7412

Aouf, L., Lefèvre, J., and Hauser, D. (2006). Assimilation of Directional Wave Spectra in the Wave Model WAM: An Impact Study from Synthetic Observations in Preparation for the SWIMSAT Satellite Mission. *Journal of Atmospheric and Oceanic Technology,* 23(3), 448-463, https://doi.org/10.1175/JTECH1861.1

Aouf, L., Danièle, H., Céline, T., Bertrand, C. (2018). On the Assimilation of Multi-Source of Directional Wave Spectra from Sentinel-1A and 1B, and CFOSAT in the Wave Model MFWAM: Toward an Operational Use in CMEMS-MFC. IGARSS 2018 - 2018 IEEE International Geoscience and Remote Sensing Symposium, 2018, pp. 5663-5666, doi: 10.1109/IGARSS.2018.8517731

Ardhuin, F., Otero, M., Merrifield, S., Grouazel, A., and Terril, E. (2020). Ice breakup controls dissipation of wind waves across Southern Ocean sea ice. *Geophysical Research Letters,* 47, e2020GL087699. https://doi.org/10.1029/2020GL087699

Ardhuin, F., Rogers, E., Babanin, A., Filipot, J.-F., Magne, R., Roland, A., van der Westhuysen, A., Queffeulou, P., Lefevre, J.-M., Aouf, L., Collard, F. (2010). Semi-empirical dissipation source functions for ocean waves. Part I: definitions, calibration and validations. *Journal of Physical Oceanography,* 40, 1917-1941, https://doi.org/10.1175/2010JPO4324.1

Babanin, A.V. (2011). Breaking and Dissipation of Ocean Surface Waves. Cambridge University Press, 480 p.

Babanin, A.V. (2018). Change of regime of air-sea dynamics in extreme Metocean conditions. Proceedings of the ASME 2018 37th International Conference on Ocean, Offshore and Arctic Engineering OMAE2018, June 17-22, 2018, Madrid, Spain, paper 77484, 6 p.

Babanin, A.V., Onorato, M., and Qiao, F. (2012). Surface waves and wave-coupled effects in lower atmosphere and upper ocean. *Journal of Geophysical Research: Ocean,* 117(C11), https://doi.org/10.1029/2012JC007932

Babanin, A.V., van der Westhuysen, A., Chalikov, D., and Rogers, W.E. (2017). Advanced wave modelling including wave-current interaction. In "The Sea: The Science of Ocean Prediction", Eds. Nadia Pinardi, Pierre F. J. Lermusiaux, Kenneth H. Brink and Ruth Preller, *Journal of Marine Research,* 75, 239-262.

Barstow, S., Mørk, G., Lønseth, L., and Schjølberg, P.. (2004). Use of satellite wave data in the world waves project. Gayana (Concepción), 68(2, Supl.TIProc), 40-47, http://dx.doi.org/10.4067/S0717-65382004000200007

Battjes, J.A., and Janssen, P.A.E..M. (1978). Energy Loss and Setup Due to Breaking in Random Waves. Proceedings of 16th Coastal Engineering Conference, Hamburg, Germany, 569-587.

Bauer, E., Hasselmann, S., Hasselmann, K. and Graber, H. C. (1992). Validation and assimilation of Seasat altimeter wave heights using the WAM wave model. *Journal of Geophysical Research: Ocean,* C97, 12671-12682, https://doi.org/10.1029/92JC01056

Berkhoff, J. C. (1972). Computation of combined refraction-diffraction. 13th International Conference on Coastal Engineering, (pp. 471-490). ASCE.

Beven J. (2019). Hurricane Pablo tropical cyclone report, NHC-NOAA.

Bidlot J. R. (2016). Twenty-one years of wave forecast verification. ECMWF Newsletter, 150, 2016.

Booij, N., Ris, R., and Holthuijsen, Leo. (1999). A third-generation wave model for coastal regions, Part I, Model description and validation. *Journal of Geophysical Research: Ocean,* 104. 7649-7656, https://doi.org/10.1029/98JC02622

Breivik, L-A., Reistad, M., Schyberg, H., Sunde, J., Krogstad, H. E., and Johnsen, H. (1998). Assimilation of ERS SAR wave spectra in an operational wave model. *Journal of Geophysical Research: Ocean,* 103, 7887-7900, https://doi.org/10.1029/97JC02728

Breivik, Ø., Gusdal, Y., Furevik, B.R., Aarnes, O.J., Reistand, M. (2009). Nearshore wave forecasting and hindcasting by dynamical and statistical downscaling. *Journal of Marine Systems,* 78, S235-S243, https://doi.org/10.1016/j.jmarsys.2009.01.025

Breivik, Ø., Mogensen, K., Bidlot, J.-R., Balmaseda, M. A., and Janssen, P. A. E. M. (2015), Surface wave effects in the NEMO ocean model: Forced and coupled experiments. *Journal of Geophysical Research: Ocean,* 120, 2973-2992, https://doi.org/10.1002/2014JC010565

Brocchini, M. (2013). A reasoned overview on Boussinesq-type models: the interplay between physics, mathematics and numerics. *Proceedings of the Royal Society A Mathematical, Physics and Engineering Science,* 469, https://doi.org/10.1098/rspa.2013.0496

Browne, M., Castelle, B., Strauss, D., Tomlinson, R., Blumenstein, M., Lane, C. (2007). Near-shore swell estimation from a global wind–wave model: spectral process, linear and artificial neural network models. *Coastal Engineering,* 54, 445-460, https://doi.org/10.1016/j.coastaleng.2006.11.007

Bunney, C., and Saulter, A. (2015). An ensemble forecast system for prediction of Atlantic-UK wind waves. *Ocean Modelling,* 96(1), 103-116, doi: 10.1016/j.ocemod.2015.07.005

Dean, R. G., Dalrymple, R. A. (1991). Water wave mechanics for engineers and scientists (Advanced series on ocean engineering - Volume 2), Singapore World Scientific Publishing.

Camus, P., Mendez, F., Medina, R. (2011). A hybrid efficient method to downscale wave climate to coastal areas. *Coastal Engineering,* 58(9), 851-862, https://doi.org/10.1016/j.coastaleng.2011.05.007

Camus, P., Mendez, F.J., Medina, R., Tomas, A., Izaguirre, C. (2013). High resolution downscaled ocean waves (DOW) reanalysis in coastal areas. *Coastal Engineering,* 72, 56-68, https://doi.org/10.1016/j.coastaleng.2012.09.002

Cavaleri, L., Alves, J.-H.G.M., Ardhuin, F., Babanin, A., Banner, M., Belibassakis, K., Benoit, M., Donelan, M., Groeneweg, J., Herbers, T.H.C., Hwang, P., Janssen, P.A.E.M., Janssen, T., Lavrenov, I.V., Magne, R., Monbaliu, J., Onorato, M., Polnikov, V., Resio, D., Rogers, W.E., Sheremet, A., McKee Smith, J., Tolman, H.L., van Vledder, G., Wolf, J., Young, I. (2007). Wave modeling - the state of the art. *Progress in Oceanography,* 75(4), 603-674, https://doi.org/10.1016/j.pocean.2007.05.005

Cavaleri, L., Abdalla, S., Benetazzo, A., Bertotti, L., Bidlot, J.-R., Breivik, Ø., Carniel, S., Jensen, R.E., Portilla-Yandun, J., Rogers, W.E., Roland, A., Sanchez-Arcilla, A., Smith, J.M., Staneva, J., Toledo, Y., van Vledder, G.Ph., and van der Westhuysen, A.J. (2018). Wave modelling in coastal and inner seas. *Progress in Oceanography,* 167, 164-233, https://doi.org/10.1016/j.pocean.2018.03.010

CERC, (1984). Shore Protection Manual. Department of the Army US. Army Corps of Engineers, Washington DC.

Chalikov, D. (2016). Numerical Modeling of Sea Waves. Springer, 330 p.

Chelton, D. B., and McCabe, P. J. (1985). A review of satellite altimeter measurement of sea surface wind speed: with a proposed new algorithm. *Journal of Geophysical Research: Oceans,* 90(3), 4707-4720, https://doi.org/10.1029/JC090iC03p04707

Chen, H.S. (2006). Ensemble Prediction of Ocean Waves at NCEP. Proceedings of 28th Ocean Engineering Conference, Taiwan.

Climate Change Initiative Coastal Sea Level Team (The). (2020). Coastal sea level anomalies and associated trends from Jason satellite altimetry over 2002-2018. *Scientific Data,* 7, 357, https://doi.org/10.1038/s41597-020-00694-w

Dean, R. G., and Dalrymple, R. A. (1991). Water wave mechanics for engineers and scientists. In: "Advanced Series on Ocean Engineering: Volume 2" by R.G. Dean and R.A. Dalrymple, World Scientific Publishing Co Pte Ltd, https://doi.org/10.1142/1232

Derkani, M. H., Alberello, A., Nelli, F., Bennetts, L.G., Hessner, K. G., MacHutchon, K., Reichert, L., Aouf, L., Khan, S., Toffoli, A. (2021). Wind, waves, and surface currents in the Southern Ocean: observations from the Antarctic Circumnavigation Expedition. *Earth System Science Data,* 13, 1189-1209, https://doi.org/10.5194/essd-13-1189-2021

Dingemanns, M. (1997). Waterwave propagation over uneven bottoms. *Advanced Series on Ocean Engineering,* 13(2), 967.

Donelan, M., Haus, B.K., Reul, N., Plant, W., Stiassnie, M., Graber, H.C., Brown, O., Saltzman, E. (2004). On the limiting aerodynamic roughness of the ocean in very strong winds. Geophysical Research Letters, 31(18), https://doi.org/10.1029/2004GL019460

Durrant, T.H., Woodcock F., and Greenslade, D.J.M. (2009). Consensus forecasts of modelled wave parameters. *Weather and Forecasting,* 24, 492-503, https://doi.org/10.1175/2008WAF2222143.1

Ebert, E. (2001). Ability of a poor man's ensemble to predict the probability and distribution of precipitation. *Monthly Weather Review,* 129(10), 2461–2480, https://doi.org/10.1175/1520-0493(2001)129<2461:AOAPMS>2.0.CO;2

Ebert, E.E. (2008). Fuzzy verification of high resolution gridded forecasts: A review and proposed framework. *Meteorological Applications,* 15, 51-64, https://doi.org/10.1002/met.25

Eckart, C. (1952). The propagation of gravity waves from deep to shallow water. *Circular 20, National Bureau of Standards,* 165-173.

Edson, J.B., Jampana, V., Weller, R.A., Bigorre, S.P., Plueddemann, A.J., Fairall, C.W., Miller, S.D., Mahrt, L., Vickers, D., and Hersbach, H. (2013). On the exchange of momentum over the open ocean. *Journal of Physical Oceanography,* 43(8), 1589-1610, https://doi.org/10.1175/JPO-D-12-0173.1

Fengyan, S., Kirby, J. T., Tehranirad, B., Harris, J. C., and Grilli, S. (2012). FUNWAVE-TVD: Fully Nonlinear Boussinesq Wave Model with TVD Solver. Documentation and User's Manual (Version 2.0). Center for Applied Coastal Research, University of Delaware, Newark, DE. Available at: https://www1.udel.edu/kirby/papers/shi-etal-cacr-11-04-version2.0.pdf

Gaslikova, L., Weisse, R. (2006). Estimating near-shore wave statistics from regional hindcasts using downscaling techniques. *Ocean Dynamics,* 56, 26-35, https://doi.org/10.1007/s10236-005-0041-2

Greenslade, D.J.M. and Young, I.R. (2004). Background errors in a global wave model determined from altimeter data. *Journal of Geophysical Research: Oceans,* 109(C9), https://doi.org/10.1029/2004JC002324

González-Marco, D., Sierra, J. P., Ybarra, O. F., Sánchez-Arcilla, A. (2008). Implications of long waves in harbour management: The Gijón port case study. *Ocean & Coastal Management,* 51(2), 180-201, https://doi.org/10.1016/j.ocecoaman.2007.04.001

Groeneweg, J., Ledden, M., Zijlema, M. (2007). Wave transformation in front of the Dutch Coast. Proceedings of the Coastal Engineering Conference, 552-564, https://doi.org/10.1142/9789812709554_0048

Gulev, S. K., Grigorieva, V., Sterl, A., and Woolf, D. (2003). Assessment of the reliability of wave observations from voluntary observing ships: Insights from the validation of a global wind wave climatology based on voluntary observing ship data. *Journal of Geophysical Research: Oceans,* 108(C7), https://doi.org/10.1029/2002JC001437

Hanley, K.E., Belcher, S.E., and Sullivan, P.P. (2010). A global climatology of wind-wave interaction. *Journal of Physical Oceanography,* 40, 1263-1282, https://doi.org/10.1175/2010JPO4377.1

Hanson, J. L., Phillips, O. M. (2001). Automated Analysis of Ocean Surface Directional Wave Spectra. *Journal of Atmospheric and Oceanic Technology,* 18(2), 277-293, https://doi.org/10.1175/1520-0426(2001)018<0277:AAOOSD>2.0.CO;2

Hansom, J. et al. (2015). Extreme Waves: Causes, Characteristics and Impact on Coastal Environments and Society January 2015. In: "Coastal and Marine Hazards, Risks, and Disasters", Edition: Hazards and Disasters Series, Elsevier Major Reference Works, Chapter 11: Extreme Waves: Causes, Characteristics and Impact on Coastal Environments and Society. Publisher: Elsevier; Editors: Ellis, J and Sherman, D. J.

Hasselmann, K. (1962). On the non-linear energy transfer in a gravity-wave spectrum part 1. General theory. *Journal of Fluid Mechanics,* 12 (4), 481-500.

Hasselmann, K., Barnett, T. P., Bouws, E., Carlson, H., Cartwright, D. E., Enke, K., Ewing, J. A.,Gienapp, H., Hasselmann, D. E., Kruseman, P., Meerburg, A., M̈uller, P., Olbers, D. J., Richter, K., Sell, W. and Walden, H. (1973). Measurements of wind-wave growth and swell decay during the Joint North Sea Wave Project (JONSWAP). *Hydraulic Engineering Reports,*. Available at: https://repository.tudelft.nl/islandora/object/uuid%3Af204e188-13b9-49d8-a6dc-4fb7c20562fc

Hasselmann, K., Hasselmann, K., Bauer, E., Janssen, P., Komen, G., Bertotti, L., Lionello, P., Guillaume, A., Cardone, V., Greenwood, J., Reistad, M., Zambresky, L., Ewing, J. (1988). The WAM model - a third generation ocean wave prediction model. *Journal of Physical Oceanography,* 18, 1775-1810.

Hasselmann, S., Hasselmann, K., Allender, J. H., and Barnett, T. P. (1985). Computations and parameterizations of the nonlinear energy transfer in a gravity wave spectrum, II, Parameterizations of the nonlinear energy transfer for application in wave models. *Journal of Physical Oceanography,* 15, 1378-1391.

Hasselmann, K. (1997). Multi-pattern fingerprint method for detection and attribution of climate change. *Climate Dynamics,* 13, 601-611, https://doi.org/10.1007/s003820050185

Hasselmann, K., Chapron, B., Aouf, L., Ardhuin, F., Collard, F., Engen, G., Hasselmann, S., Heimbach, P., Janssen, P., Johnsen, H., et al. (2013). The ERS SAR wave mode: A breakthrough in global ocean wave observations. In: "ERS Missions: 20 Years of Observing Earth", 1st ed.; Fletcher, K., Ed.; European Space Agency: Noordwijk, The Netherlands, 2013; pp. 165-198.

Herman, A., Kaiser, R., Niemeyer, H.D. (2009). Wind-wave variability in shallow tidal sea - spectral modelling combined with neural network methods. *Coastal Engineering,* 56(7), 759-772, https://doi.org/10.1016/j.coastaleng.2009.02.007

Hersbach H. (2000). Decomposition of the continuous ranked probability score for ensemble prediction systems. *Weather and Forecasting,* 5(15), 1697-1709, https://doi.org/10.1175/WAF-D-16-0164.1

Hewitt, J. E, Cummings, V. J., Elis, J. I., Funnell, G., Norkko, A., Talley, T.S., Thrush, S.F. (2003). The role of waves in the colonisation of terrestrial sediments deposited in the marine environment. *Journal of Experimental Marine Biology and Ecology,* 290, 19-47, https://doi.org/10.1016/S0022-0981(03)00051-0

Higuera, P., Lara, L. J., Losada, I.J. (2014a). Three-dimensional interaction of waves and porous coastal structures using OpenFOAM®. Part I: Formulation and validation. *Coastal Engineering,* 83, 243-258, https://doi.org/10.1016/j.coastaleng.2013.08.010

Higuera, P., Lara, L. J., Losada, I.J. (2014b). Three-dimensional interaction of waves and porous coastal structures using OpenFOAM®. Part II: Application. *Coastal Engineering,* 83, 259-270, https://doi.org/10.1016/j.coastaleng.2013.09.002

Holthuijsen, L.H. (2007). Waves in Oceanic and Coastal Waters. Cambridge University Press, https://doi.org/10.1017/CBO9780511618536

Iafrati, A., Babanin, A.V., Onorato, M. (2013). Modulational instability, wave breaking and formation of large scale dipoles. *Physical Review Letters,* 110, 184504, :https://doi.org/10.1103/PhysRevLett.110.184504

Janssen, P.A.E.M (1989). Wave-induced stress and the drag of air flow over sea waves. *Journal of Physical Oceanography,* 19(6), 745-754, https://doi.org/10.1175/1520-0485(1989)019<0745:WISATD>2.0.CO;2

Janssen, P.A.E.M (1991). Quasi-linear theory of wind wave generation applied to wave forecasting. *Journal of Physical Oceanography,* 21, 1631-1642.

Janssen, P.A.E.M. (2004). The Interaction of Ocean Waves and Wind. Cambridge University Press, 308 p.

Janssen, P.A.E.M. (2012). Ocean wave effects on the daily cycle in SST. J*ournal of Geophysical Research: Oceans,* 117, C00J32, https://doi.org/10.1029/2012JC007943

Janssen, P.A.E.M., Lionello, P., Reistad, M. and Hollingsworth, A. (1989). Hindcasts and data assimilation studies with the WAM model during the Seasat period. *Journal of Geophysical Research: Oceans,* C94, 973-993.

Janssen, P.A.E.M., Abdalla, S., Hersbach, H., Bidlot, J.R. (2007). Error estimation of buoy, satellite, and model wave height data. Journal of Atmospheric and Oceanic Technology, 24:1665-1677, https://doi.org/10.1175/JTECH2069.1

Kalra, R., Deo, M.C., Kumar, R., Agarwal, V.K. (2005). Artificial neural network to translate offshore satellite waves to data to coastal locations. *Ocean Engineering,* 32, 1917-1932, https://doi.org/10.1016/j.oceaneng.2005.01.007

Kirby, J., Dalrymple, R. (1983). Propagation of weakly nonlinear surface waves in the presence of varying depth and current. In: Proceedings of the 20th Congress, Int. Assoc. Hydraul. Res.(IAHR), Moscow, 1983, Paper S.1.5.3, pp. 198-202.

Komen, G.J., Hasselmann, K., and Hasselmann, S. (1984). On the existence of a fully developed windsea spectrum. *Journal of Physical Oceanography,* 14, 1271-1285.

Koutitas, C. G. (1990). Mathematical models in coastal engineering. *Applied Ocean Research,* 12(1), 52, https://doi.org/10.1016/S0141-1187(05)80022-7

Kudryavtsev, V.N., Makin, V.K., and Meirink, J.F. (2001). Simplified model of air flow above the waves. *Boundary Layer Meteorology,* 100, 63-90, https://doi.org/10.1023/A:1018914113697

Lalaurette, F. (2003). Early detection of abnormal weather conditions using a probabilistic extreme forecast index. *Quarterly Journal of the Royal Meteorological Society,* 129, 3037-3057, https://doi.org/10.1256/qj.02.152

Lara, J.L., Garcia, N., Losada, I.J. (2006). RANS modelling applied to random wave interaction with submerged permeable structures. *Coastal Engineering,* 53(5-6), 395-417, https://doi.org/10.1016/j.coastaleng.2005.11.003

Law Chune, S., Aouf, L. (2018). Wave effects in global ocean modeling: parametrizations vs. forcing from a wave model. *Ocean Dynamics,* 68, 1739-1758, https://doi.org/10.1007/s10236-018-1220-2

Le Traon, P.Y., Reppucci, A., Alvarez Fanjul, E., Aouf, L., Behrens, A., Belmonte, M., Bentamy, A., Bertino, L., Brando, V.E., Kreiner, M.B., Benkiran, M., Carval, T., Ciliberti, S.A., Claustre, H., Clementi, E., Coppini, G., Cossarini, G., De Alfonso Alonso-Muñoyerro, M., Delamarche, A., Dibarboure, G., Dinessen, F., Drevillon, M., Drillet, Y., Faugere, Y., Fernández, V., Fleming, A., Garcia-Hermosa, M.I., Sotillo, M.G., Garric, G., Gasparin, F., Giordan, C., Gehlen, M., Gregoire, M.L., Guinehut, S., Hamon, M., Harris, C., Hernandez, F., Hinkler, J.B., Hoyer, J., Karvonen, J., Kay, S., King, R., Lavergne, T., Lemieux-Dudon, B., Lima, L., Mao, C., Martin, M.J., Masina, S., Melet, A., Buongiorno Nardelli, B., Nolan, G., Pascual, A., Pistoia, J., Palazov, A., Piolle, J.F., Pujol, M.I., Pequignet, A.C., Peneva, E., Pérez Gómez, B., Petit de la Villeon, L., Pinardi, N., Pisano, A., Pouliquen, S., Reid, R., Remy, E., Santoleri, R., Siddorn, J., She, J., Staneva, J., Stoffelen, A., Tonani, M., Vandenbulcke, L., von Schuckmann, K., Volpe, G., Wettre, C.. and Zacharioudaki, A. (2019). From Observation to Information and Users: The Copernicus Marine Service Perspective. Frontiers in Marine Science, 6, 23, https://doi.org/10.3389/fmars.2019.00234

Lin, P. (2008). Numerical modeling of water waves (1st ed.). New York: Taylor and Francis.

Lionello, P., Gunther, H., and Janssen, P.A.E M. (1992). Assimilation of altimeter data in a global third generation wave model. *Journal of Geophysical Research: Oceans,* C97, 14453-14474, https://doi.org/10.1029/92JC01055

Madsen, P. A., and Larsen, J. (1987). An efficient finite-difference approach to the mild-slope equation. Coastal Engineering, 11, 329-351, https://doi.org/10.1016/0378-3839(87)90032-9

Marti F., Cazenave, A., Birol, F., Passaro, M., Léger, F., Niño, F., Almar, R., Benveniste, J., Legeais, J.F. (2021). Altimetry-based sea level trends along the coasts of Western Africa. *Advances in Space Research,* 68(2), 504-522, https://doi.org/10.1016/j.asr.2019.05.033

Maza, M., Lara, J. L., Losada, I. J. (2016). Solitary wave attenuation by vegetation patches. *Advances in Water Resources,* 98, 159-172, https://doi.org/10.1016/j.advwatres.2016.10.021

McCowan, J. (1894). On the Highest Waves of a Permanent Type. *Philosophical Magazine,* Edinburgh 38, 351-358.

Losada, I.J., Lara, J.L., Guanche, R., Gonzalez-Ondina, J.M. (2008). Numerical analysis of wave overtopping of rubble mound breakwaters. Coastal Engineering, 55, 47-62, https://doi.org/10.1016/j.coastaleng.2007.06.003

Mitsuyasu, H. (1970). On the growth of the spectrum of wind-generated waves. *Coastal Engineering in Japan,* 13(1), 1-14, https://doi.org/10.1080/05785634.1970.11924105

Mittermaier M. P., Csima, G. (2017). Ensemble versus deterministic Performance at kilometric scale. *Weather and Forecasting,* 32(5), https://doi.org/10.1175/WAF-D-16-0164.1

Molteni, F., Buizza, R., Palmer, T.N., Petroliagis, T. (1996). The ECMWF ensemble prediction system: methodology and validation. *Quarterly Journal of the Royal Meteorological Society,* 122(529), 73-119, https://doi.org/10.1002/qj.49712252905

Munk, W. H. (1950). Origin and generation of waves. *Coastal Engineering Proceedings,* 1, https://doi.org/10.9753/icce.v1.1

National Centers for Environmental Prediction (2012). Output fields from the NOAA WAVEWATCH III® wave model monthly hindcasts. NOAA National Centers for Environmental Information. Dataset.

Parkinson, C. L., and Cavalieri, D. J. (2012). Antarctic Sea ice variability and trends, 1979-2010. *The Cryosphere,* 6, 881–889, https://doi.org/10.5194/tc-6-881-2012

Pérez, B., Álvarez Fanjul, E., Pérez, S., de Alfonso, M., Vela, J. (2013). Use of tide gauge data in operational oceanography and sea level hazard warning systems, *Journal of Operational Oceanography,* 6(2), 1-18, https://doi.org/10.1080/1755876X.2013.11020147

Perez, J., Menendez, M., and Losada, I. J. (2017). GOW2: A global wave hindcast for coastal applications. *Coastal Engineering,* 124, 1-11, https://doi.org/10.1016/j.coastaleng.2017.03.005

Petroliagis, T.I., and Pinson, P. (2012). Early warnings of extreme winds using the ECMWF Extreme Forecast Index. *Meteorological Applications,* 21(2), 171-185, https://doi.org/10.1002/met.1339

Pezzutto P., Saulter A., Cavaleri L., Bunney, C., Marcucci, F., Sebastianelli, S. (2016). Performance comparison of meso-scale ensemble wave forecasting systems for Mediterranean Sea states. *Ocean Modelling,* 104, 171-186, https://doi.org/10.1016/j.ocemod.2016.06.002

Rascle N., Ardhuin, F., Queffeulou, P., Croizé-Fillon, D. (2008). A global wave parameter database for geophysical applications. Part 1: Wave-current–turbulence interaction parameters for the open ocean based on traditional parameterizations. *Ocean Modelling,* 25(3-4), 154-171, doi:10.1016/j.ocemod.2008.07.006

Reguero, B.G., Menéndez, M., Méndez, F.J., Mínguez, R., Losada, I.J. (2012). A global Ocean Wave (GOW) calibrated reanalysis from 1948 onwards. *Coastal Engineering,* 65, 38-55, https://doi.org/10.1016/j.coastaleng.2012.03.003

Ribal, A., Young, I.R. (2019). 33 years of globally calibrated wave height and wind speed data based on altimeter observations. *Scientific Data,* 6, 77, https://doi.org/10.1038/s41597-019-0083-9

Rusu, L., Pilar, P., Guedes Soares, C. (2008). Hindcast of the wave conditions along the west Iberian coast. *Coastal Engineering,* 55(11), 906-919, https://doi.org/10.1016/j.coastaleng.2008.02.029

Saetra, O., and Bidlot, J.-R. (2004). Potential benefit of using probabilistic forecasts for waves and marine winds based on the ECMWF ensemble prediction system. *Weather and Forecasting,* 19(4), 673-689, https://doi.org/10.1175/1520-0434(2004)019<0673:PBOUPF>2.0.CO;2

Saha, S., Moorthi, S., Pan, H.-L., Wu, X., Wang, J., Nadiga, S., … Goldberg, M. (2010). The NCEP Climate Fore-cast System Reanalysis. *Bulletin of the American Meteorological Society,* 91(8), 1015-1057, https://doi.org/10.1175/2010BAMS3001.1

Saulter A. N., Bunney, C., King, R., Water, J. (2020). An Application of NEMOVAR for Regional Wave Model Data Assimilation, Frontiers in Marine Science, 7, 579834, https://doi.org/10.3389/fmars.2020.579834

Shapiro, R. (1970). Smoothing filtering and boundary effects. *Reviews of Geophysics,* 8(2), 359-387, https://doi.org/10.1029/RG008i002p00359

State of the Global Climate 2020 (WMO-No. 1264).

Staneva, J., Alari, V., Breivik, Ø. et al. (2017). Effects of wave-induced forcing on a circulation model of the North Sea. *Ocean Dynamics,* 67, 81-101, https://doi.org/10.1007/s10236-016-1009-0

Staneva, J., Grayek, S., Behrens, A., and Günther, H. (2021). GCOAST: skill assessments of coupling wave and circulation models (NEMO-WAM). Journal of Physics: Conference Series, 1730, 012071. doi:10.1088/1742-6596/1730/1/012071

Stansby, P., Zhou, J., Kuang, C., Walkden, M., Hall, J., Dickson, M. (2007). Long-term prediction of nearshore wave climate with an application to cliff erosion. In: McKee Smith, Jane (Ed.), Proc. of International Con-ference Coastal Engineering, ASCE, pp. 616-627.

Stopa, J.E. (2018). Wind forcing calibration and wave hindcast comparison using multiple reanaly-sis and merged satellite wind datasets. *Ocean Modelling,* 127, 55-69, https://doi.org/10.1016/j.oce-mod.2018.04.008

Swail, V., Jensen, R., Lee, B., Turton, J., Thomas, J., Gulev, S., Yelland, M., Etala, P., Meldrum, D., Birkemeier, W., Burnett, W., Warren, G. (2010). Wave Measurements, Needs and Developments for the Next Decade. Pro-ceedings of OceanObs'09: Sustained Ocean Observations and Information for Society Conference (Volume 2), Venice, Italy, 21-25 September 2009 (J. Hall, D.E. Harrison and D. Stammer, eds.). ESA Publication WPP-306.

Thomson, J., Ackley, S., Girard-Ardhuin, F., Ardhuin, F., Babanin, A.V., Boutin, G., Brozena, J., Cheng, S., Col-lins, C., Doble, M., Fairall, C., Guest, P., Gebhardt, C., Gemmrich, J., Graber, H.C., Holt, B., Lehner, S., Lund, B., Meylan, M.H., Maksym, T., Montiel, F., Perrie, W., Persson, O., Rainville, L., Rogers, W.E., Shen, H., Shen, H., Squire, V., Stammerjohn, S., Stopa, J., Smith, M.M., Sutherland, P., Wadhams, P. (2018). Overview of the Arctic Sea State and Boundary Layer Physics Program. *Journal of Geophysical Research: Oceans,* 123(12), 8674-8687, https://doi.org/10.1002/2018JC013766

Tolman, H. L. (1989). The numerical model WAVEWATCH: a third generation model for the hindcasting of wind waves on tides in shelf seas. *Communications on Hydraulic and Geotechnical Engineering,* Delft Univ. of Techn., ISSN 0169-6548, Rep. no. 89-2, 72 pp.

Tolman, H.L. (2010). WAVEWATCH III development best practices. Camp Springs.

Tolman H.L., and the WAVEWATCH III® Development Group (2014). User Manual and System Documenta-tion of WAVEWATCH III® version 4.18. Technical Note 316, NOAA/NWS/NCEP/MMAB. Available at: https://polar.ncep.noaa.gov/waves/wavewatch/manual.v4.18.pdf

Thomas, A., Mendez, F. J., and Losada, I. J. (2008). A method for spatial calibration of wave hindcast data bases. *Continental Shelf Research,* 28(3), 391-398, https://doi.org/10.1016/j.csr.2007.09.009

Trulsen, K. C., Nieto Borge, J., Gramstad, O., Aouf, L., and Lefèvre, J.-M. (2015). Crossing sea state and rogue wave probability during the Prestige accident. *Journal of Geophysical Research: Oceans,* 120, 7113-7136, https://doi.org/10.1002/2015JC011161

.Tsagareli, K.N., Babanin, A.V., Walker, D.J., and Young, I.R. (2010). Numerical investigation of spectral evolution of wind waves. Part 1. Wind input source function. *Journal of Physical Oceanography,* 40(4), 656-666, https://doi.org/10.1175/2009JPO4370.1

Tsay, T. K., Zhu, W., and Liu, P. L.-F. (1989) A finite element model for wave refraction, diffraction, reflection and dissipation. *Applied Ocean Research,* 11, 33-38, https://doi.org/10.1016/0141-1187(89)90005-9

Van der Meer, J., Allsop, W., Bruce, T., Rouck, J., Kortenhaus, A., Pullen, T., Schüttrumpf, H., Troch, P., Zanuttigh, B. (2016). EurOtop: Manual on wave overtopping of sea defences and related structures - An overtopping manual largely based on European research, but for worldwide application, 2nd edition.

Van der Ven, P., Reijmerink, B., Van der Hout, A., De Jong, M. (2018). Comparison of Validation Studies of Wave - Penetration Models using Open Benchmark Datasets of Deltares, PIANC World Congress 2018, At Panama City, Panama.

Veron, F. (2015). Ocean spray. Annual Review of Fluid Mechanics, 47, 507-538, https://doi.org/10.1146/annurev-fluid-010814-014651

Visbeck, M. (2018). Ocean science research is key for a sustainable future. *Nature Communication,* 9, 690, https://doi.org/10.1038/s41467-018-03158-3

Voorrips, A. C., Makin V. K., and Hasselmann S. (1997). Assimilation of wave spectra from pitch-and-roll buoys in a North Sea wave model. *Journal of Geophysical Research: Oceans,* 102, 5829-5849, https://doi.org/10.1029/96JC03242

WAMDI group (The) (1988). The WAM Model - A Third Generation Ocean Wave Prediction Model. *Journal of Physical Oceanography,* 18, 1775-1810, https://doi.org/10.1175/1520-0485(1988)018<1775:TWMTGO>2.0.CO;2

Wang, J. K., Aouf, L., Dalphinet, A., Zhang, Y. G., Xu, Y., Hauser, D., Liu, J. Q. (2021). The Wide Swath Significant Wave Height: An Innovative Reconstruction of Significant Wave Heights From CFOSAT's SWIM and Scatterometer Using Deep Learning. *Geophysical Research Lettera,* 48(6), https://doi.org/10.1029/2020GL091276

Wilby, R. and Dessai, S. (2010). Robust adaptation to climate change. *Weather,* 65, 180-185, https://doi.org/10.1002/wea.543

Young, I.R. (1999). Wind Generated Ocean Waves, Elsevier, Amsterdam, 288 p.

Zakharov, V.E. (1968). Stability of periodic waves of finite amplitude on the surface of a deep fluid. *Journal of Applied Mechanics and Technical Physics,* 9(2), 190-194

Zieger, S., Greenslade, D.J.M., and Kepert, J.D. (2018). Wave ensemble forecast system for tropical cyclones in the Australian region. *Ocean Dynamics,* 68(4-5):603-625, https://doi.org/10.1007/s10236-018-1145-9

Zijlema, M. (2009). Parallel, unstructured mesh implementation for SWAN. Proceedings of the Coastal Engineering Conference. 470-482, https://doi.org/10.1142/9789814277426_0040

Zijlema, M., Stelling, G., and Smit, P. (2011). SWASH: An operational public domain code for simulating wave fields and rapidly varied flows in coastal waters. *Coastal Engineering,* 58, 992-1012, https://doi.org/10.1016/j.coastaleng.2011.05.015